FIFTH ANNUAL
CLIMATE ASSESSMENT
1993

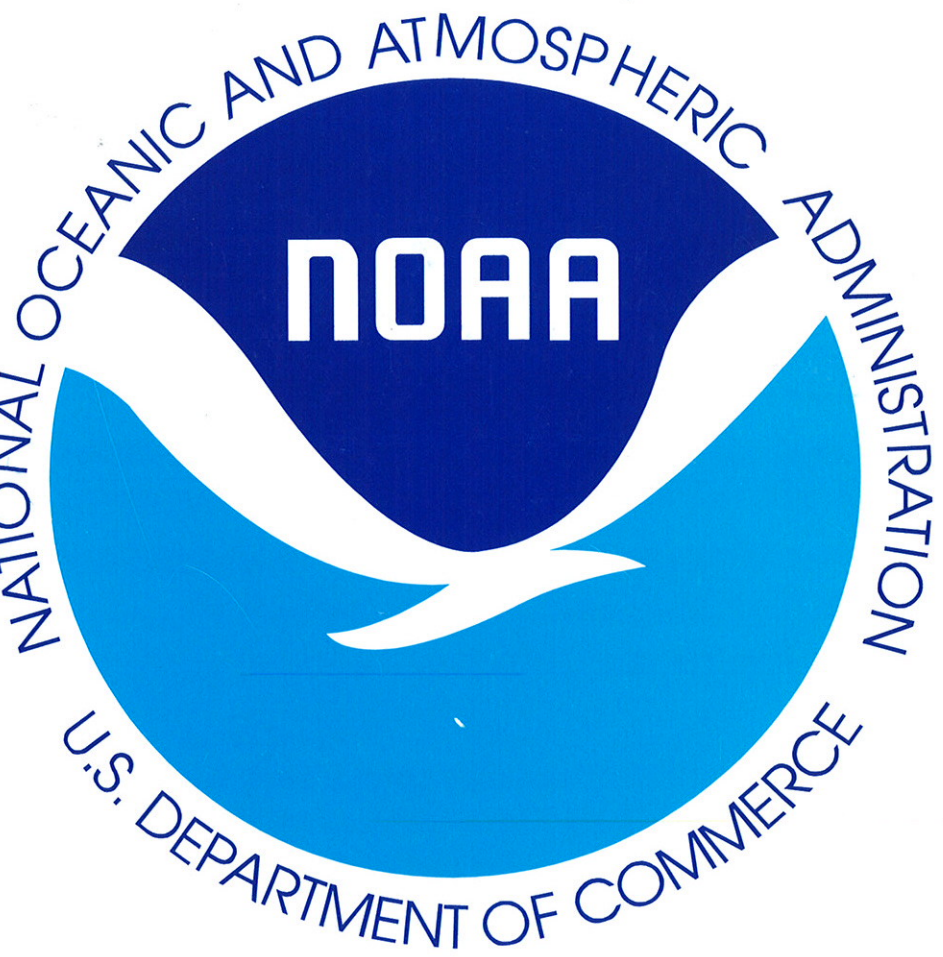

U. S. DEPARTMENT OF COMMERCE
National Weather Service
National Meteorological Center
Climate Analysis Center

Climate Analysis Center
Camp Springs, Md
March 1994

FIFTH ANNUAL
CLIMATE ASSESSMENT
1993

EDITORS: M. S. Halpert
G. D. Bell
V. E. Kousky
C. F. Ropelewski

U. S. DEPARTMENT OF COMMERCE
NATIONAL OCEANIC AND ATMOSPHERIC ADMINISTRATION
NATIONAL WEATHER SERVICE
NATIONAL METEOROLOGICAL CENTER

TABLE OF CONTENTS

LIST OF FIGURES

PREFACE

The possibility of long-term climate change continues to be a concern and focus for scientific investigations, development of government policy, and planning of commercial interests, especially in agriculture and water resources. However, the year-by-year evaluation of the global climate system also includes seasonal climate anomalies and decadal variability, as well as possible long-term trends.

The report you are now reading is the best description of recent climatic variations and changes that we can assemble immediately after the end of the past calendar year. Subsequently, more thorough studies by the scientific community will examine in greater detail the evidence we have put forward.

Although many components of the global climate system are not fully described, this report intends to assess annual changes in the circulation, structure and constituents of the atmosphere, and changes in surface conditions of temperature, precipitation, snow and ice. It describes the evolution of ENSO during the past year, and identifies major, regional climatic events around the world.

As we plan improvements to this report and expand its scope during 1994, your comments and suggestions for improvements would be most welcome.

Acknowledgments - This assessment was assembled with the cooperation and the contributions from NOAA scientists representing a wide range of climate interests. We also would like to acknowledge several contributions from outside NOAA. These scientists are identified on the proceeding page, and we thank them for their timely and useful input. In addition, we would like to thank the reviewers for their comments and quick response: T. Karl, E. Rasmusson, J. Hansen, M. Coughlan, P. Arkin and D. Phillips. The manuscript was also reviewed by A. Lessard and L. Mannello at the Climate Analysis Center.

David R. Rodenhuis
Director
Climate Analysis Center/NMC
February 28, 1994

CONTRIBUTORS

Air Resources Laboratory/ERL/NOAA

J. Angell

Center for Ocean-Land-Atmosphere Interactions, Univ. of Maryland

B. E. Doty

Climate Analysis Center/NMC/NWS/NOAA

A. N. Basist
G. D. Bell
D. R. Garrett
M. E. Gelman
M. S. Halpert
J. E. Janowiak
V. E. Kousky
C. S. Long
A. J. Miller
D. Miskus
R. Nagatani
C. F. Ropelewski
T. M. Smith
R. J. Tinker

Climate Monitoring and Diagnostics Laboratory/ERL/NOAA

E. Dutton
J. Peterson
P. Tans

Climatic Research Unit, University of East Anglia, (UK)

P. D. Jones

Coupled Model Project/NMC/NWS/NOAA

M. Ji
A. Leetmaa
R. W. Reynolds

Department of Geography, Rutgers University

D. A. Robinson

Hadley Centre for Climate Prediction and Research, (UK)

D. E. Parker

Institute for Global Climate and Ecology, (Russia)

G. Gruza

Johnson Research Center, University of Alabama in Huntsville

J. R. Christy

NASA Goddard Institute for Space Studies

J. Hansen

NASA Marshall Space Flight Center

R. W. Spencer

National Climatic Data Center/NESDIS/NOAA

R. R. Heim Jr.
T. R. Karl

Office of Hydrology/NWS/NOAA

S. Kroczynski
A. Morgan

Satellite Research Laboratory/NESDIS/NOAA

L. L. Stowe

EXECUTIVE SUMMARY

The global climate during 1993 was dominated by mature warm episode [El Niño/Southern Oscillation (ENSO)] conditions in the east-central equatorial Pacific. This period of warm episode conditions, which first developed in late 1991, is one of the three most prolonged ENSO episodes observed in this century, being similar in duration to the ENSO episodes of 1911-1913 and 1939-1941.

During 1993, these ENSO conditions were associated with anomalous temperature and rainfall patterns throughout the tropical and subtropical Pacific, and with a host of persistent anomalous weather patterns in the extratropical latitudes of both hemispheres. For example, preliminary evidence suggests that the warm episode was a contributing factor in ending severe drought conditions which had plagued California since 1986. By the end of the year, conditions in the equatorial Pacific showed definitive signs of returning to normal.

Among the major surface climatic events during 1993 was the devastating flood that inundated the central United States during June-July. Severe flooding was also observed over sections of central South America early in the year, and over large sections of the Indian Subcontinent during the peak of the Indian Monsoon. Flooding was also observed in southeastern China during June-August, and in large portions of both Europe and southeastern Australia during the latter part of the year. In contrast, drought conditions became entrenched over northeastern Australia, with unprecedented long-term rainfall deficiencies observed in some areas. Moderate drought conditions were also observed in the monsoon regions of West Africa, central India, northeastern Brazil, and the southeastern United States.

The annual global temperature anomaly pattern during 1993 resembled the pattern that dominated both hemispheres during the 1980s. The global (land only) surface temperature anomaly for 1993 of 0.18°C was comparable to the anomaly observed last year. Snow cover in the Northern Hemisphere increased compared to 1992, especially during the boreal fall. September - November 1993 featured the largest snow-cover area during this season since 1976.

In the stratosphere, aerosol concentrations returned to near-normal levels. However, global lower-stratospheric temperatures steadily declined during 1993, with the anomalies reaching -0.9°C in December. This was the largest negative temperature anomaly observed in the 15-year record. Temperatures during most of 1993 were well below the six-year mean value observed immediately prior to the Mt. Pinatubo eruption. Total ozone values were also below-normal in 1993 during the spring seasons of both hemispheres. In the Southern Hemisphere, record low total ozone values were observed over Antarctica during September and October, and the areal extent of the ozone hole was one of the largest ever recorded.

1. CLIMATE AND GLOBAL CHANGE ISSUES

a. Surface Temperature

The pattern of global temperature anomalies during 1993 (**Fig. 1.1**) is similar to the one observed during the decade of the 1980's (*Climate Analysis Center 1991*), except for the cooler than normal regions in the western United States and western Asia. The largest anomalies were found in the Northern Hemisphere, with positive anomalies observed over northwestern North America, and over central and northern Russia, and negative anomalies over northeastern Canada, sections of the western United States, and southwestern Russia. In the Southern Hemisphere, the mean temperature anomaly pattern primarily reflected above-normal sea surface temperatures (SSTs) in the equatorial and subtropical Pacific Ocean and in the southwestern and south-central South Atlantic Ocean. Above-normal temperatures were also observed in South Africa and adjacent waters, and in east-central Australia. The estimated global (land only) surface temperature anomaly of +0.18°C (relative to the 1951-1980 base period) was similar to that observed in 1992 (**Fig. 1.2**). Other estimates of the global temperature anomaly for 1993 vary from between +0.18°C and +0.24°C.

Values of the global land-only temperature were computed on a 2^{o} x 2^{o} grid from data received over the Global Telecommunications System (GTS). Monthly anomalies for the past four years (**Fig. 1.3**) show a general decrease during the period from 1991 through 1993. All monthly values during 1990 and 1991 were positive, with the largest anomalies occurring during the January - March period. This tendency for well above-normal temperatures during the early part of the year persisted during both 1992 and 1993. However, global temperature anomalies during the latter half of both 1992 and 1993 were much smaller than during 1990 and 1991, with negative values observed during some individual months.

Stratification of the global land temperature anomalies into three latitude bands [tropics (20°N-20°S), northern extratropics (20°N-90°N) and southern extratropics (20°S-90°S)] (**Fig. 1.4**), shows that during the past four years, the mean annual tropical temperature anomaly (**Fig. 1.4, middle**) has consistently averaged about +0.4°C, with all individual monthly values ranging between +0.01°C and +0.69°C. Much of this warmth has been related to the long-lived El Niño/ Southern Oscillation (ENSO) episode in the tropical Pacific (see section 2). In the Southern Hemisphere extratropics (**Fig. 1.4, bottom**), surface land temperature anomalies averaged +0.33°C during 1990 and 1991, but decreased to +0.09 in 1992, as volcanic aerosols from the eruption of Mt. Pinatubo became dispersed throughout the hemisphere. As aerosol concentrations decreased during 1993, the temperature anomaly increased to approximately +0.3°C. In the Northern Hemisphere extratropics (**Fig. 1.4, top**), a steady decrease in temperature occurred from 1990 through 1993. Although global stratospheric aerosols during 1993 decreased to levels observed prior to the eruption of Mt. Pinatubo, the mean annual temperature anomaly in the northern extratropics fell to the lowest value (+0.09°C) since 1986.

Global land-marine temperature anomalies computed relative to the period April-June 1991 are compared to general circulation model forecasts using the Goddard Institute for Space Studies (GISS) global coupled atmosphere-ocean climate model (**Fig. 1.5**). This model attempts to simulate the global climate effects of heat-dependent variations of atmospheric aerosols and trace gases (*Hansen et al. 1988; 1992*). The land-marine anomalies were computed by combining land station air temperatures (*Jones 1988*) and nighttime marine-air temperatures (*Bottomley et al. 1990*). Daytime marine air temperatures were not used because they are affected by solar heating of ships' surfaces. Air temperatures rather than sea surface temperatures (SSTs) were used for compatibility with the GISS model results. The observed time series shows an overall cooling of about 0.5°C between the time of the eruption of Mt. Pinatubo and the northern summer of 1992 (**Fig. 1.5**). Two runs of the GISS model (initialized with random atmospheric conditions (black and blue lines)), successfully simulated the observed overall cooling. However, the model failed to capture global temperature increases during the Northern Hemisphere winters of 1991-92 and

1992-93. Seasonal fields of surface temperature (see section 4) and mid-tropospheric circulation anomalies for 1993 show that the warmth during the northern winter was concentrated over northern Eurasia and central North America.

Global and hemispheric annual averages of combined land-air and sea surface temperature (SST) anomalies, for each year from 1861 to 1993 (October), are shown in **Figs. 1.6-1.8**. The land-air temperatures are an update of the *Jones (1988)* data base and the sea surface temperatures are updated from *Bottomley et al. (1990)*, but with improved corrections for the use of uninsulated and semi-insulated buckets before 1942 (*Folland and Parker 1994*). These series differ from those presented in the 1992 Supplementary Report to the IPCC Scientific Assessment (*Folland et al. 1992*) because the latter also incorporated the University of East Anglia's version of the Comprehensive Ocean-Atmosphere Data Set (COADS) SSTs with different instrumental corrections. The three time series are all similar in that they each show a warming of approximately 0.5°C over the past 135 years. However, the character of the hemispheric time series is different, as the Northern Hemisphere (**Fig. 1.7**) warmed more during the late 1930s and early 1940s, while the Southern Hemisphere (**Fig. 1.8**) has been warmer during the past 15 years. The global (**Fig. 1.6**) and Northern Hemisphere (**Fig. 1.7**) annual land-marine temperature anomalies show a partial recovery in 1993 following the post-Pinatubo cooling evident in 1992. The true cooling may, however, have been partly masked by the recent long-lived tropical Pacific warm episode, which lasted for about three years and finally declined late in 1993 (see section 2). In the predominantly oceanic Southern Hemisphere (**Fig. 1.8**), the cooling during 1992 continued through 1993, although this cooling was less than that observed in the Northern Hemisphere.

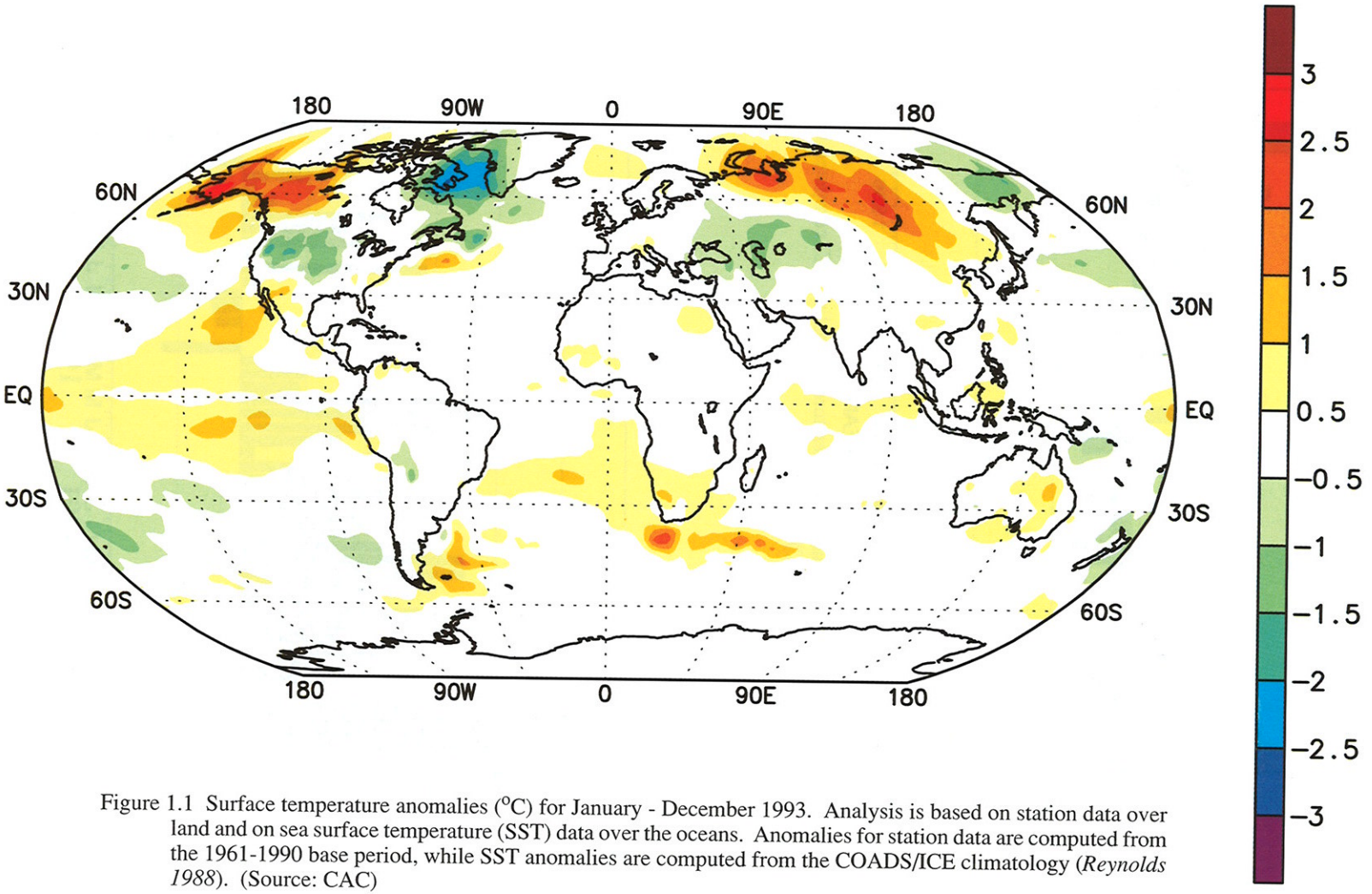

Figure 1.1 Surface temperature anomalies (°C) for January - December 1993. Analysis is based on station data over land and on sea surface temperature (SST) data over the oceans. Anomalies for station data are computed from the 1961-1990 base period, while SST anomalies are computed from the COADS/ICE climatology (*Reynolds 1988*). (Source: CAC)

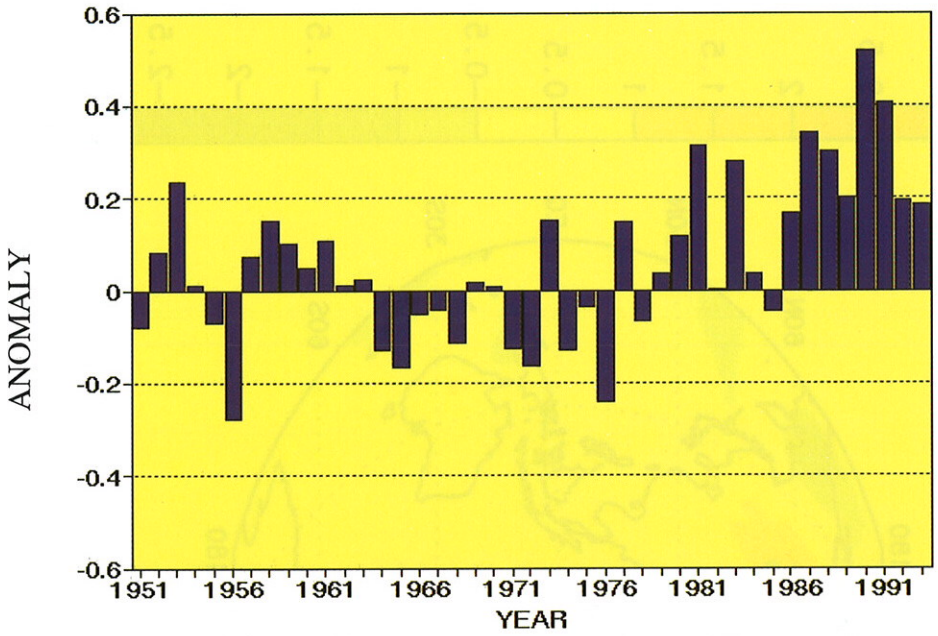

Figure 1.2 Annual global (land only) surface temperature anomalies (°C) computed from the 1951-1980 base period. (Source: CAC)

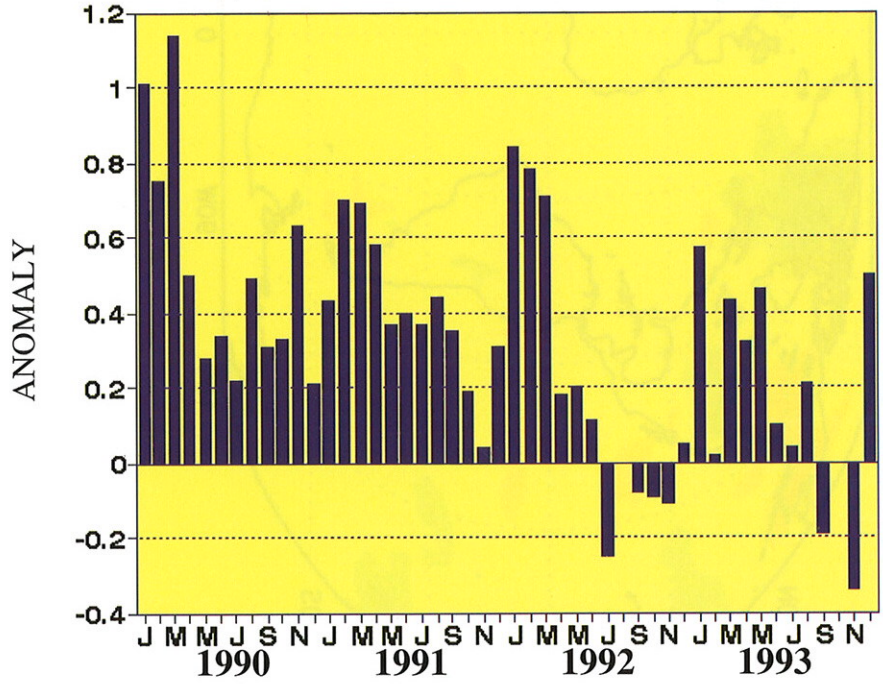

Figure 1.3 Monthly global (land only) surface temperature anomalies (°C) from January 1990 - December 1993 computed from the 1951-1980 base period. (Source: CAC)

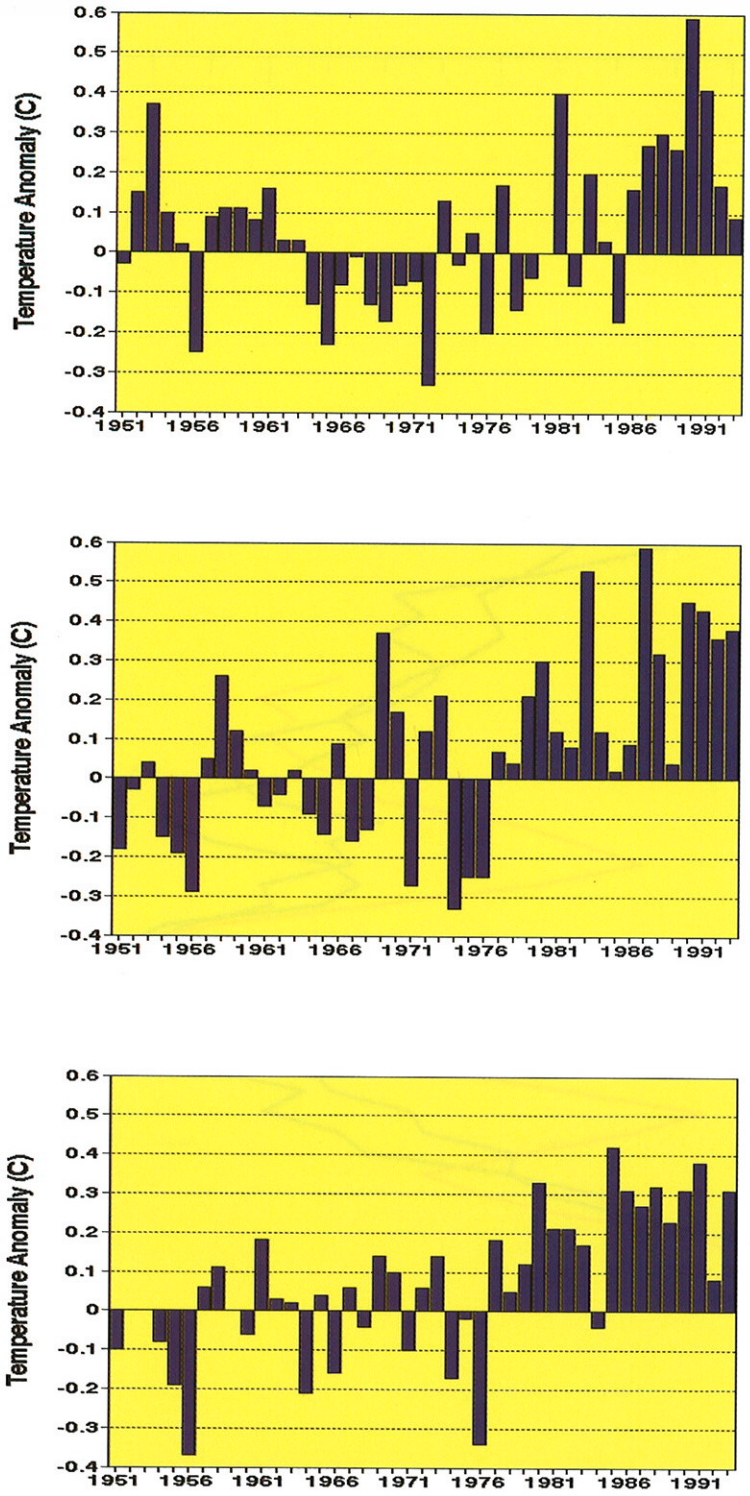

Figure 1.4 Annual global (land only) surface temperature anomalies (°C) computed from the 1951-1980 base period for the Northern Hemisphere extratropics (top), tropics (middle) and Southern Hemisphere extratropics (bottom). (Source: CAC)

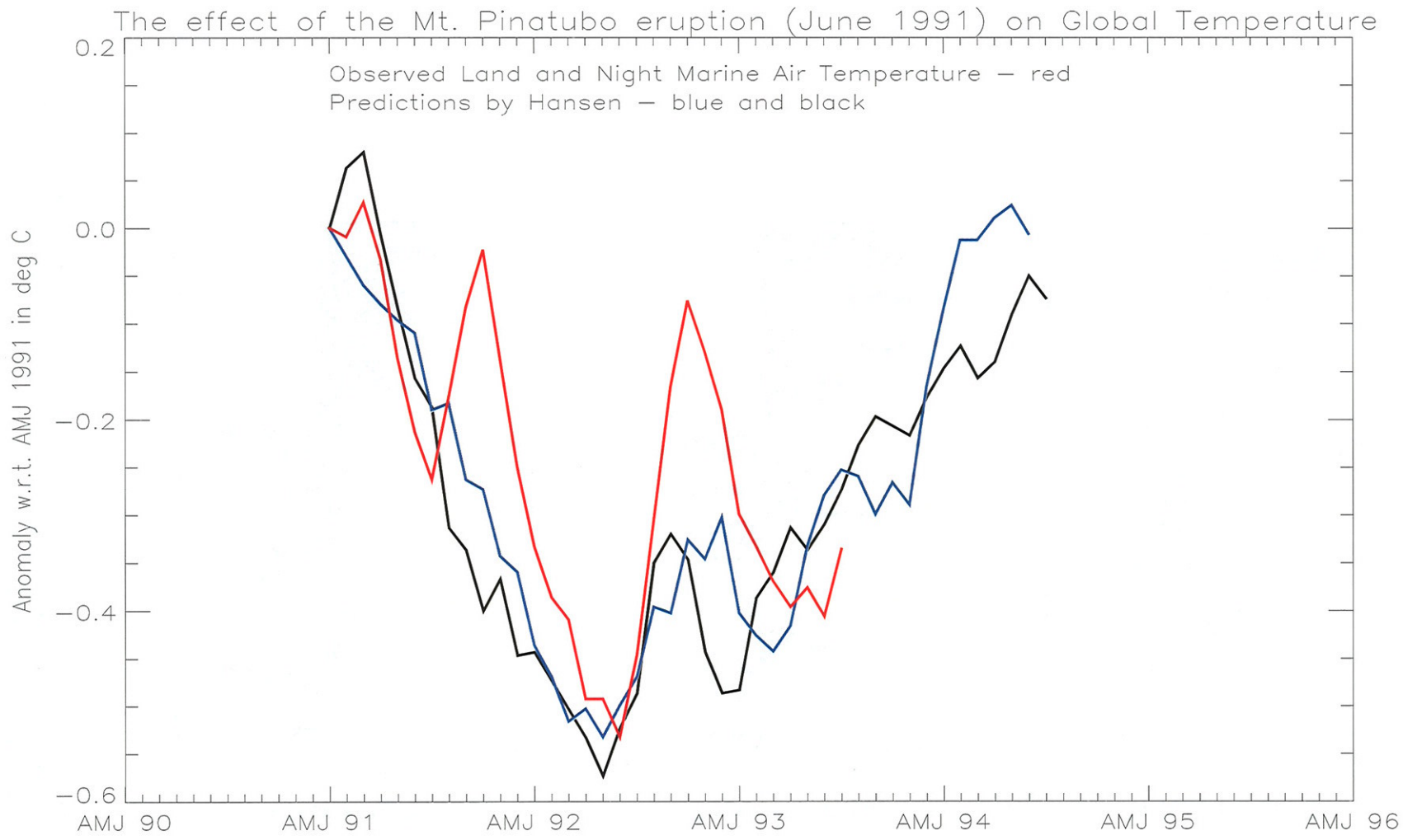

Figure 1.5 Global surface air temperature anomalies (red line) following the June 1991 eruption of Mt. Pinatubo, relative to the global anomaly for the 3-month period April-June 1991. Values are 3-month running mean anomalies ending with September-November 1993. The anomalies are computed from the 1951-1980 base period. Model results are indicated by blue and black lines. (Source: Hadley Centre for Climate Prediction and Research, UK)

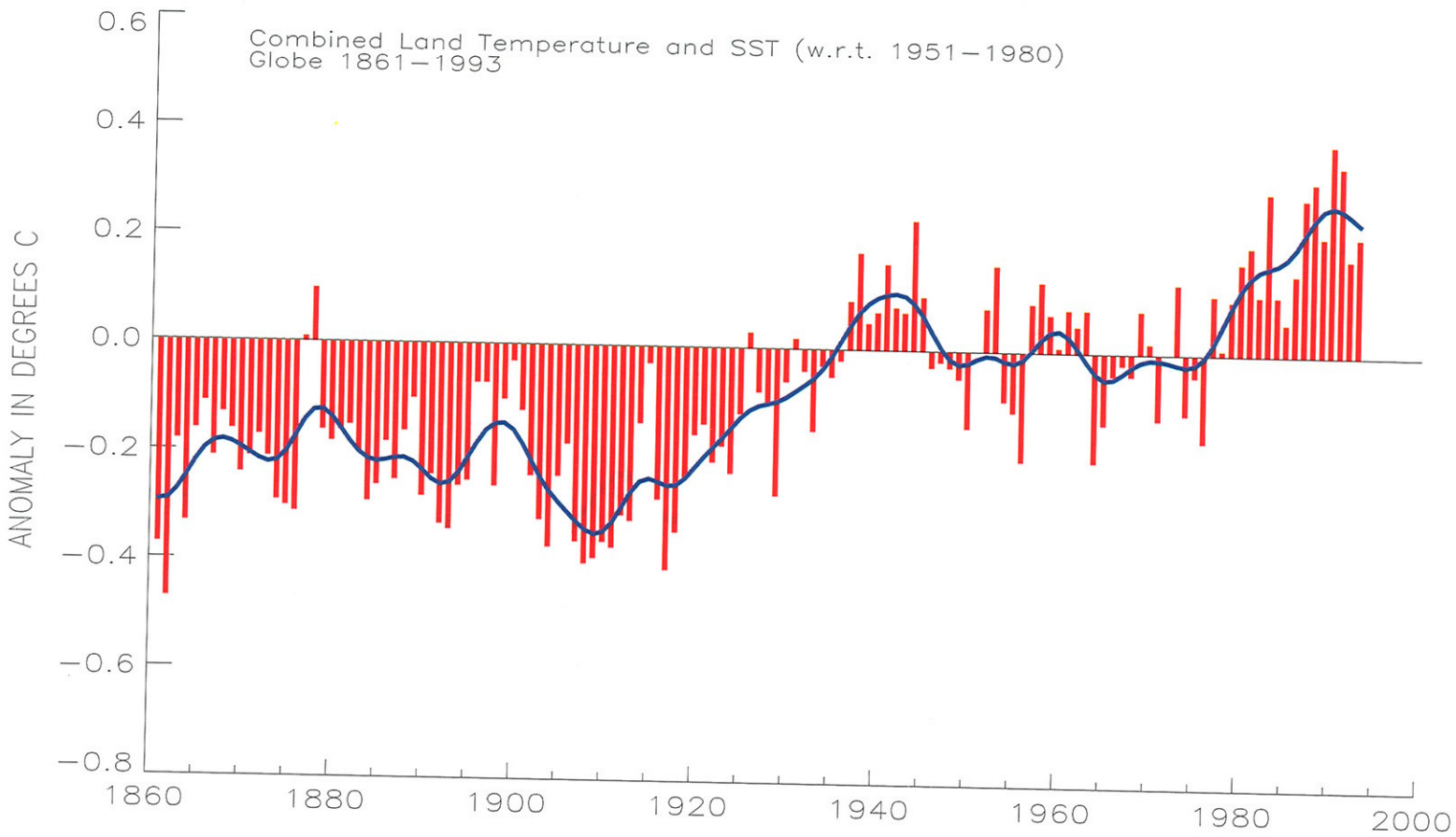

Figure 1.6 Global annual averages of combined land-air and sea surface temperature (SST) anomalies for each year from 1861-1993 (October). Anomalies are computed with respect to the 1951-1980 base period. The blue curve is a 13-term Gaussian filter designed to suppress variations on time scales less than 10 years. (Source: Hadley Centre for Climate Prediction and Research, UK)

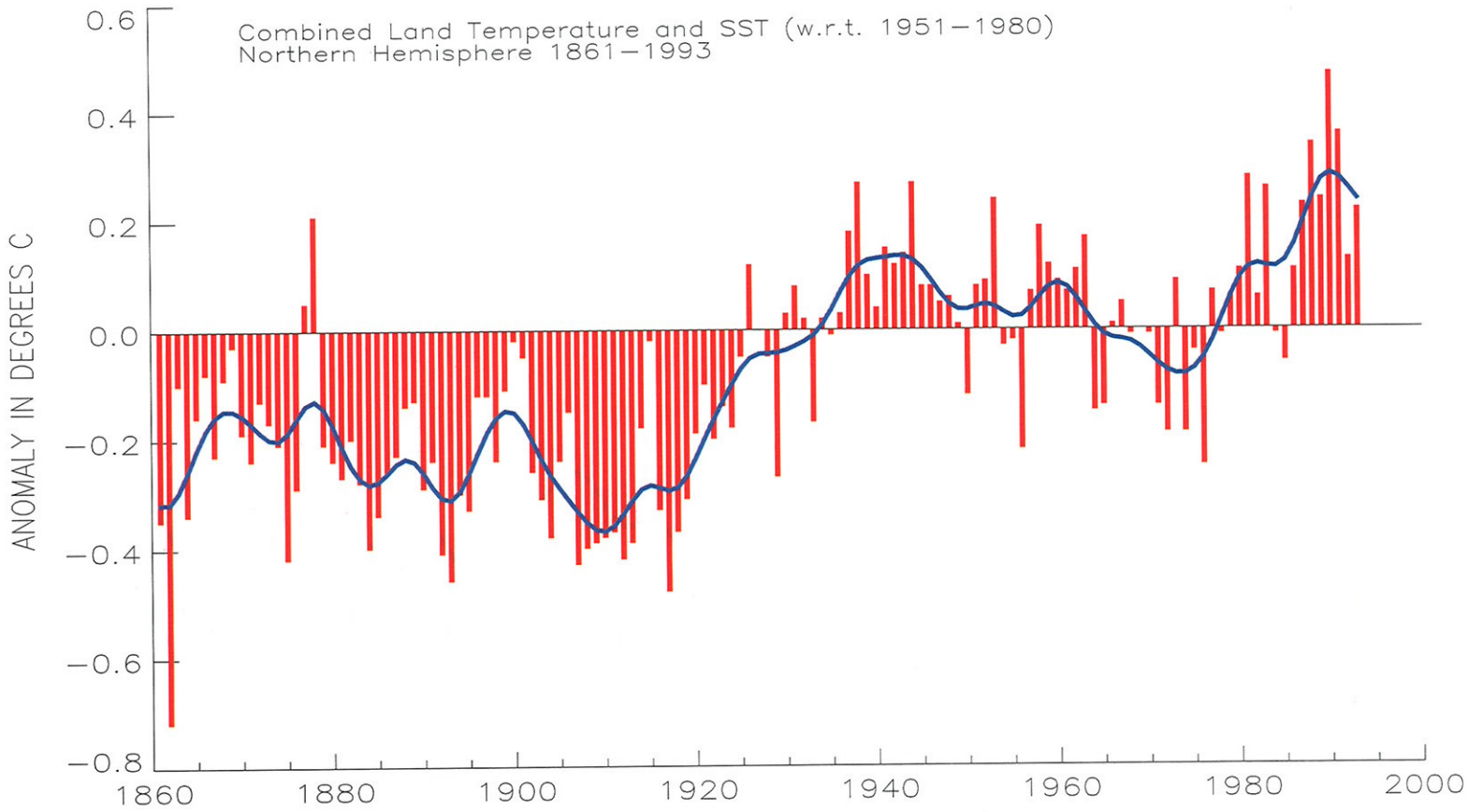

Figure 1.7 Northern Hemisphere annual averages of combined land-air and sea surface temperature (SST) anomalies for each year from 1861-1993 (October). Anomalies are computed with respect to the 1951-1980 base period. The blue curve is a 13-term Gaussian filter designed to suppress variations on time scales less than 10 years. (Source: Hadley Centre for Climate Prediction and Research, UK)

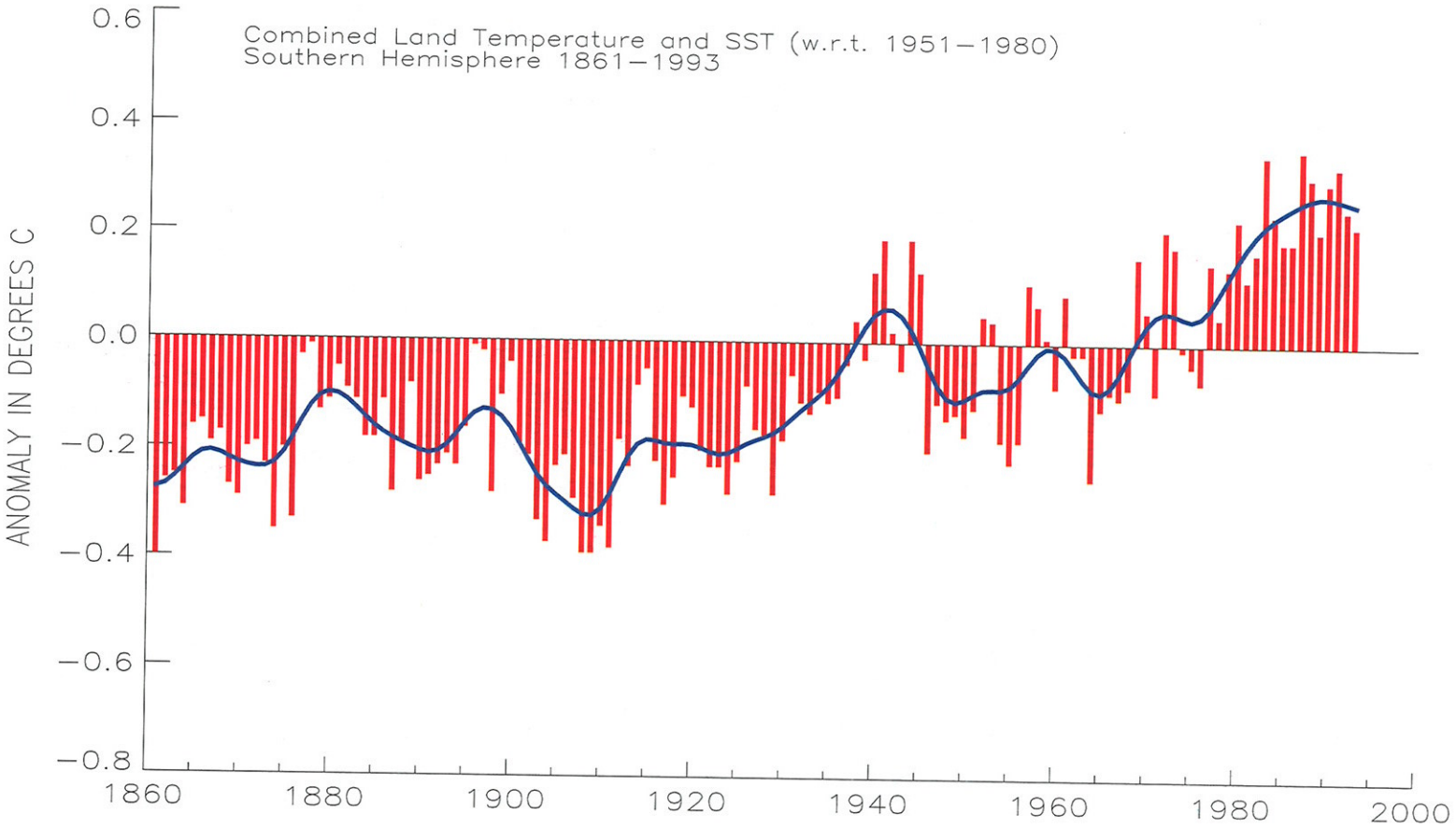

Figure 1.8 Southern Hemisphere annual averages of combined land-air and sea surface temperature (SST) anomalies for each year from 1861-1993 (October). Anomalies are computed with respect to the 1951-1980 base period. The blue curve is a 13-term Gaussian filter designed to suppress variations on time scales less than 10 years. (Source: Hadley Centre for Climate Prediction and Research, UK)

b. Tropospheric/Stratospheric Temperatures

1) Lower Troposphere

Lower-tropospheric temperature fields are derived globally on a 2.5° x 2.5° latitude-longitude grid from channel-2R of the Microwave Sounding Unit (MSU) flown aboard the NOAA polar-orbiting satellites (*Spencer et al. 1990*). Global tropospheric temperatures declined rapidly following the eruption of Mt. Pinatubo in June 1991 (**Fig. 1.9a**), as atmospheric aerosols reflected incoming solar radiation back to space. This decline ended approximately one year later, with temperatures averaging 0.3°C below normal during the period from June 1991 - June 1992. These results are consistent with mean tropospheric temperatures derived from radiosonde data (**Fig. 1.10**). A significant and prolonged cooling in the troposphere also followed the eruption of Mt. Agung in 1963, while no such cooling trend was evident following the eruption of El Chichon in 1982 (**Fig. 1.10**).

During the first three months of 1993, global lower-tropospheric temperatures averaged 0.23°C below normal (**Fig. 1.9a**). Temperatures returned to normal by October, and rose to slightly above-normal during the final months of 1993, marking the first period of above-normal global temperatures since the Mt. Pinatubo eruption.

The recent global tropospheric temperature variations are most evident in the tropics (30°N-30°S) (**Fig. 1.9b**), where temperatures were nearly 0.4°C below normal in the beginning of 1993, but rapidly returned toward normal as the year progressed. By the end of the year, temperatures were 0.2°C above the 1982-1991 normal in the tropics. In contrast, tropospheric temperatures in both the Northern Hemisphere (**Fig. 1.9c**) and Southern Hemisphere extratropics (**Fig. 1.9d**) have remained below-normal since the eruption of Mt. Pinatubo.

The spatial pattern of MSU-derived annual tropospheric temperature anomalies for 1993 (**Fig. 1.11**) shows considerable similarity to the surface temperature anomaly pattern (**Fig. 1.1**). In the tropical and subtropical Pacific, above-normal temperatures in the east and below-normal temperatures in the west are coincident with the sea surface temperature anomaly pattern associated with the El Niño/ Southern Oscillation. Farther west, below-normal temperature anomalies covered much of the Indian Ocean, Africa and southeastern Asia. In the northern extratropics, below-normal temperatures covered the middle latitudes near 40°N, while above-normal temperatures dominated the high latitudes, particularly over western North America and eastern Siberia. In the southern extratropics, below-normal temperatures also tended to dominate the middle latitudes. Above-normal temperatures were found farther south near the southern regions of all three Southern Hemisphere continents, where above-normal sea surface temperatures also prevailed during much of the year.

The time-latitude cross-section of mean tropospheric temperature anomalies (**Fig. 1.12**) shows negative temperature anomalies dominating most latitudes immediately following the eruption of Mt. Pinatubo. In the tropics, weak positive anomalies developed during December 1991-March 1992 in association with the onset of mature ENSO conditions in the tropical Pacific. Weak negative temperature anomalies reappeared during June 1992 and subsequently persisted until March 1993. Slightly above-normal temperatures dominated the tropics during the remainder of 1993.

In the northern extratropics, negative temperature anomalies dominated the region between 30°N and 40°N during 1992 and 1993 (**Fig. 1.12**). This pattern was associated with enhanced westerlies and with an overall southward shift of the storm track in the lower extratropics throughout the period. These conditions likely were associated with the magnitude and extent of the Midwest U. S. floods during June-July 1993 (see section 3d). Negative temperature anomalies also dominated the southern extratropics during 1992 and 1993, although these anomalies were weaker and less persistent than those observed in the middle latitudes of the Northern Hemisphere.

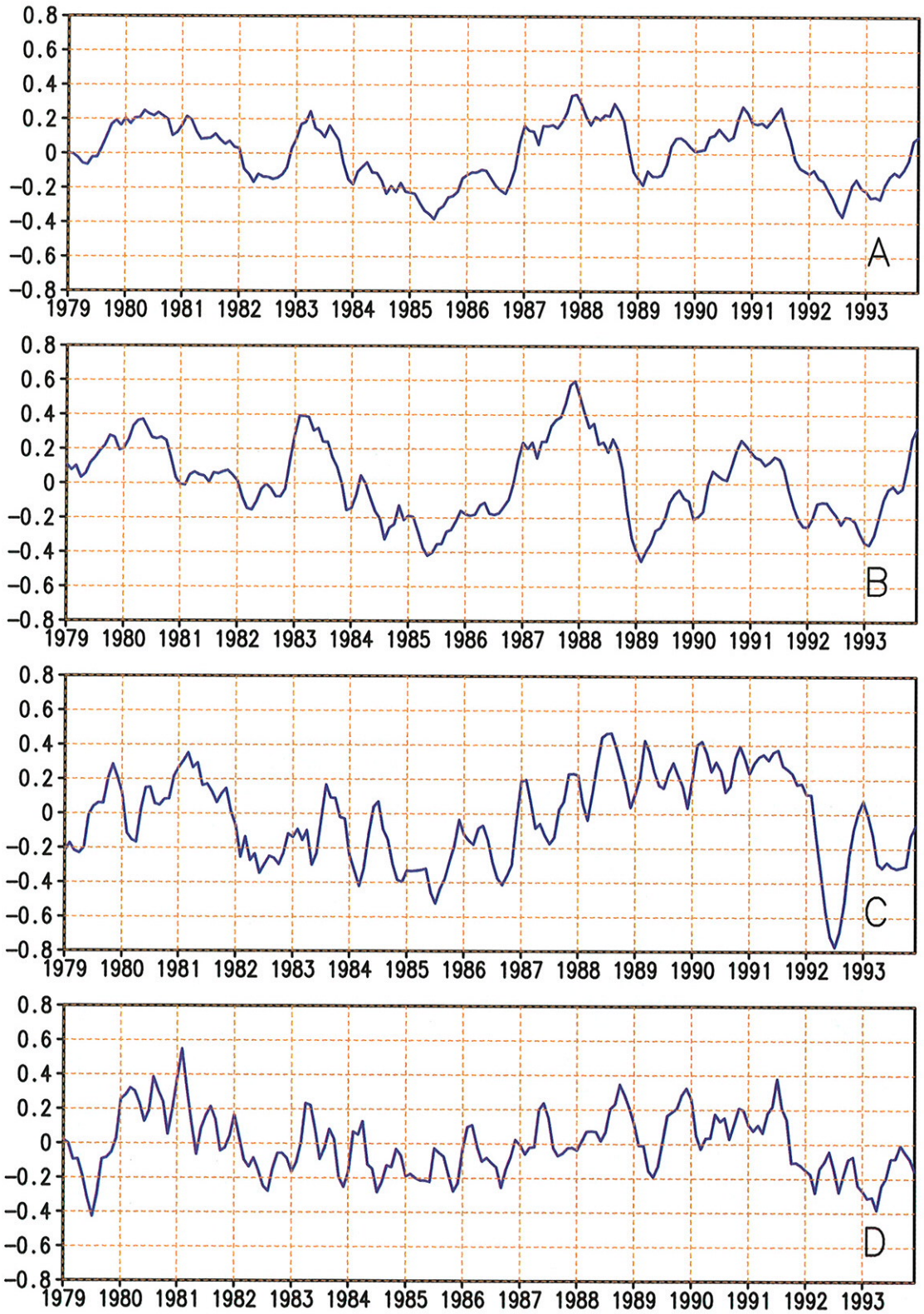

Figure 1.9 Mean tropospheric temperature anomalies from the Microwave Sounding Unit (MSU) channel 2r for the a) globe (85°S-85°N), b) tropics (30°N-30°S), c) Northern Hemisphere extratropics (30°N-85°N) and d) Southern Hemisphere extratropics (30°S-85°S). Anomalies are computed from the 1982-1991 base period. (Data provided by R. W. Spencer and J. R. Christy.)

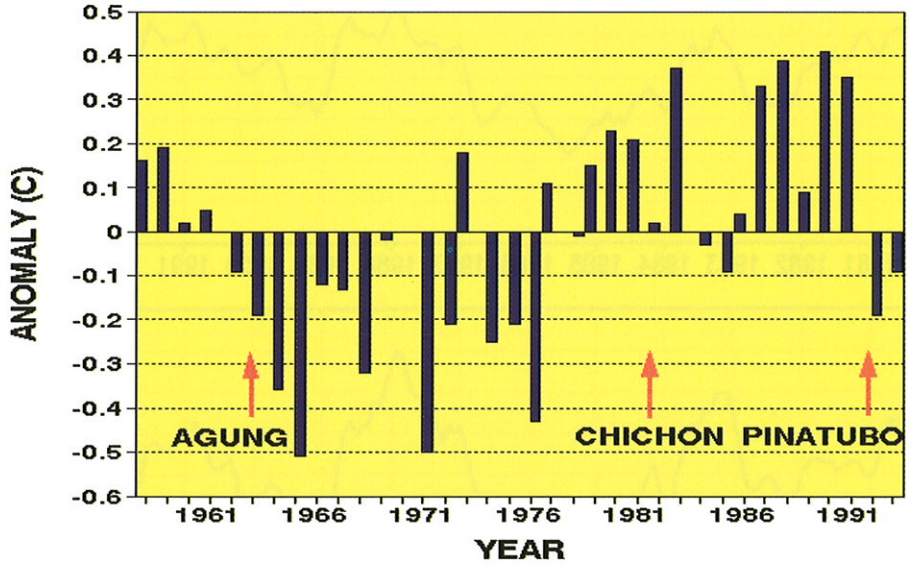

Figure 1.10 Annual global tropospheric (850-300 mb) temperature anomalies derived from radiosonde data. Annual values of global tropospheric temperature anomalies are based on a 63-station network and computed from the 1958-1991 base period. (Data provided by J. Angell.)

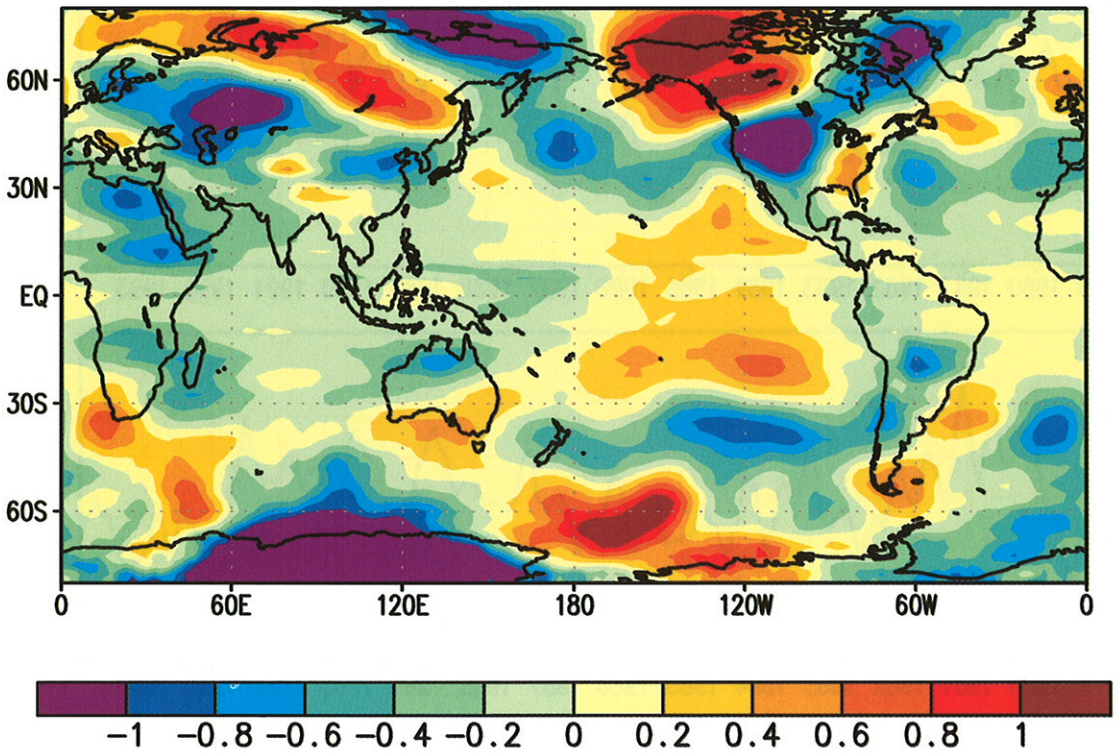

Figure 1.11. Mean annual tropospheric temperature anomalies for 1993 derived from the Microwave Sounding Unit (MSU) channel 2r. Anomalies are departures from the 1982-1991 base period. (Data provided by R. W. Spencer and J. R. Christy.)

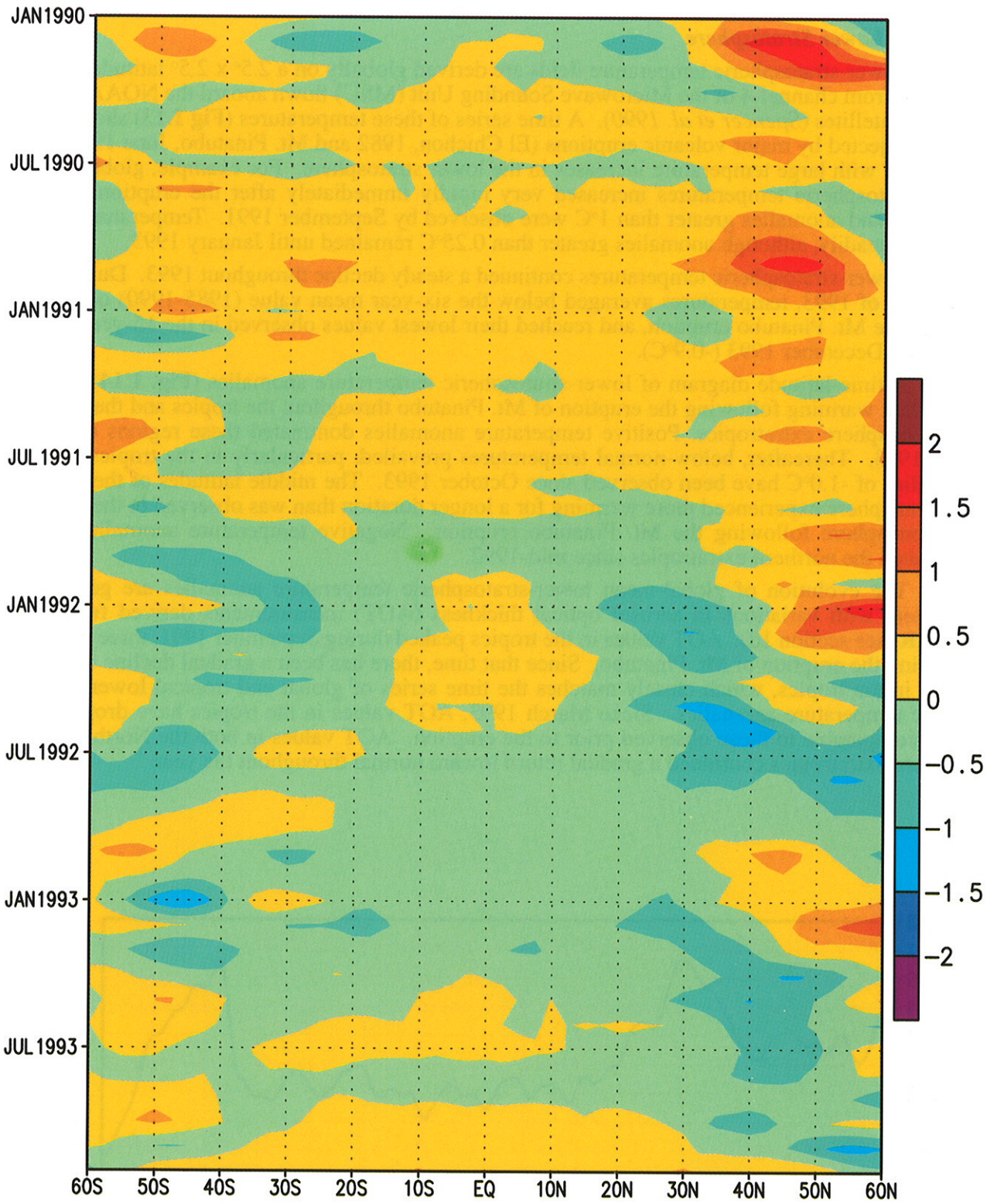

Figure 1.12 Time-latitude cross-section of zonally-averaged mean tropospheric temperature anomalies (°C) from the Microwave Sounding Unit (MSU) channel 2r. Anomalies are computed from the 1982-1991 base period. (Data provided by R. W. Spencer and J. R. Christy.)

2) Lower Stratosphere

Lower-stratospheric temperature fields are derived globally on a 2.5° x 2.5° latitude-longitude grid from channel-4 of the Microwave Sounding Unit (MSU) flown aboard the NOAA polar-orbiting satellites (*Spencer et al. 1990*). A time series of these temperatures (**Fig 1.13**) shows that aerosols ejected by major volcanic eruptions (El Chichon, 1982 and Mt. Pinatubo, June 1991) are associated with large temperature increases in the lower stratosphere. For example, global mean lower-stratospheric temperatures increased very rapidly immediately after the eruption of Mt. Pinatubo, and anomalies greater than 1°C were observed by September 1991. Temperatures then declined steadily, although anomalies greater than 0.25°C remained until January 1993.

Lower-stratospheric temperatures continued a steady decline throughout 1993. During the latter half of 1993, temperatures averaged below the six-year mean value (1985-1990) observed prior to the Mt. Pinatubo eruption, and reached their lowest values observed in the 15-year MSU record by December 1993 (-0.9°C).

A time-latitude diagram of lower-stratospheric temperature anomalies (**Fig. 1.14**) shows significant warming following the eruption of Mt. Pinatubo throughout the tropics and the Southern Hemisphere extratropics. Positive temperature anomalies dominated these regions through April 1993. Thereafter, below-normal temperatures prevailed, particularly in the tropics where anomalies of -1.0°C have been observed since October 1993. The middle latitudes of the Southern Hemisphere experienced more warming for a longer duration than was observed in the Northern Hemisphere following the Mt. Pinatubo eruption. Negative temperature anomalies have dominated the northern extratropics since mid-1992.

The evolution of global-mean lower-stratospheric temperature anomalies are generally consistent with variations in aerosol optical thickness (AOT) measurements derived from the AVHRR (see section 1d). AOT values in the tropics peaked during September 1991, three months following the eruption of Mt. Pinatubo. Since that time, there has been a gradual decline of AOT values in the tropics, which closely matches the time series of global and tropical lower-stratospheric temperature anomalies. Since March 1993, AOT values in the tropics have dropped to levels comparable to those observed prior to the eruption. AOT values in both the Northern and Southern extratropics continued a gradual return toward normal throughout the year.

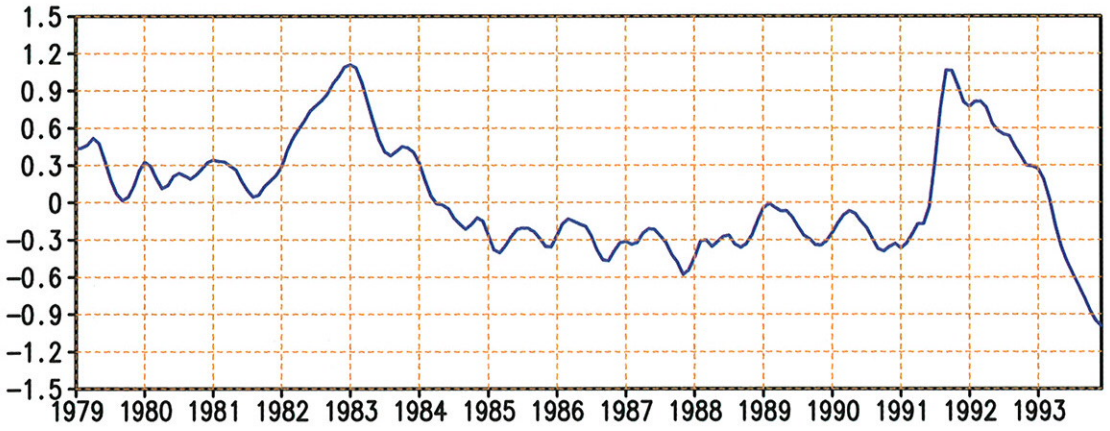

Figure 1.13 Lower-stratospheric temperature anomalies from the Microwave Sounding Unit (MSU) channel 4 for the globe (85°S-85°N). Anomalies are computed from the 1982-1991 base period. (Data provided by R. W. Spencer and J. R. Christy.)

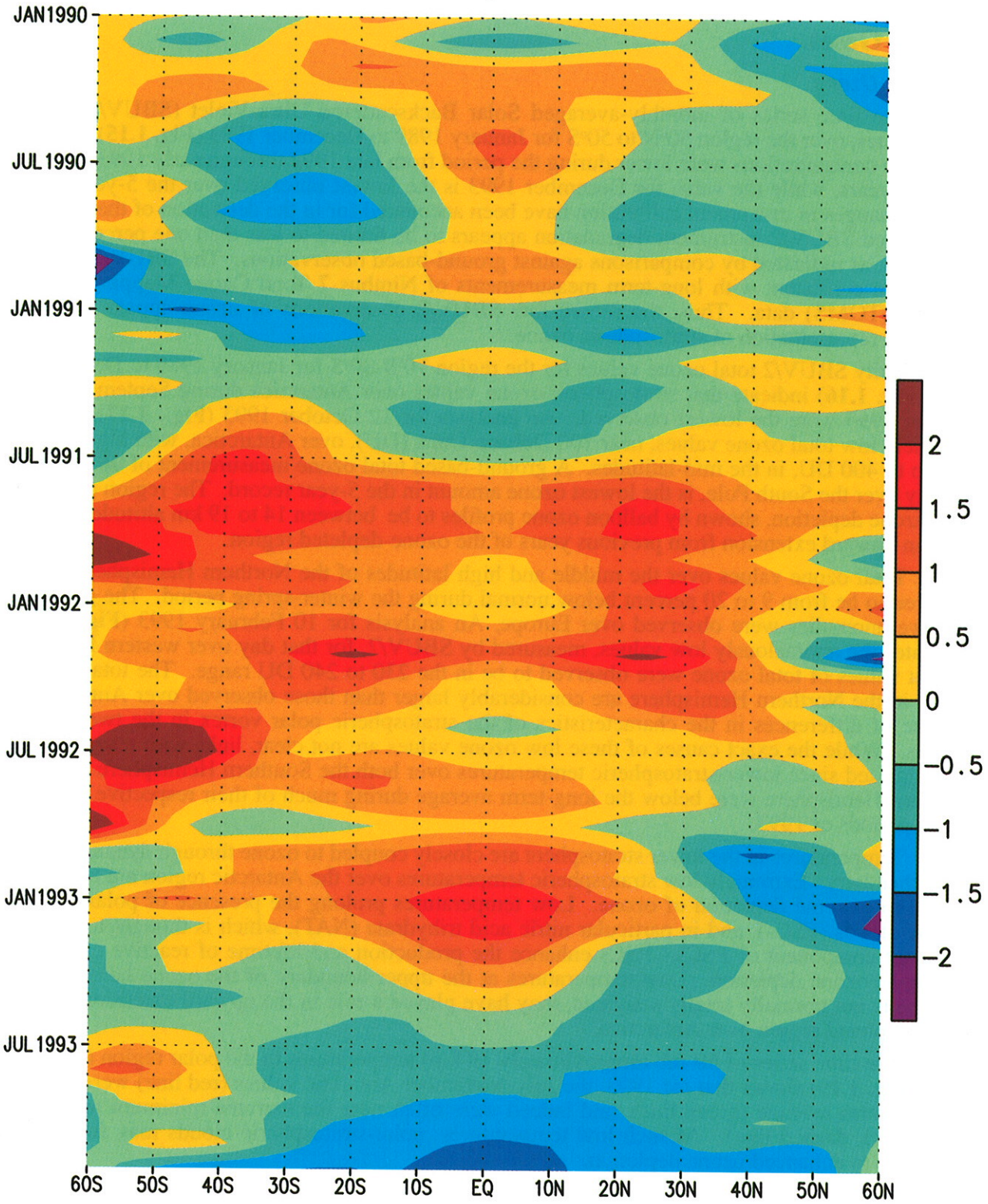

Figure 1.14 Time-latitude section of zonally-averaged lower-stratospheric temperature anomalies (°C) from the Microwave Sounding Unit (MSU) channel 4. Anomalies are computed from the 1982-1991 base period. (Data provided by R. W. Spencer and J. R. Christy.)

c. Trace Gases

1) Ozone

The time series of monthly-averaged Solar Backscattered Ultra-Violet (SBUV/2) total ozone values, over the region 50°N to 50°S for January 1989 to December 1993 (**Fig. 1.15**), shows that ozone concentrations were lower during the period from late 1992 through early 1993 than in previous years, while the value for December 1993 is the lowest observed over the 5-year time series. Changes in instrument calibration have been accounted for in the derivation of these data. Uncorrected SBUV/2 instrument degradation appears to be limited to less than one percent over the period, as indicated by comparisons against ground-based observations. The SBUV/2 observations are consistent with long-term measurements of Nimbus 7 Total Ozone Mapping Spectrometer (TOMS) data. Thus, the record low SBUV/2 observations of ozone appear to be a consistent representation of stratospheric ozone.

Daily SBUV/2 total ozone values for the region 70°S-80°S for January 1989 to December 1993 (**Fig. 1.16**) indicate that stratospheric ozone values over Antarctica during September and October 1993 were the lowest observed. An analysis for 12 October 1993 (**Fig. 1.17**), shows extremely low total ozone values, near 100 Dobson Units (DU), over Antarctica, with higher values, up to 400 DU, in the mid-latitudes. A ground-based total ozone measurement of 96 DU for this day over the South Pole, is the lowest ozone amount in the 5-year record. The region of complete ozone depletion, shown by balloon ozone profiles to be between 14 to 19 km altitude, represents an upward extension from previous years of the ozone-depleted region.

Total ozone values over the middle and high latitudes of the Northern Hemisphere were observed to be from 9 to 20 percent below normal during the winter-spring period. The greatest negative anomalies were observed over Europe. An analysis for 10 February 1993 (**Fig. 1.18**) illustrates the anomalously low values, measured by SBUV/2, for that day over western Europe. Lowest values of total ozone were observed to be in the 230 to 240 DU range. The total ozone values in the Northern Hemisphere are considerably larger than those observed over Antarctica, because of differences in the characteristics of the stratospheric polar vortex in the two hemispheres. While the exact causes of these low ozone values are not clear, links with temperature are suggested since lower-stratospheric temperatures over both the Southern Hemisphere and the Northern Hemisphere were below the long-term average during much of their respective winter-spring periods of 1993.

Temperatures in the lower stratosphere are closely coupled to ozone through dynamics and photochemistry. Extremely low stratospheric temperatures over the Antarctic region are believed to lead to extreme depletion of ozone. Low temperatures prolong the presence of polar-stratospheric clouds (PSCs), and in particular nitric acid trihydrate (NAT), which is thought to be the dominant component of PSCs. PSCs enhance the production and lifetime of reactive chlorine, leading to ozone depletion. Low temperatures at the upper boundary of the ozone hole, where chlorine is not normally totally activated, may have played a role in the upward extension of the ozone-depleted region over Antarctica.

The time series of 50-mb (approximately 19 km) temperatures in the polar region (65°S to 90°S) (**Fig. 1.19**) shows that for 1993, the July-November Antarctic values (red line) were below the long-term average (green line), and indeed were often near the extreme minimum temperatures (black dashed line). At such low temperatures, polar-stratospheric clouds may form and contribute to enhanced ozone depletion.

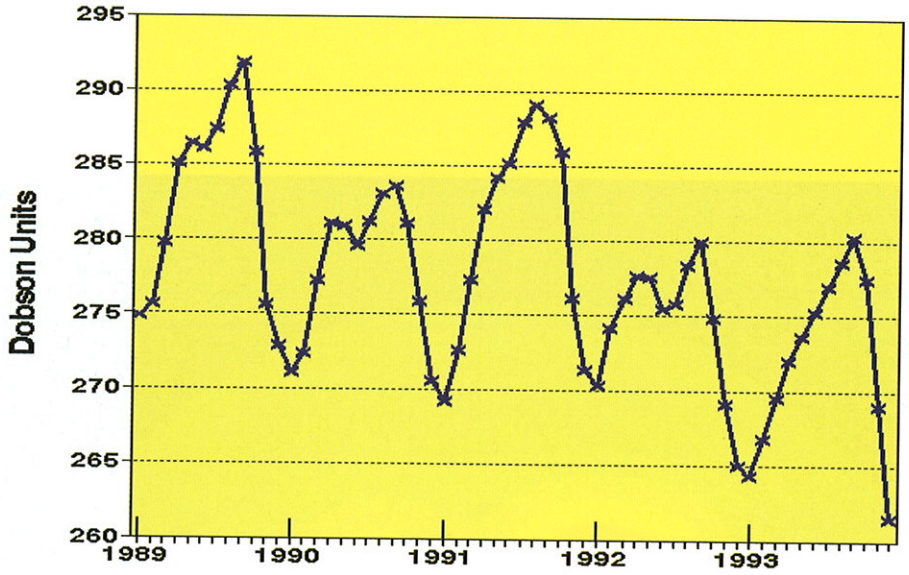

Figure 1.15 Time series of monthly NOAA-11 SBUV/2 total ozone (January 1989 to December 1993) for the region 50°N-50°S. (Source: CAC)

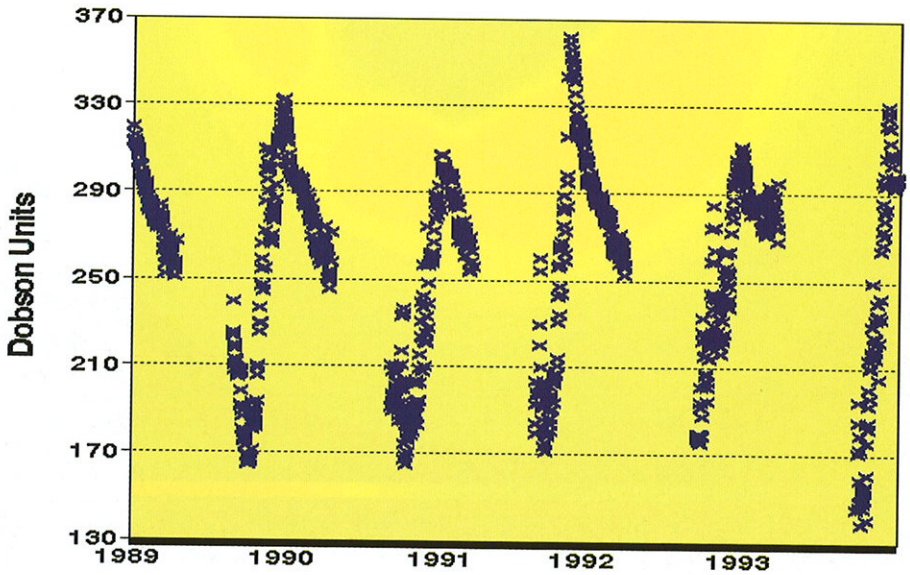

Figure 1.16 Time series of daily SBUV/2 total ozone (January 1989 to December 1993) for the 70°S-80°S region. Missing data occur each winter due to a lack of sunlight when SBUV/2 views the polar region. (Source: CAC)

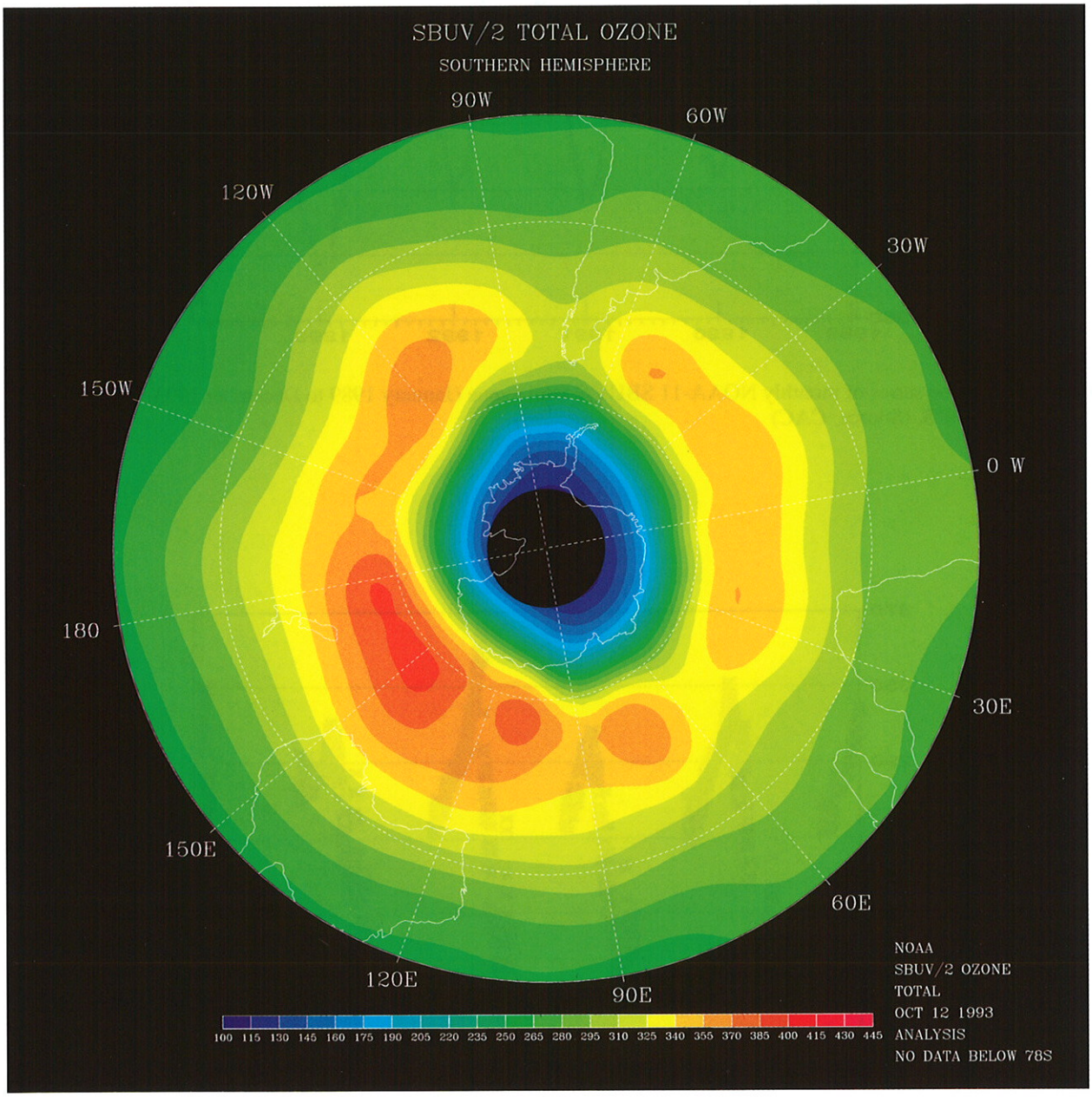

Figure 1.17 Southern Hemisphere NOAA-11 SBUV/2 total ozone (DU) for 12 October 1993. Areas of lowest ozone are shown in blue and purple, with highest values in yellow and red. Regions of no data are shown in black. (Source: CAC)

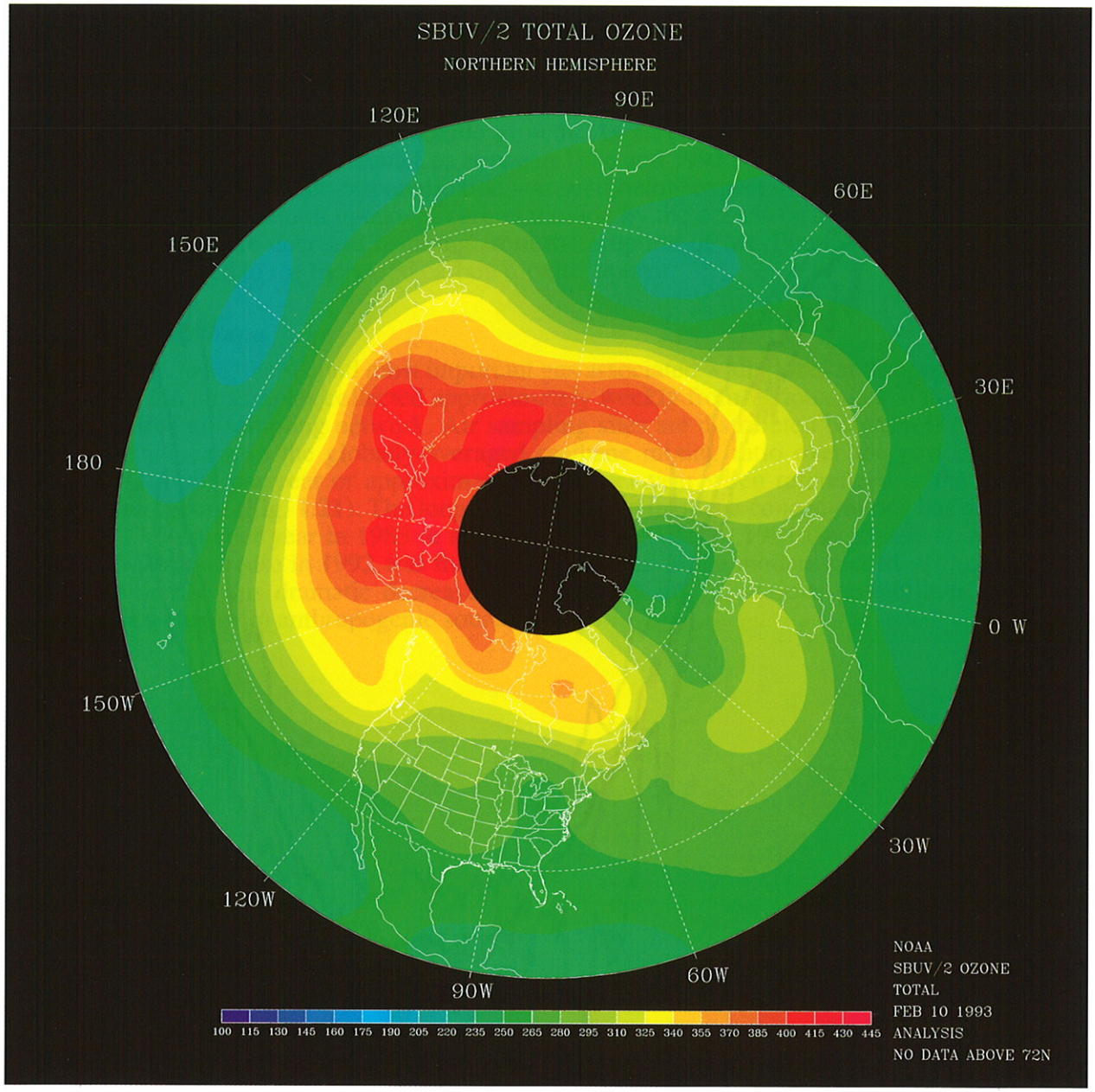

Figure 1.18 Northern Hemisphere NOAA-11 SBUV/2 total ozone (DU) for 10 February 1993. Areas of lowest ozone are shown in blue and purple, with highest values in yellow and red. Regions of no data are shown in black. (Source: CAC)

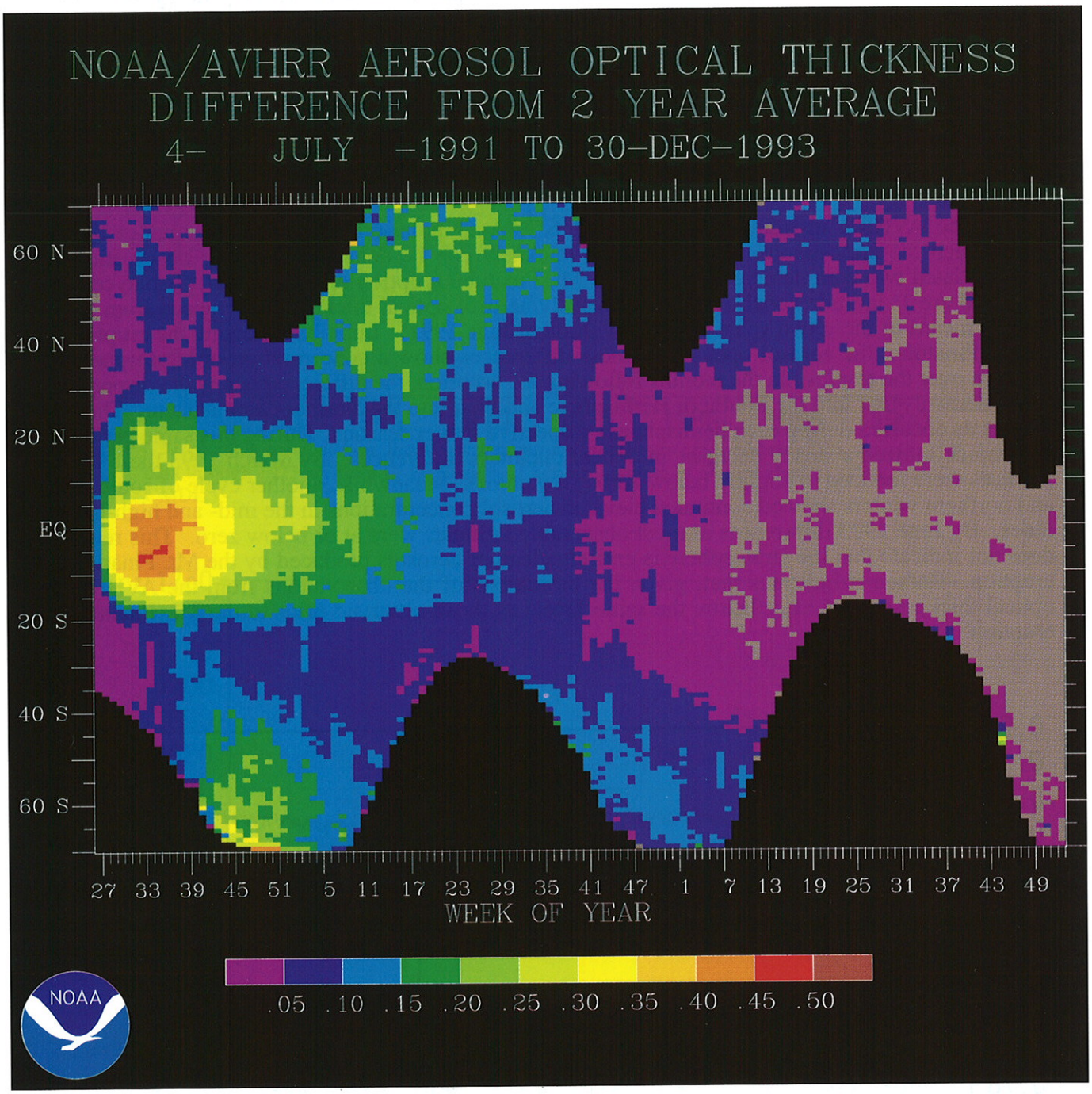

Figure 1.23 Weekly zonal averages of the aerosol optical thickness (AOT) differences from 70°S to 70°N for the period 4 July 1991 through 30 December 1993. Differences are from the July 1989 - June 1991 base period. (Data provided by L. Stowe.)

e. Cryosphere

1) Snow Cover

Large-scale variations in seasonal snow cover and sea-ice extent are important for the earth's radiation balance, through the albedo, and also for the global hydrologic cycle, through water storage. Indices of snow cover and sea ice may also reflect important interactions with other components of the climate system such as the global surface temperature.

During December 1992 through February 1993, the Northern Hemisphere experienced its largest extent of snow cover since 1986 (**Fig. 1.24**). Snow cover was especially heavy and persistent over western North America, Asia Minor, and western Siberia (**Fig. 1.25**). In contrast, less-than-normal snow cover was experienced in the eastern United States, northern Europe and Scandinavia, and the southern flanks of the Great Siberian Plain. The snow cover anomaly pattern seems to mirror the surface temperature anomaly patterns (see section 4).

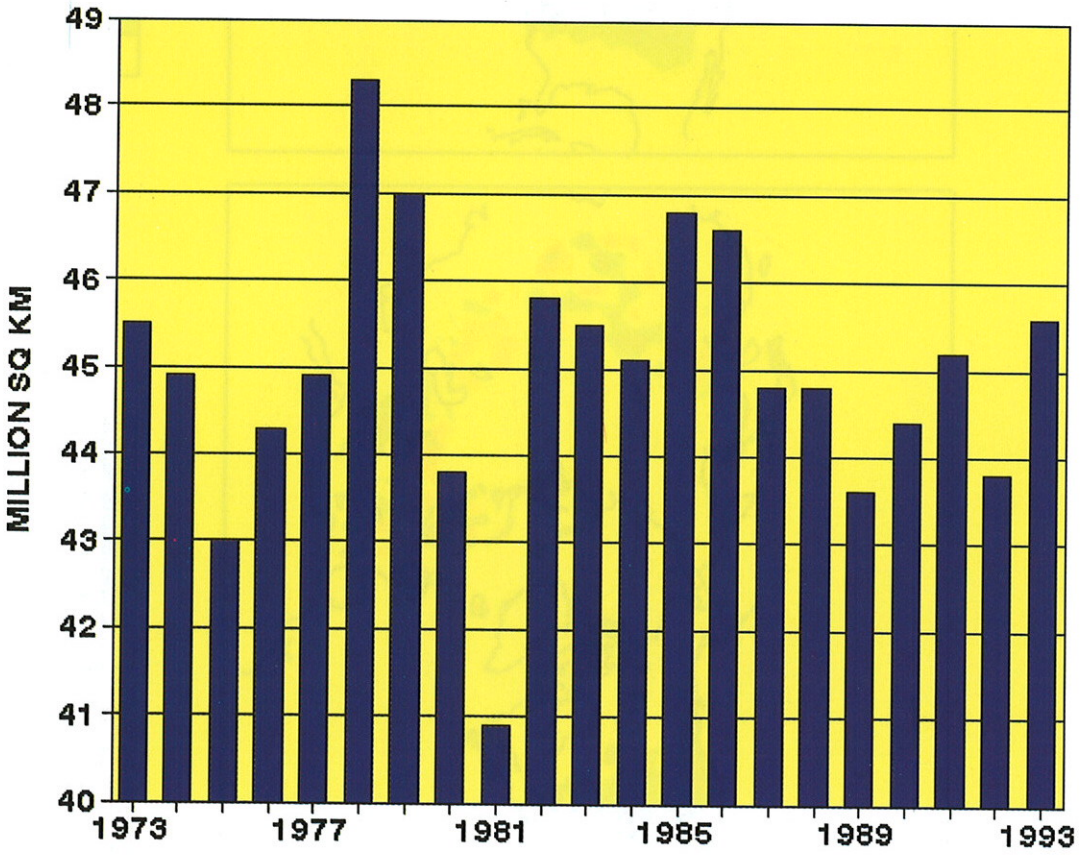

Figure 1.24 Time series of Northern Hemisphere snow-cover area (10^6 km^2) for winter (December through February), estimated from satellite imagery. (Data provided by NOAA/NESDIS and D. Robinson, Rutgers University.)

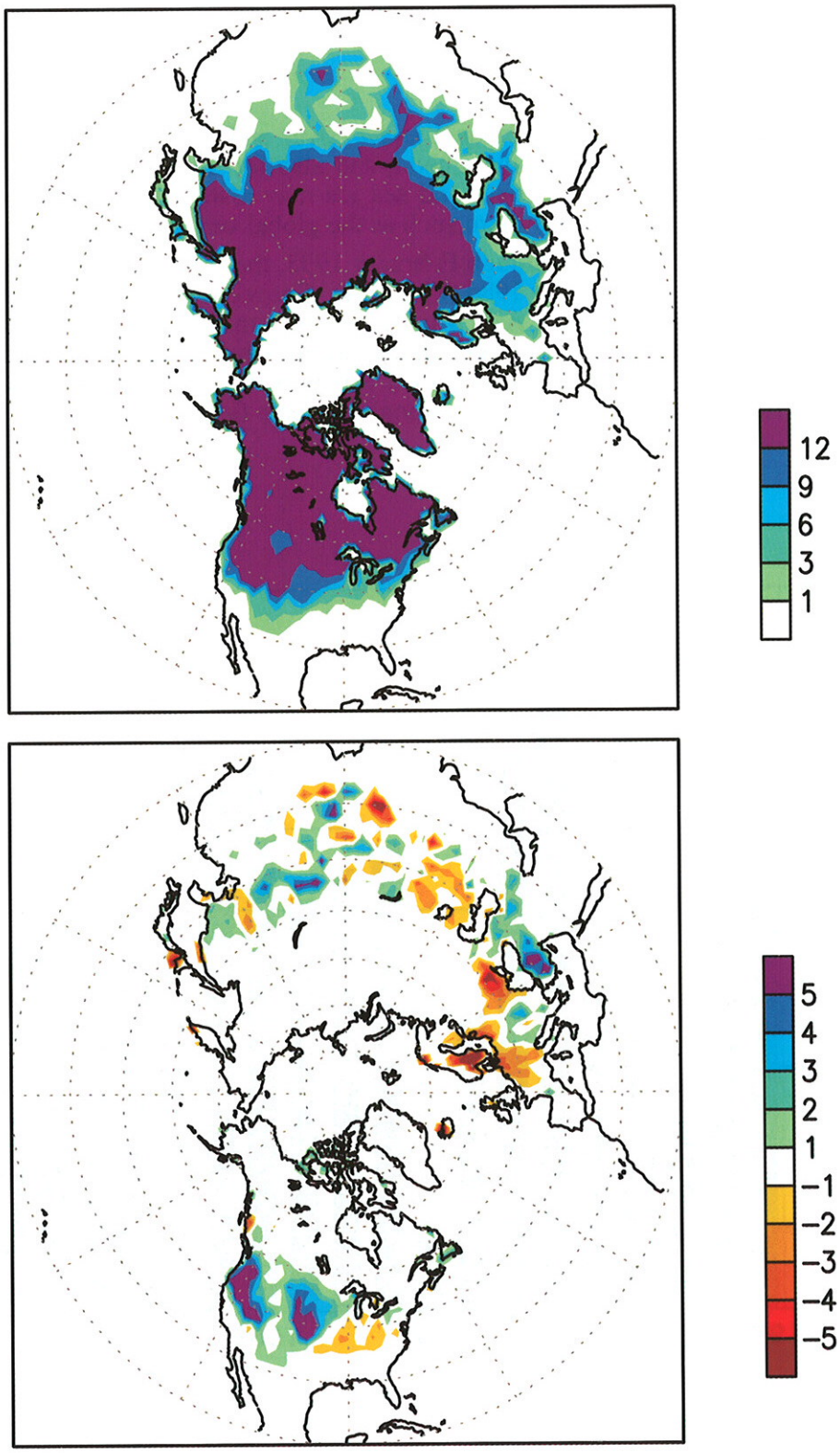

Figure 1.25 Winter snow-cover extent in weeks of snow cover (top) and anomaly (bottom), derived from subjective analysis of visual imagery by NOAA/NESDIS. Anomalies are departures from the 1973-1993 base period. (Source: CAC)

During March-May 1993, approximately 29×10^6 km^2 were covered by snow in the Northern Hemisphere (**Fig. 1.26**). This areal coverage is approximately 1.5×10^6 km^2 below-normal, thus continuing a trend of below-normal springtime snow cover that began in 1988. During this 6-year period, the lowest springtime snow cover was observed in 1990, which coincided with the warmest year on record for the hemisphere. During 1993, reduced snow cover was most evident over western Canada and portions of central Alaska, and also over eastern Siberia, northern China and Scandinavia (**Fig. 1.27**). These regions coincided with warmer-than-normal surface temperatures during the season (see section 4). Above-normal snow cover during the season was observed over portions of the northeastern and north-central United States, and over scattered regions of central Asia.

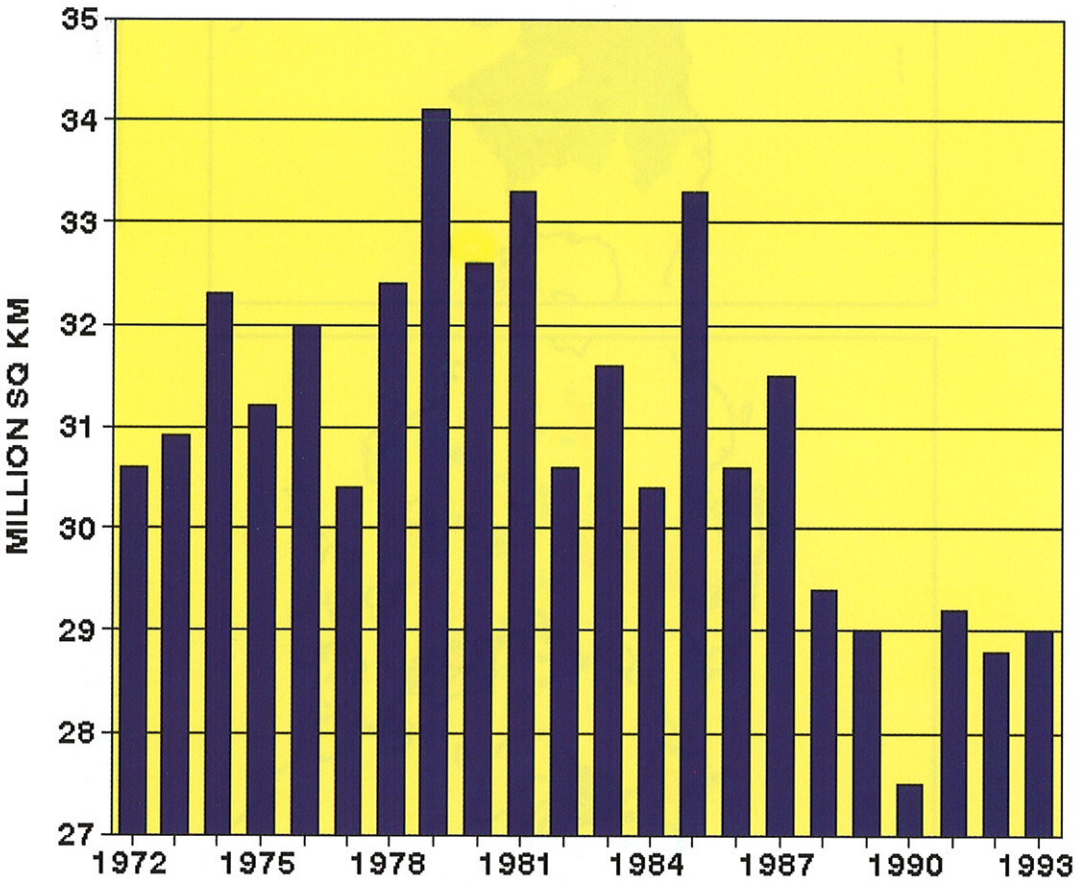

Figure 1.26 Time series of Northern Hemisphere snow-cover area (10^6 km^2) for spring (March through May), estimated from satellite imagery. (Data provided by NOAA/NESDIS and D. Robinson, Rutgers University.)

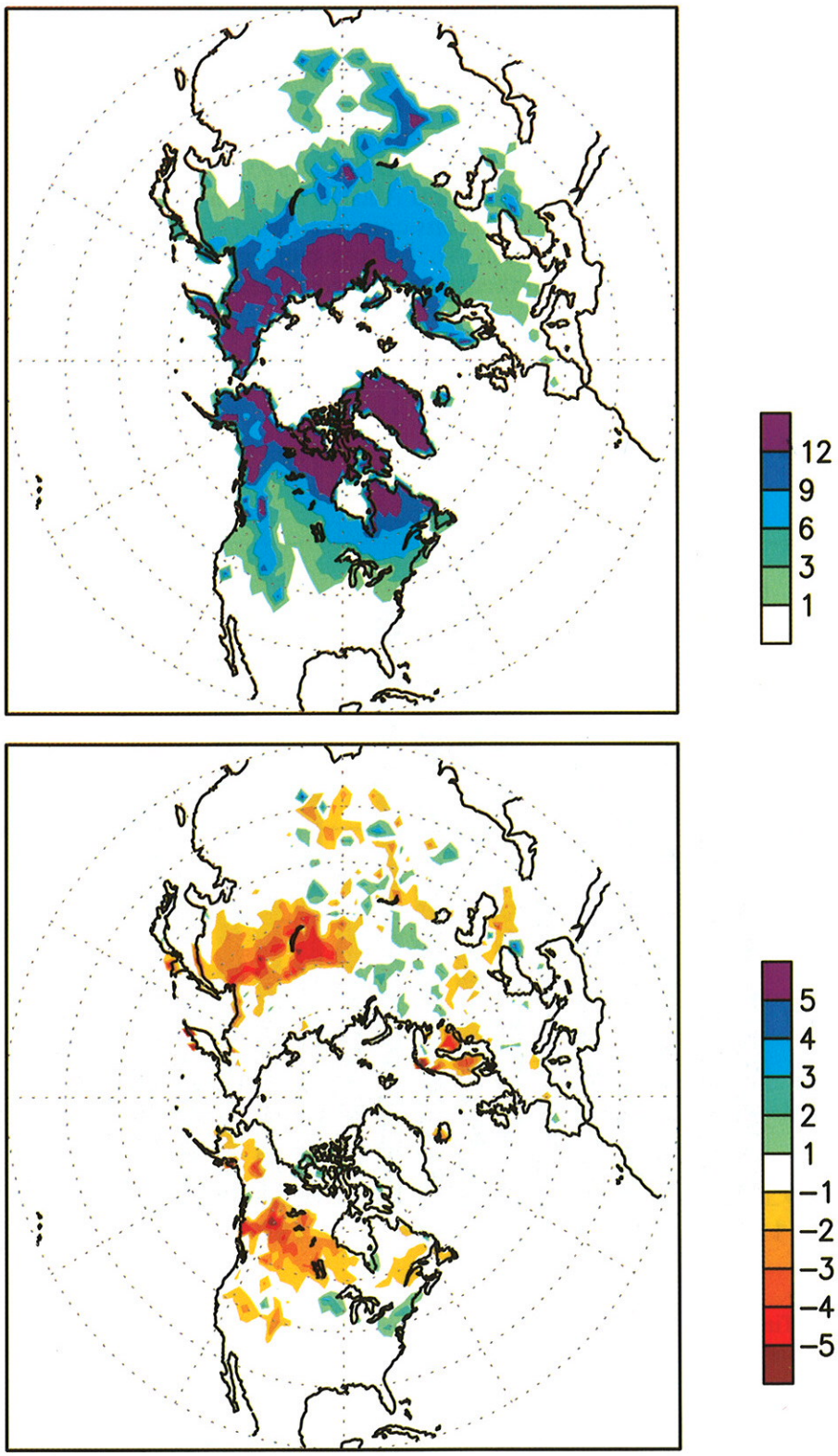

Figure 1.27 Spring snow-cover extent in weeks of snow cover (top) and anomaly (bottom), derived from subjective analysis of visual imagery by NOAA/NESDIS. Anomalies are departures from the 1973-1993 base period. (Source: CAC)

The areal extent of Northern Hemisphere fall season snow cover has shown steady increases since the fall of 1990 (**Fig. 1.28**). Snow-cover area during 1993 was the largest since 1976 and the third highest in the 22-year record. Colder conditions in western Russia and northern Europe during the fall of 1993 were reflected in large areas with increased duration of snow cover (**Fig. 1.29**). Snowfall was large enough over these regions to maintain an excess of snow cover even though overall precipitation was generally at or below normal. Canada was characterized by below-normal snow cover in the west and above-normal snow cover in the east during the season.

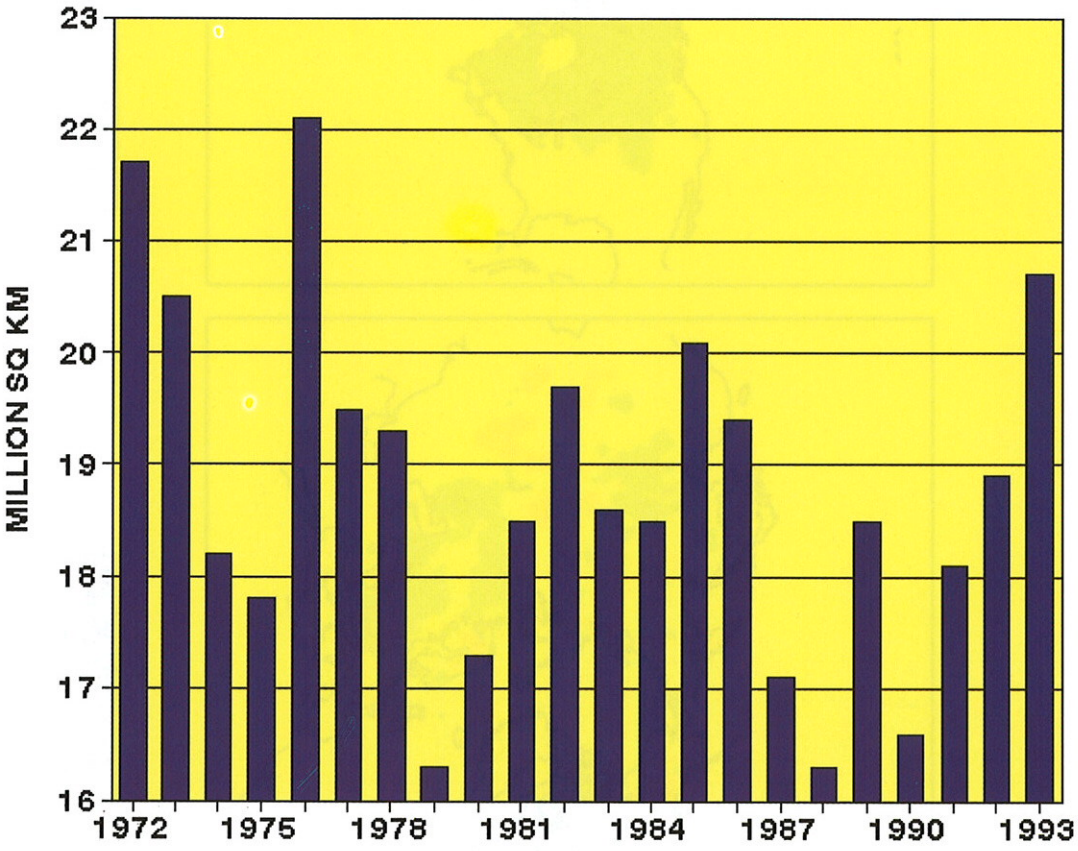

Figure 1.28 Time series of Northern Hemisphere snow-cover area (10^6 km^2) for fall (September through November), estimated from satellite imagery. (Data provided by NOAA/NESDIS and D. Robinson, Rutgers University.)

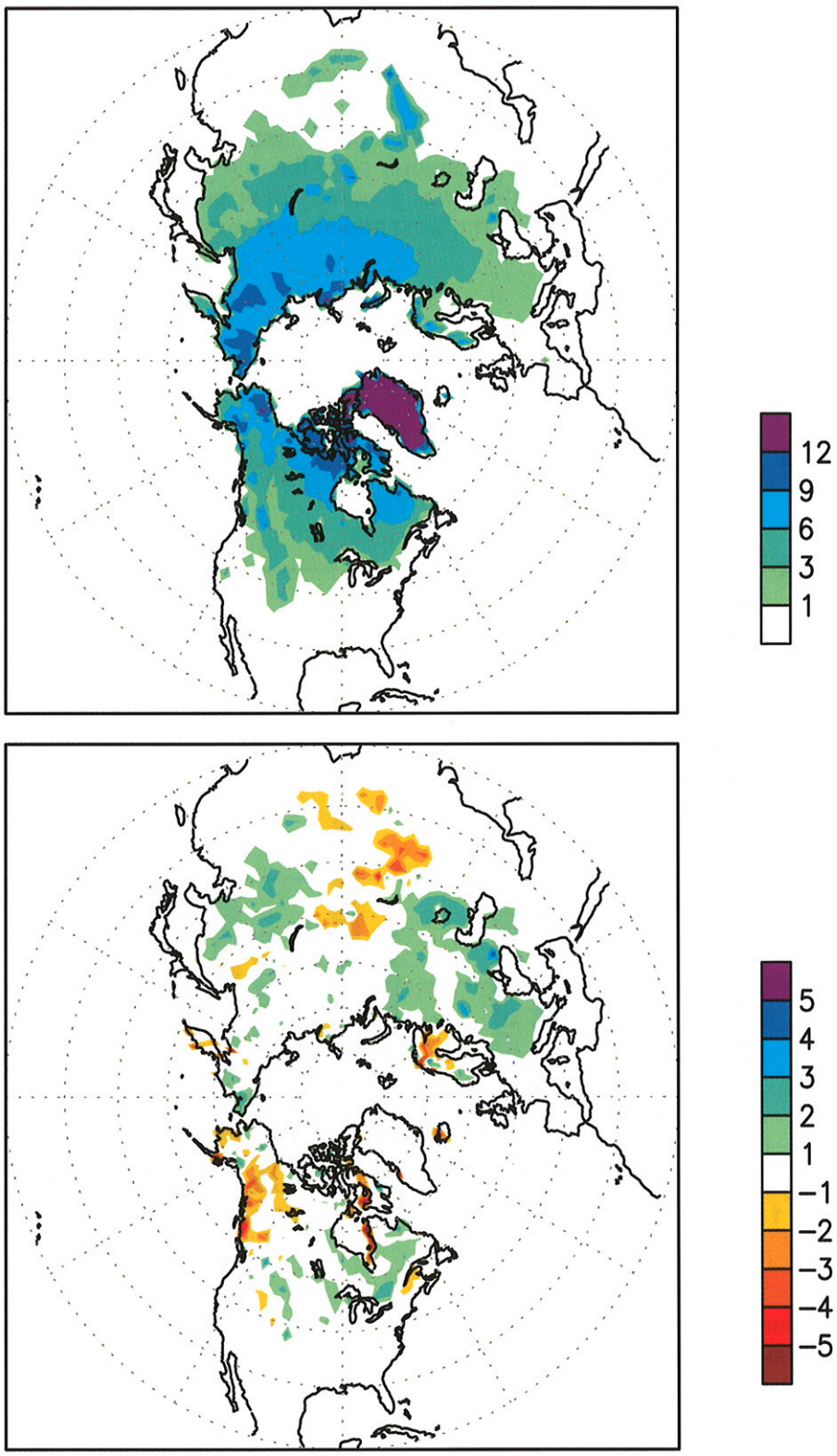

Figure 1.29 Fall 1993 snow-cover extent in weeks of snow cover (top) and anomaly (bottom), derived from subjective analysis of visual imagery by NOAA/NESDIS. Anomalies are departures from the 1973-1993 base period. (Source: CAC)

2) Sea ice

Arctic sea-ice extent is generally at a maximum in February and a minimum in August. Time series of sea-ice area for each of these months (**Figs. 1.30 and 1.31**) show increases since 1991. However, the August values have remained below the 21-year average since 1989. The February 1993 values were above average for the first time since 1988. Neither of these time series show evidence of systematic trends.

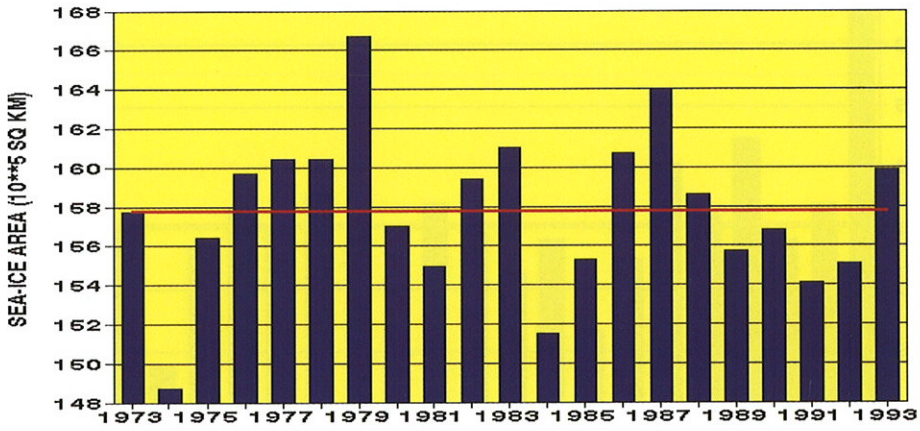

Figure 1.30 Time series of arctic sea ice (10^5 km^2) for February. Solid red line depicts the 1973-1993 mean. (Source: CAC)

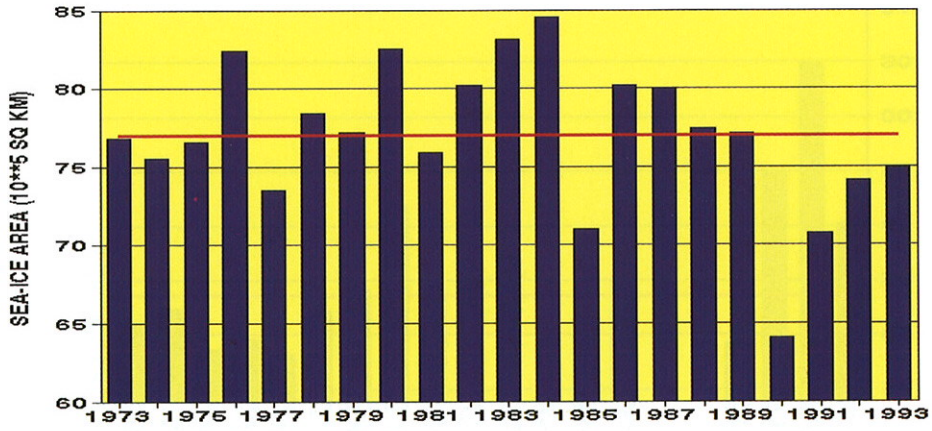

Figure 1.31 Time series of arctic sea ice (10^5 km^2) for August. Solid red line depicts the 1973-1993 mean. (Source: CAC)

Antarctic sea-ice extent was above the 21-year mean in both February 1993 (**Fig. 1.32**) and August 1993 (**Fig. 1.33**) the time of minimum and maximum areal coverage, respectively. The August 1993 antarctic sea-ice extent is the largest since 1985. There appears to be no relationship between sea-ice area and global trends in surface temperature over the limited period of satellite records.

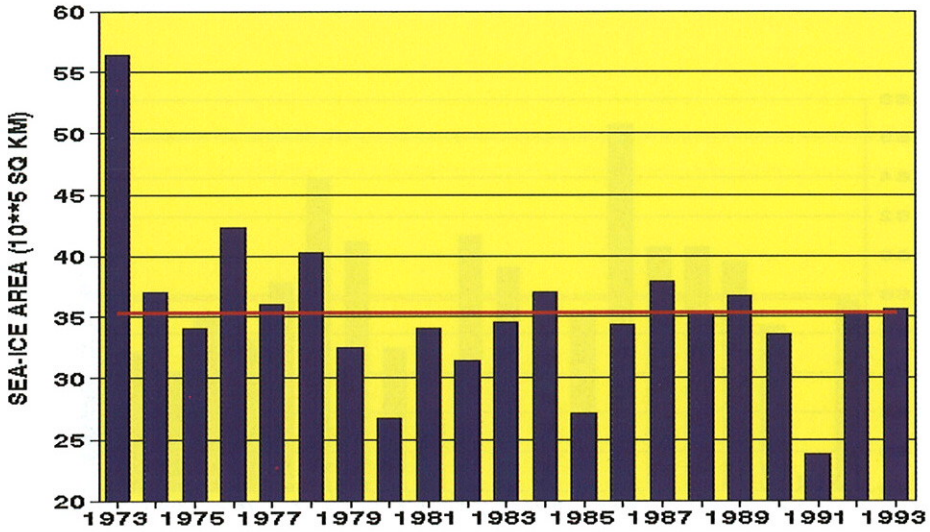

Figure 1.32 Time series of antarctic sea ice (10^5 km^2) for February. Solid red line depicts the 1973-1993 mean. (Source: CAC)

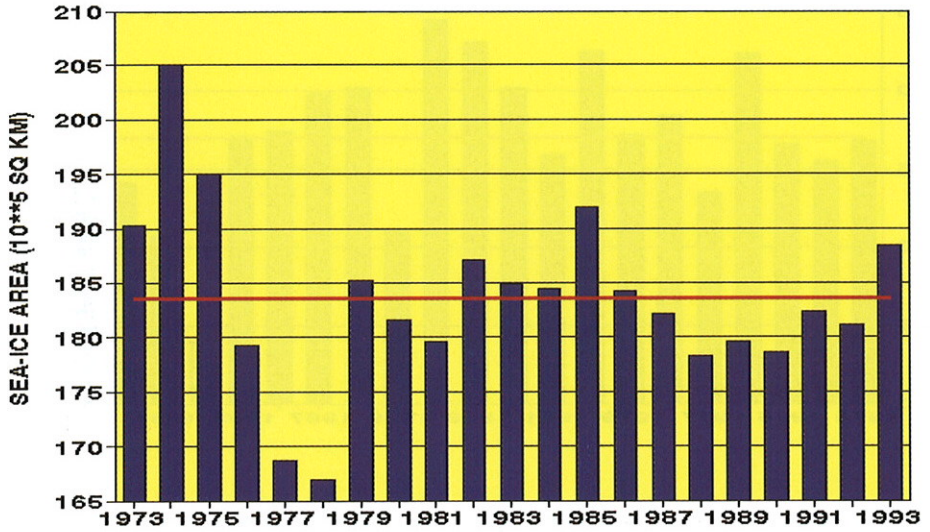

Figure 1.33 Time series of antarctic sea ice (10^5 km^2) for August. Solid red line depicts the 1973-1993 mean. (Source: CAC)

f. Cloud Cover

Cloud cover is derived from a subjective analysis of visual and infrared imagery originating on a number of different satellites and instruments in the "METEOR" series of weather satellites (*Matveev 1986; Mokhov and Schlesinger 1993*). Changes in global cloud cover are another indicator of feedback of the global climate system. However, it is difficult to measure accurately, and it is difficult to model because of microscale cloud properties.

The original METEOR imagery was analyzed onto a 5° latitude by 10° longitude global grid. Interannual variability in this data is a factor of 3 to 4 larger than observed in the International Satellite Cloud Climatology Project (ISCCP) analysis, (*Rossow et al. 1993*). Part of the differences in interannual variability in these data sets may have resulted from changes in the orbital characteristics of various satellites in the METEOR series. Despite these differences and uncertainties, the METEOR data provide a quick first look at global cloud cover.

The time series of anomalous global cloud cover based on the METEOR analysis (**Fig. 1.34 top**) indicates an increase in global cloudiness from 1966 to the mid-1980's and a decrease after 1986. These features are evident in the METEOR analysis in both the Northern and Southern Hemispheres (**Fig 1.34, middle and bottom**). The ISCCP analysis for 1984 to 1990 also suggests a decrease in global cloudiness from 1986 through 1990 but of much smaller magnitude.

According to the METEOR analysis, global cloud cover increased slightly during 1993 when compared to the 1992 values, with the most pronounced increases occurring in the second half of the year. Both the Northern and Southern Hemispheres showed this relative increase in cloud cover during 1993.

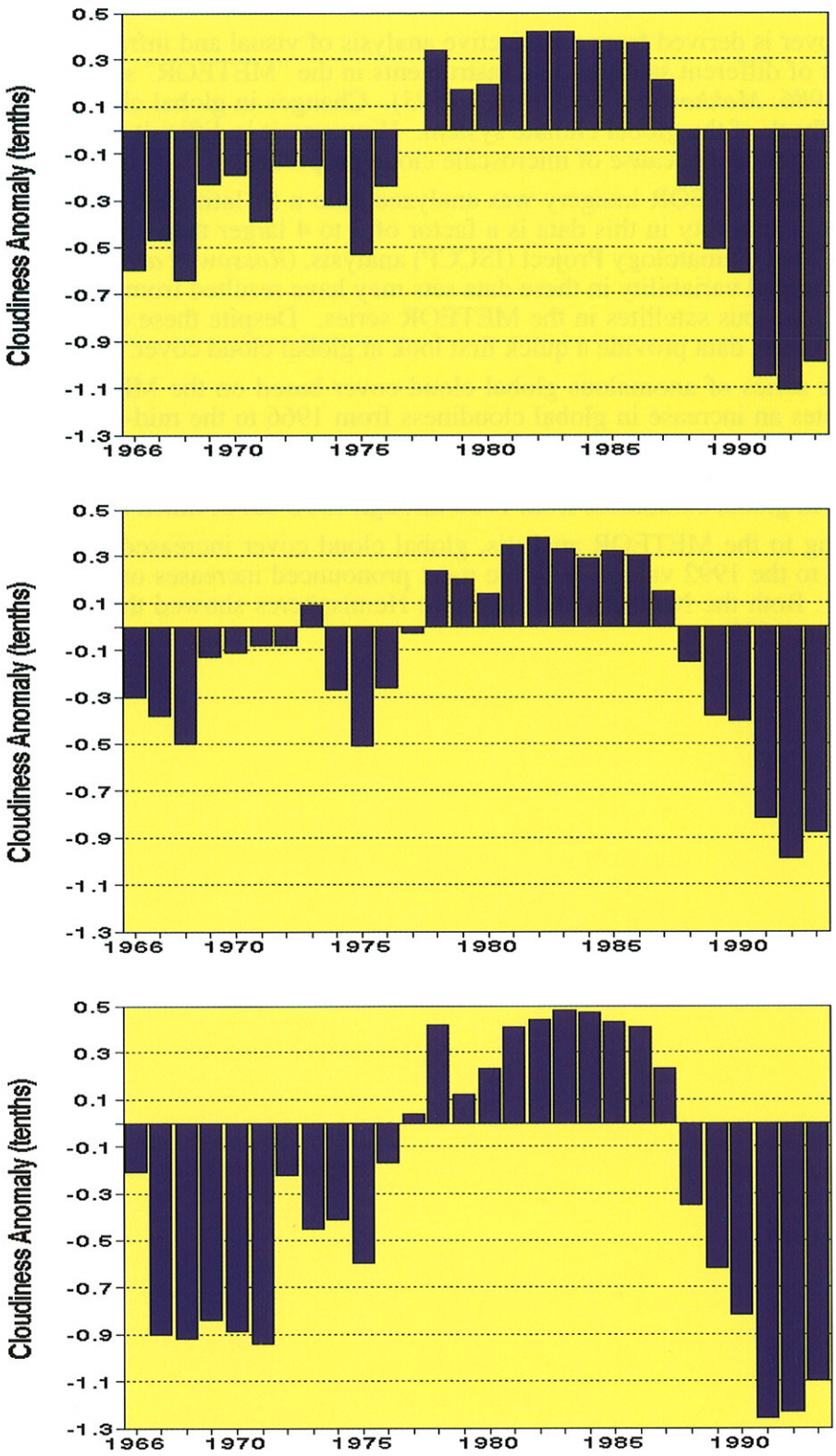

Figure 1.34. Regionally-averaged annual total cloud cover anomalies: global (top), Northern Hemisphere (middle), and Southern Hemisphere (bottom). Anomalies (expressed in tenths) are computed from the 1966-1985 base period. (Source: Institute for Global Climate and Ecology, Moscow)

2. EL NIÑO/SOUTHERN OSCILLATION (ENSO)

Since 1990, warm (ENSO) episode-like conditions have dominated the tropical Pacific. The current episode is the longest period of warm episode conditions in half a century, but it is not unprecedented. Extended warm episode-like conditions were also evident for the periods 1911-1913 and 1939-1942 (**Fig. 2.1**). For the present period, mature warm episode conditions first developed in late 1991. Positive sea surface temperature anomalies (**Fig. 2.2**) and enhanced convection [negative outgoing longwave radiation anomalies (**Fig. 2.3**)] dominated the central and eastern equatorial Pacific, accompanied by weaker-than-normal low-level easterlies throughout the equatorial Pacific (**Fig. 2.4**). During the period December 1991 through April 1992, precipitation anomalies in many regions of the tropics and subtropics were consistent with those generally observed during the mature phase of a warm episode (*Ropelewski and Halpert 1987*).

Mature warm episode conditions redeveloped in early 1993 and continued until mid-1993. Once again precipitation anomalies characteristic of warm episodes were observed in many areas. Estimated rainfall anomalies (1986-93 base period) are routinely produced by applying the GOES Precipitation Index (GPI) technique (*Arkin and Meisner, 1987*) to geostationary and polar orbiting IR data provided by the Global Precipitation Climatology Project (*Arkin and Xie, 1994*). The rainfall anomaly patterns for 1993 (**Fig. 2.5**) reflect the warm episode conditions that were observed in the tropical Pacific during the year. Along the equator near the date line, monthly rainfall was estimated to be in excess of 150 mm above normal during the period December 1992 through August 1993, while in the North Pacific ITCZ rainfall was heavier-than-normal during March-May 1993. In contrast, below-normal rainfall occurred over Indonesia throughout the nine-month period and over Northeast Brazil from March-August. Slightly weaker-than-normal monsoon rainfall was also estimated for the region of western India. These rainfall anomaly features are generally consistent with those observed during previous warm episodes (*Ropelewski and Halpert 1987*).

Excessive rainfall, observed during early 1993 over California and other parts of the southwestern United States (see section 3a for more details), appears to be related, in part, to the pattern of warmer-than-normal sea surface temperatures in the central equatorial Pacific and the anomalous pattern of tropical cloudiness and precipitation that accompanied the unusually warm water.

During March-May 1993, the oceanic thermocline (as indicated by the depth of the 20°C isotherm) was deeper than normal in the eastern equatorial Pacific and shallower than normal in the western equatorial Pacific (**Fig. 2.6**), indicating mature warm episode subsurface conditions. However, the depth anomalies along the equator were considerably weaker than at the same time in 1992 (**Fig. 2.7**).

As in 1992, positive sea surface temperature anomalies persisted in the central equatorial Pacific during most of 1993 (**Fig. 2.8**), accompanied by enhanced convection (**Fig. 2.9**). However, by the end of 1993, warm episode conditions were steadily weakening throughout the tropical Pacific as the low-level equatorial easterlies returned to near-normal intensity (**Fig. 2.4**), and the Southern Oscillation Index was near zero.

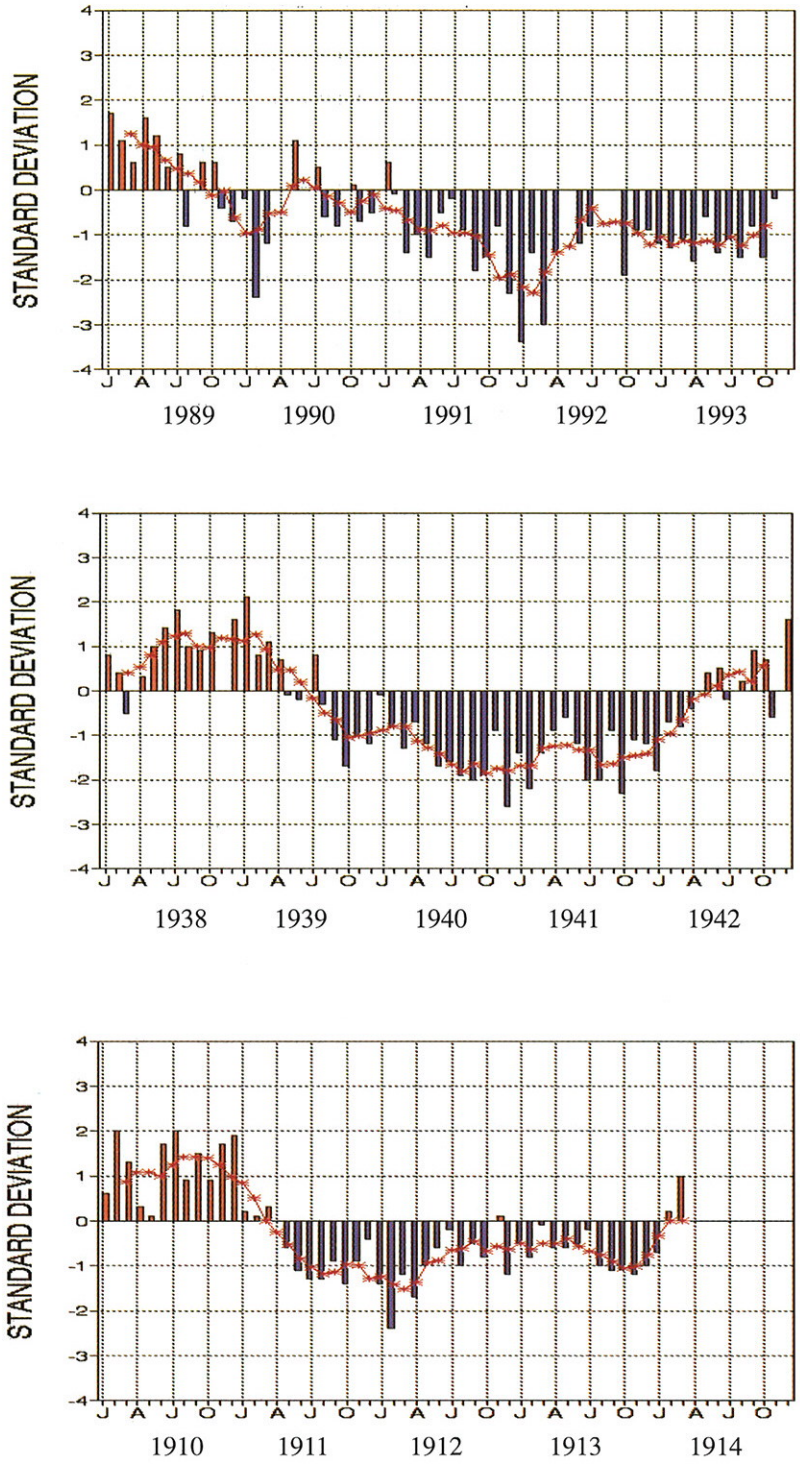

Figure 2.1 The Southern Oscillation Index (SOI) for the three longest warm episodes in the historical record. Monthly (five month running mean) values are indicated by the bar (red line) graph. (Source: CAC)

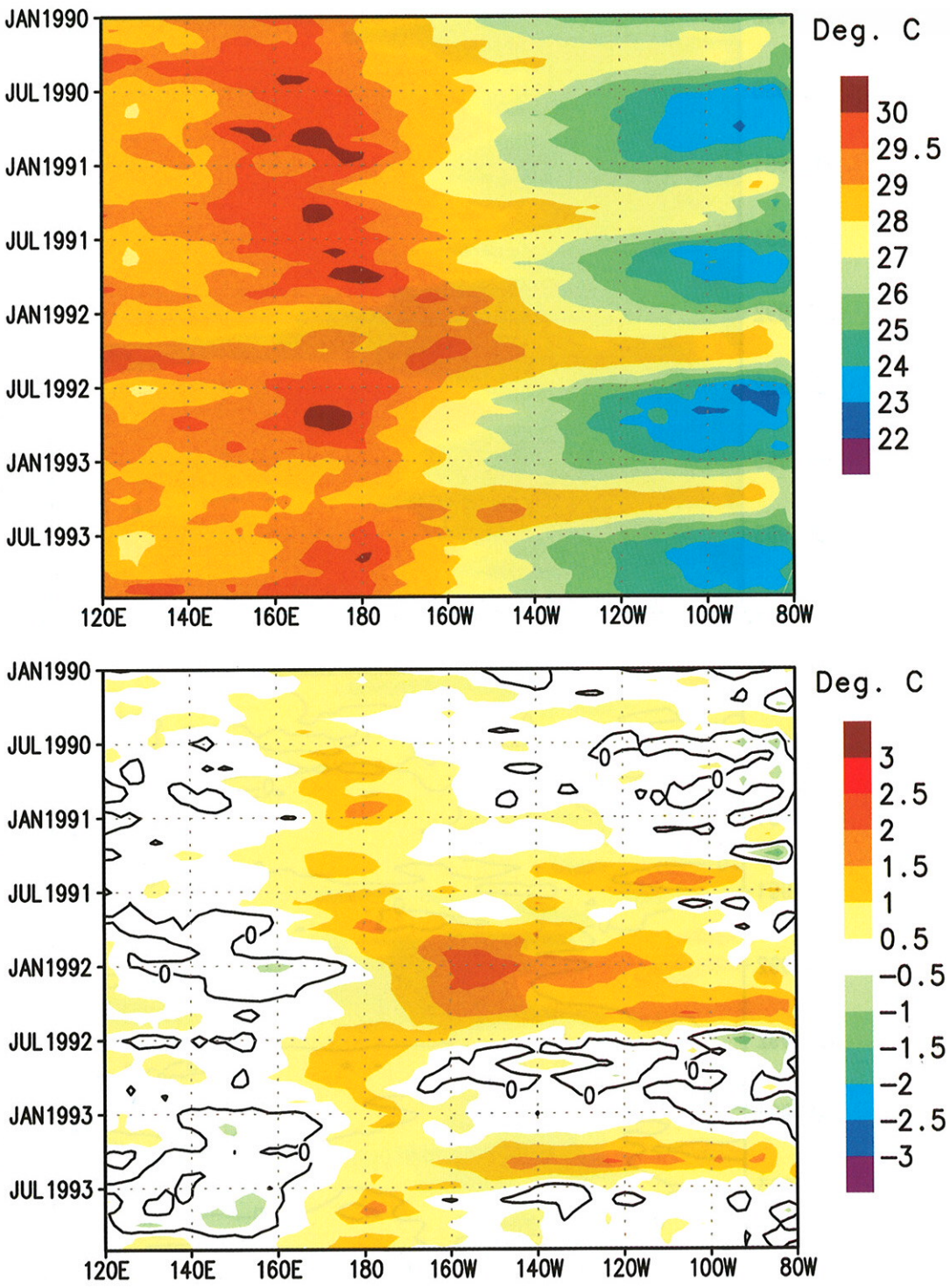

Figure 2.2 Time-longitude section of mean (top) and anomalous (bottom) sea surface temperature (SST) averaged from 5°N-5°S. Anomalies are departures from the COADS/ICE climatology (*Reynolds 1988*). (Data provided by the NMC Coupled Model Project.)

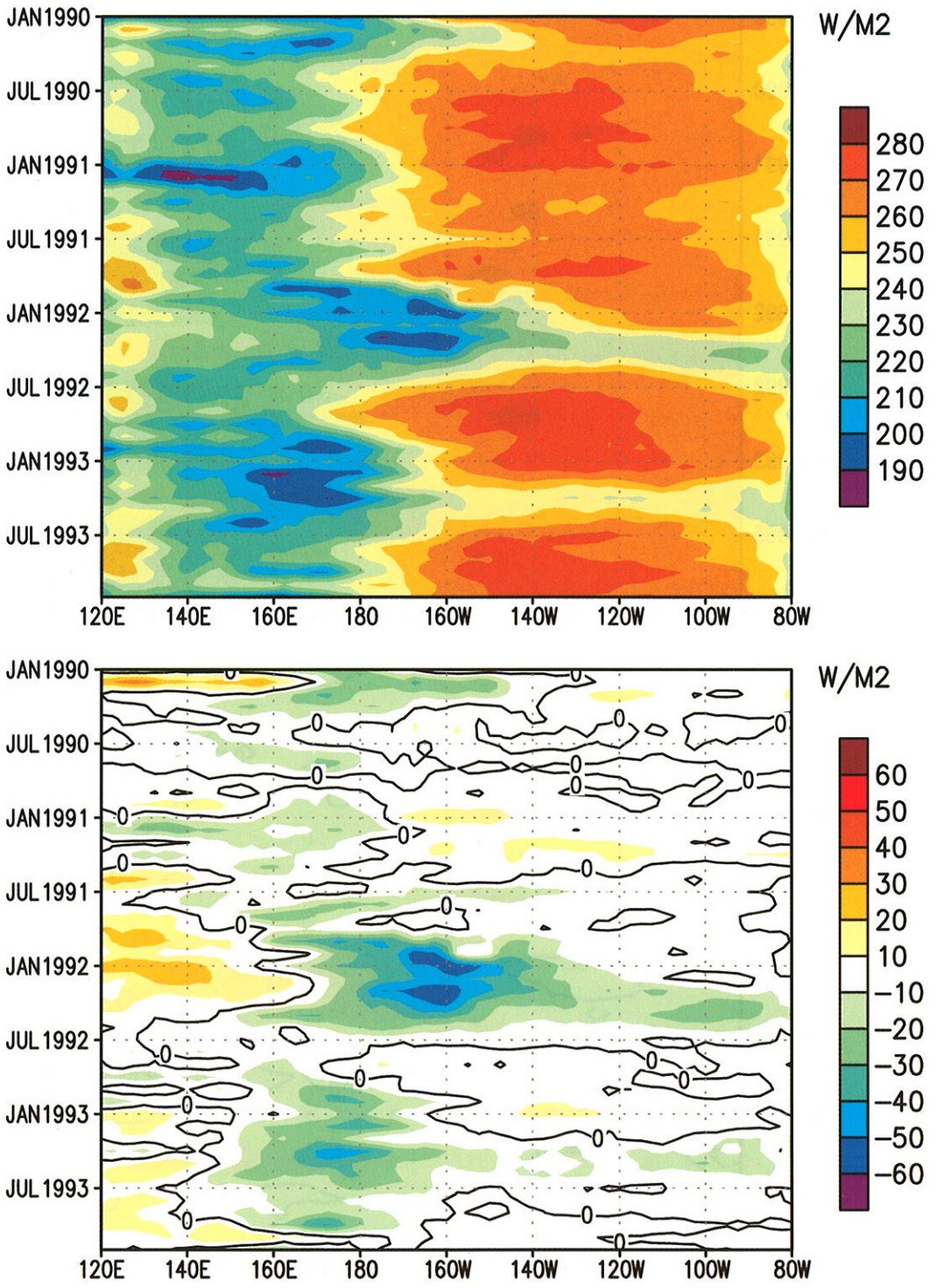

Figure 2.3 Time-longitude section of mean (top) and anomalous (bottom) outgoing longwave radiation averaged from 5°N-5°S. Anomalies are departures from the 1979-1988 base period. (Source: CAC)

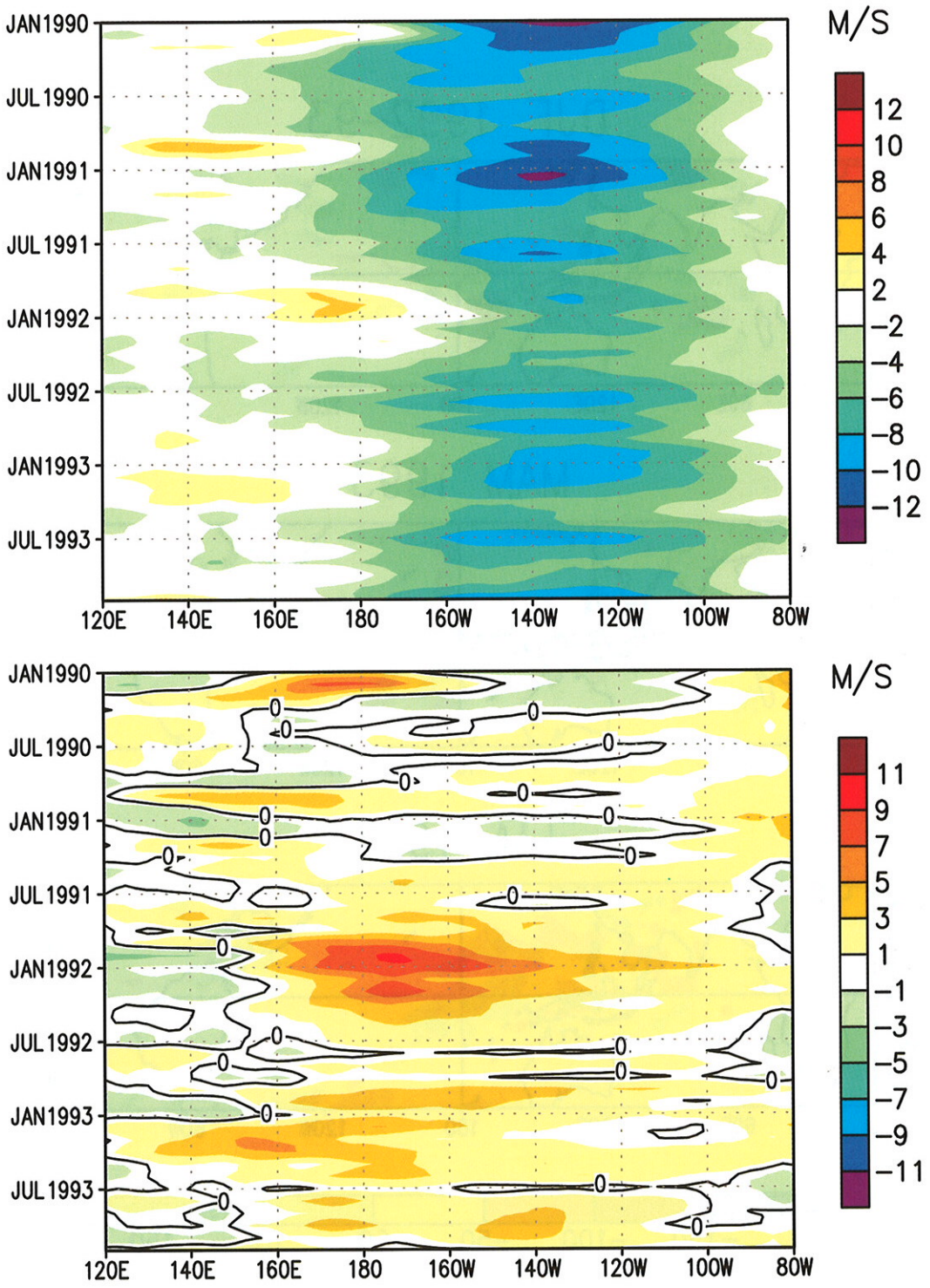

Figure 2.4 Time-longitude section of mean (top) and anomalous (bottom) 850-mb zonal wind averaged from 5°N-5°S. Anomalies are departures from the 1979-1988 base period. (Source: CAC)

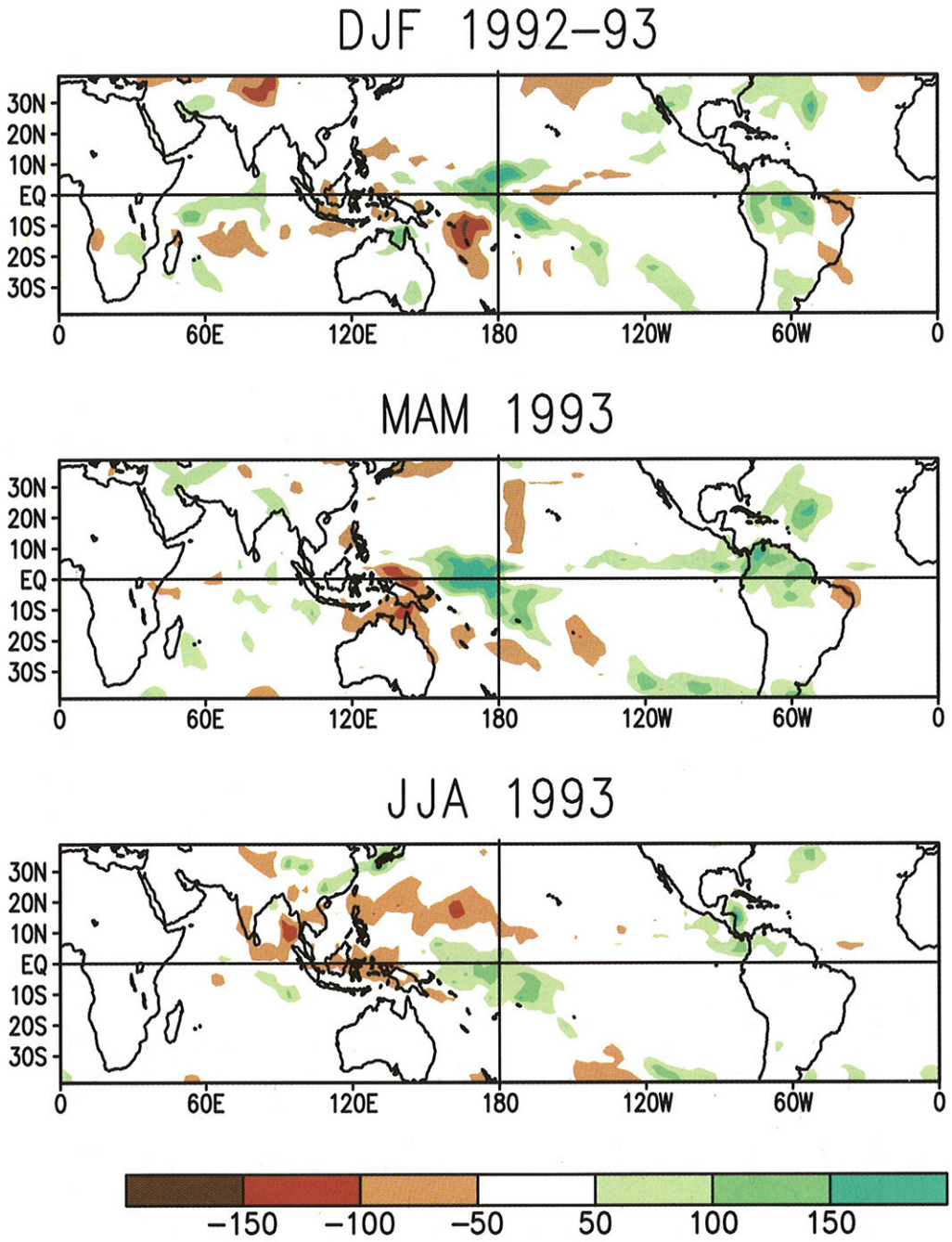

Figure 2.5 Satellite-derived rainfall anomaly estimates in mm per month. Anomalies are computed from the 1986-1993 base period. (Source: CAC)

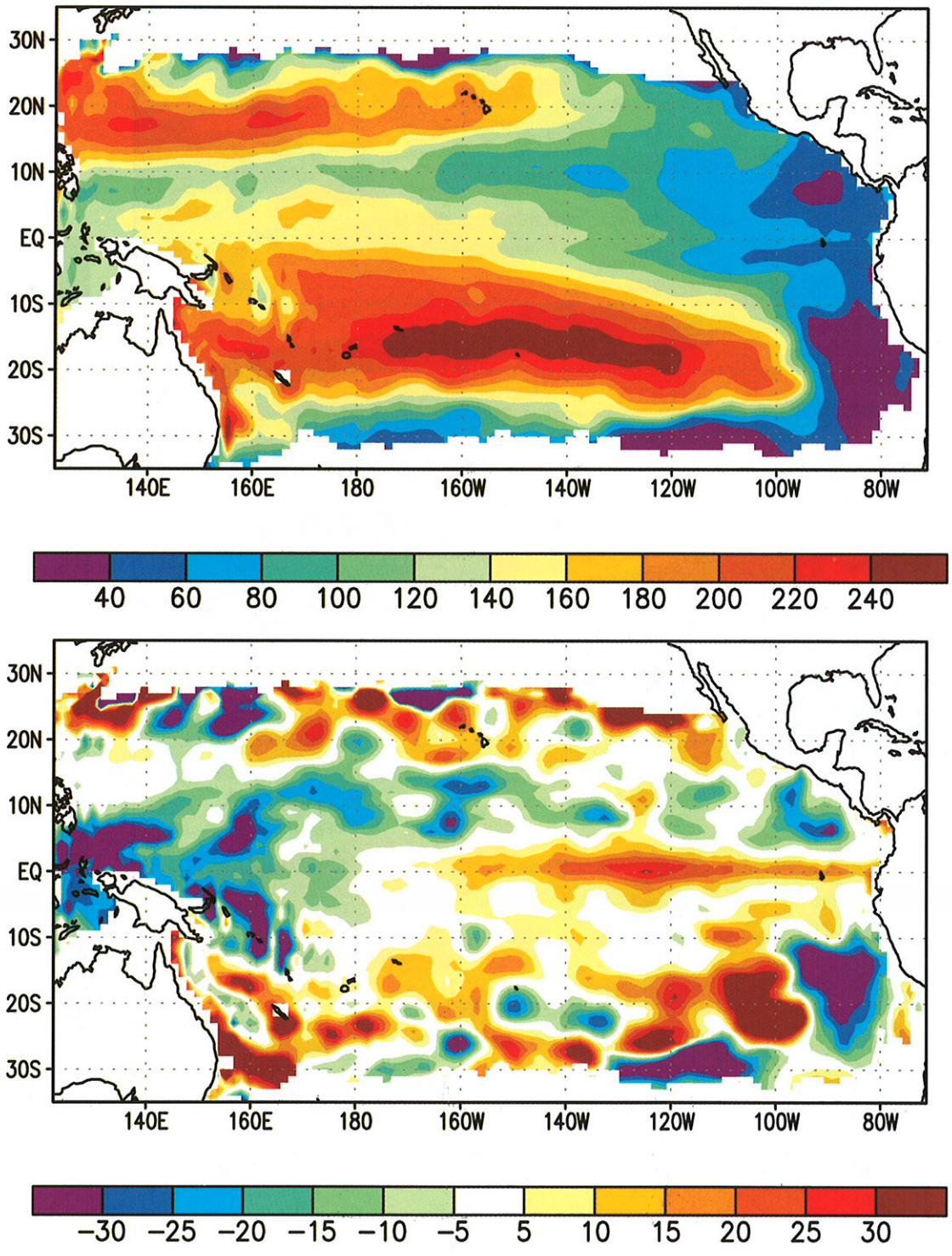

Figure 2.6 Mean (top) and anomalous (bottom) depth (m) of the 20°C isotherm for the period March - May 1993. Anomalies are departures from the 1983-1992 base period. (Data provided by the NMC Coupled Model Project.)

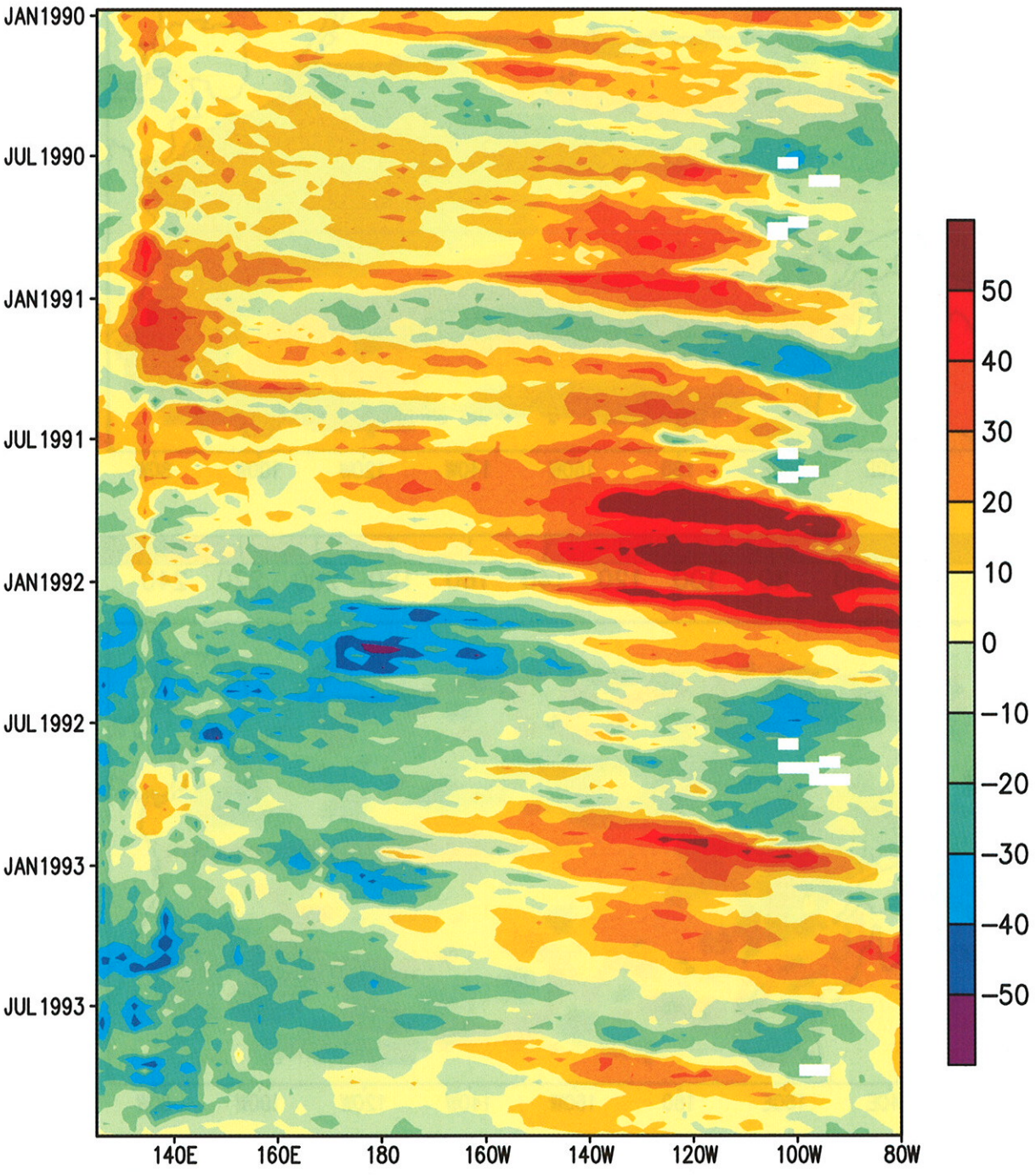

Figure 2.7. Anomalous depth (m) of the 20°C isotherm along the equator in the Pacific Ocean. Data are derived from an analysis which assimilates oceanic observations into an oceanic GCM (*Leetmaa and Ji 1989*). Anomalies are departures from the 1983-1992 base period. (Data provided by the NMC Coupled Model Project.)

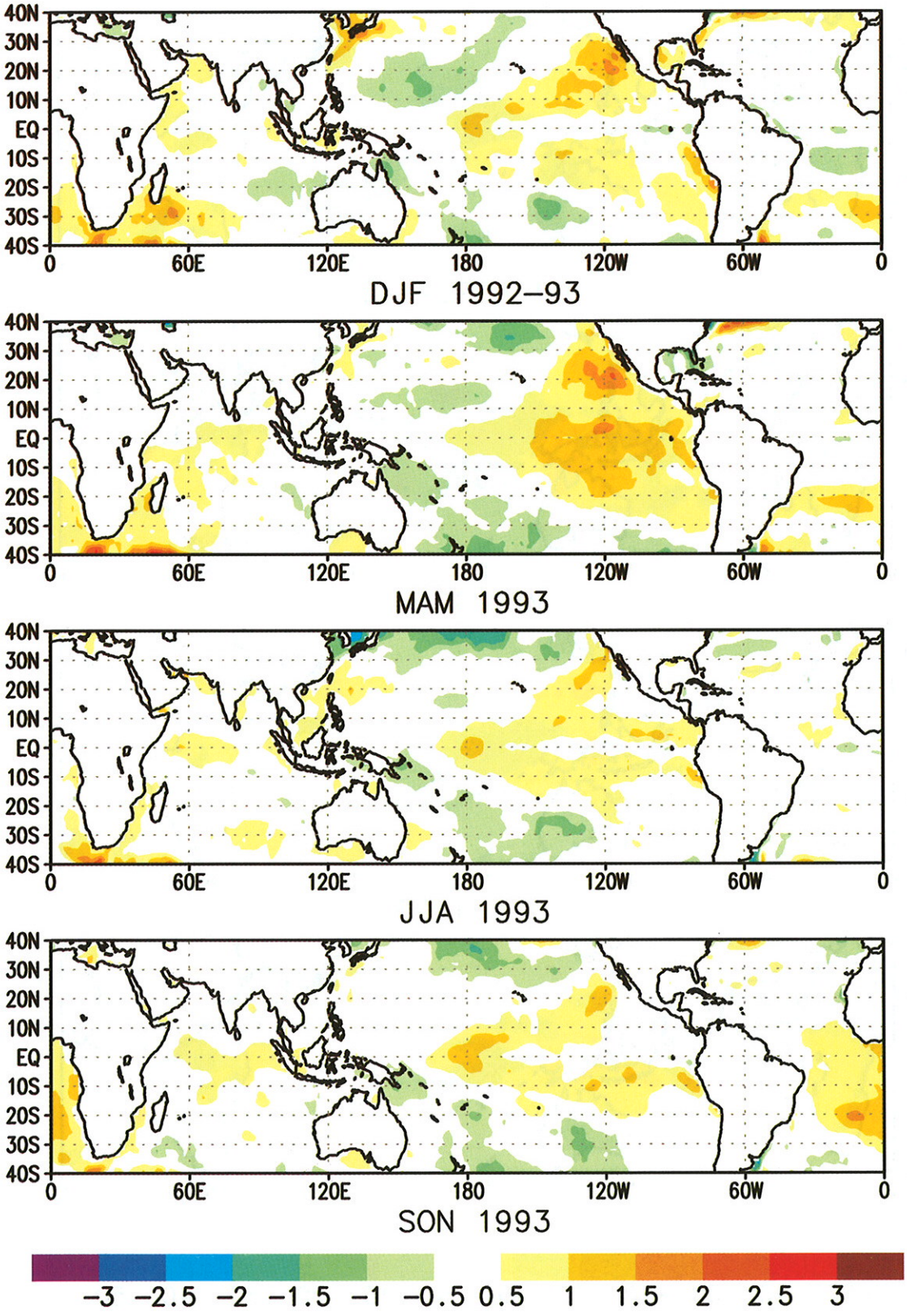

Figure 2.8 Seasonal sea surface temperature (SST) anomalies (°C) computed as departures from the COADS/ICE climatology (*Reynolds 1988*). (Data provided by the NMC Coupled Model Project.)

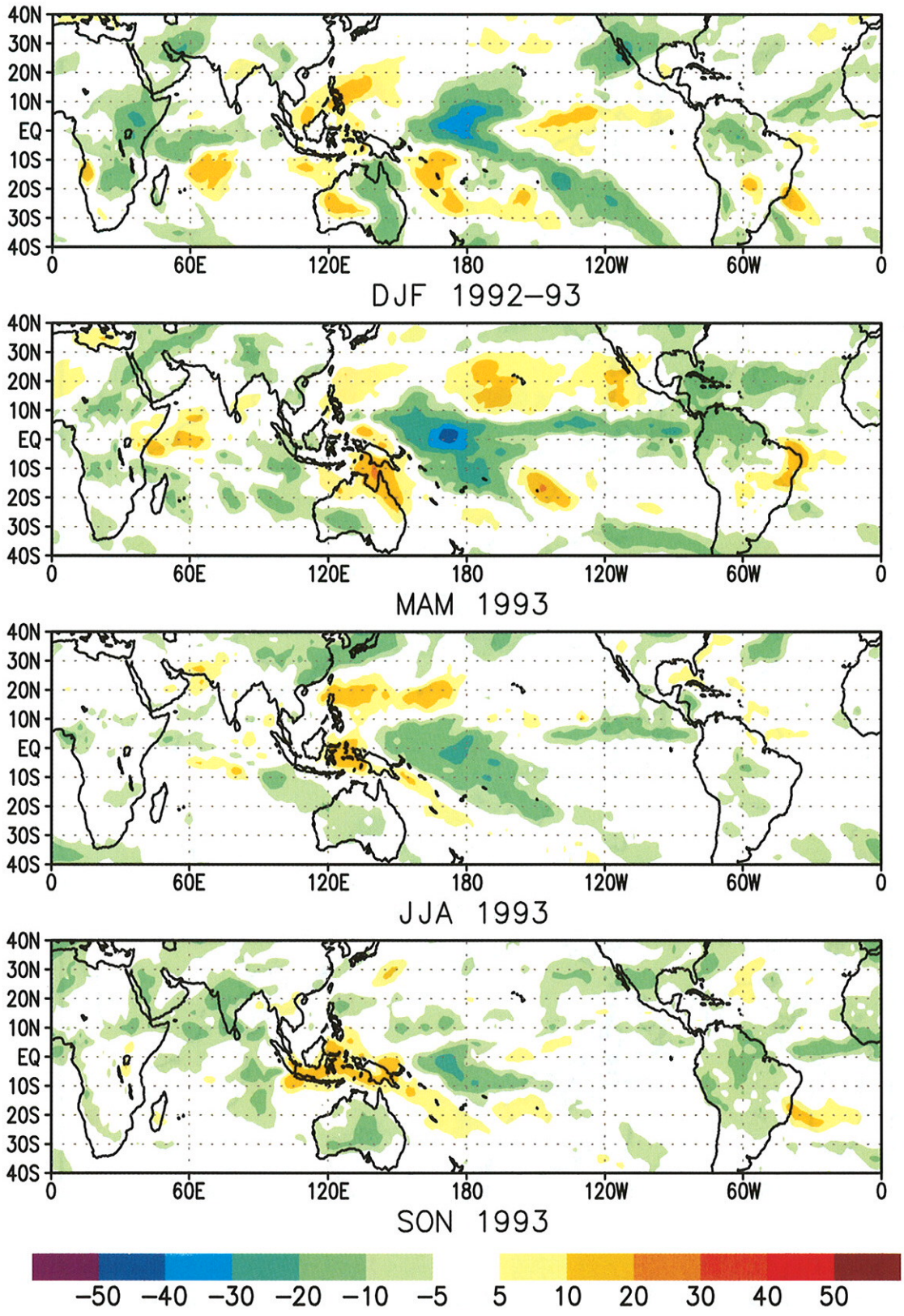

Figure 2.9 Seasonal outgoing longwave radiation (OLR) anomalies (WM^{-2}) computed as departures from the 1979-1988 base period. (Source: CAC)

3. REGIONAL CLIMATE SUMMARIES

a. Drought Abates in California, Continues in Pacific Northwest

California and the Pacific Northwest receive much of their mean annual precipitation during the winter months, which significantly influences the region's hydrologic conditions throughout the year. However, for the period encompassing the winters of 1983/1984 through 1991/1992, the region received significantly below-normal precipitation (**Fig. 3.1, top**). For example, during this nine-year period, much-below-normal precipitation was observed during seven winters in California, and near-normal precipitation was observed in the other two winters (1985/1986 and 1991/1992). These conditions resulted in severe long-term drought, which dominated the state's hydrology since approximately the winter of 1986/1987. Similar conditions have also been observed throughout the Pacific Northwest since the winter of 1986/1987. During the winter of 1992/1993, significantly above-normal precipitation finally fell throughout California, thus alleviating the long-term drought conditions that had previously plagued the state. However, precipitation remained below normal in the Pacific Northwest. Winter precipitation deficiencies again developed in California during late 1993, with below-normal precipitation falling during November and December (**Fig. 3.1, bottom**).

Precipitation totals in California during December-February 1992/93 were the largest recorded by the state since 1968, and the second largest observed in the past 40 years. By the end of the season, overall reservoir storage increased to 85% of capacity, and water storage content increased by 5 million acre-feet from the previous year. However, since much of this increase in water storage was due primarily to the excessive rainfall, it was considered only a short-term remedy to the state's severe hydrologic problems. Fortunately, excessive snowfall dominated the season at high elevations, resulting in the heaviest snowpack water content in the California mountains since early 1983. This increased snowpack played a crucial factor in improving the state's long-term hydrologic outlook, as substantial snow-melt extended throughout the spring season and prevented reservoir levels from returning to pre-winter drought levels.

Monthly mean precipitation totals and departures from normal during December 1992, January and February 1993 are shown in **Fig. 3.2**. December rainfall totals (**Fig. 3.2a**) of 150-225 mm covered western Oregon and much of northern California. Farther south, precipitation totals of 50-100 mm covered central and southern California, and much of southern Arizona. The precipitation totals were substantially above normal in northern California and southern Arizona where anomalies in excess of 50 mm were observed, and in southern California where anomalies in excess of 25 mm were observed (**Fig. 3.2d**). Precipitation deficits of 25 - 75 mm were recorded in western Washington.

The region of heavy precipitation expanded considerably during January to include much of Nevada and Utah (**Fig. 3.2b**). During this period, precipitation totals in excess of 200 mm were observed across much of coastal northern and central California and extreme southern California, while totals of 100-150 mm fell over much of the remainder of the state. Farther east, precipitation totals of 50-100 mm fell over much of Nevada, Utah and Arizona, with totals of 100-150 mm over southeastern Arizona. These totals were highly anomalous, particularly throughout California and Arizona where anomalies exceeded 75-100 mm (**Fig. 3.2e**). However, below-normal precipitation was again observed in the Pacific Northwest.

During February, the area of heavy precipitation diminished and the area of greater than 50 mm was confined primarily to California (**Fig. 3.2c**). However, the heaviest precipitation was again observed over northern California, which received more than 125 mm during the month. Elsewhere, much of the remainder of California received 50-100 mm of precipitation, with anomalies of 25-75 mm observed over many areas of both the northern and extreme southern portions of the state (**Fig. 3.2f**). Less than 50 mm of precipitation fell on Washington and Oregon during February, with deficits greater than 75 mm recorded.

Winter precipitation in California tends to be strongly dependent on the prevailing wind direction and on the location and intensity of the storm track. For example, southwesterly flow and above-normal cyclone activity is associated with above-normal precipitation, while northwesterly flow and below-normal cyclone activity is associated with below-normal precipitation. From December to mid-January, the circulation was dominated by a long-lived blocking anticyclone over the eastern North Pacific (**Figs. 3.3, top**), and by negative height anomalies over the western United States. This anomaly pattern was accompanied by a highly anomalous storm track throughout the Gulf of Alaska and western United States (**Fig. 3.4**). For example, storms west of the block tended to weaken and move northeastward from the central North Pacific to the Aleutians, while storms east of the block generally amplified while moving southeastward from the Aleutians into California. Anomalously strong southwesterly geostrophic flow was also observed throughout California and the southwestern United States during this period (**Fig. 3.5**). These conditions, along with above-normal moisture transport into California from the tropics by the anomalous southwesterly flow, contributed to the extremely heavy precipitation totals observed over California during the period.

The blocking anticyclone dissipated in mid-January, but negative height anomalies persisted off the southwest coast of the United States for the remainder of the season (**Fig. 3.3, bottom**). This anomalous circulation was associated with a continuation of both the amplified subtropical jet stream and abnormally strong southwesterly flow over California, along with an anomalously strong influx of tropical moisture over the southwestern United States. Thus, California continued to receive excessive precipitation from mid-January through the end of February. In contrast, the Pacific Northwest remained anomalously dry during the period, as the primary storm track and enhanced westerly flow remained displaced well south of the region.

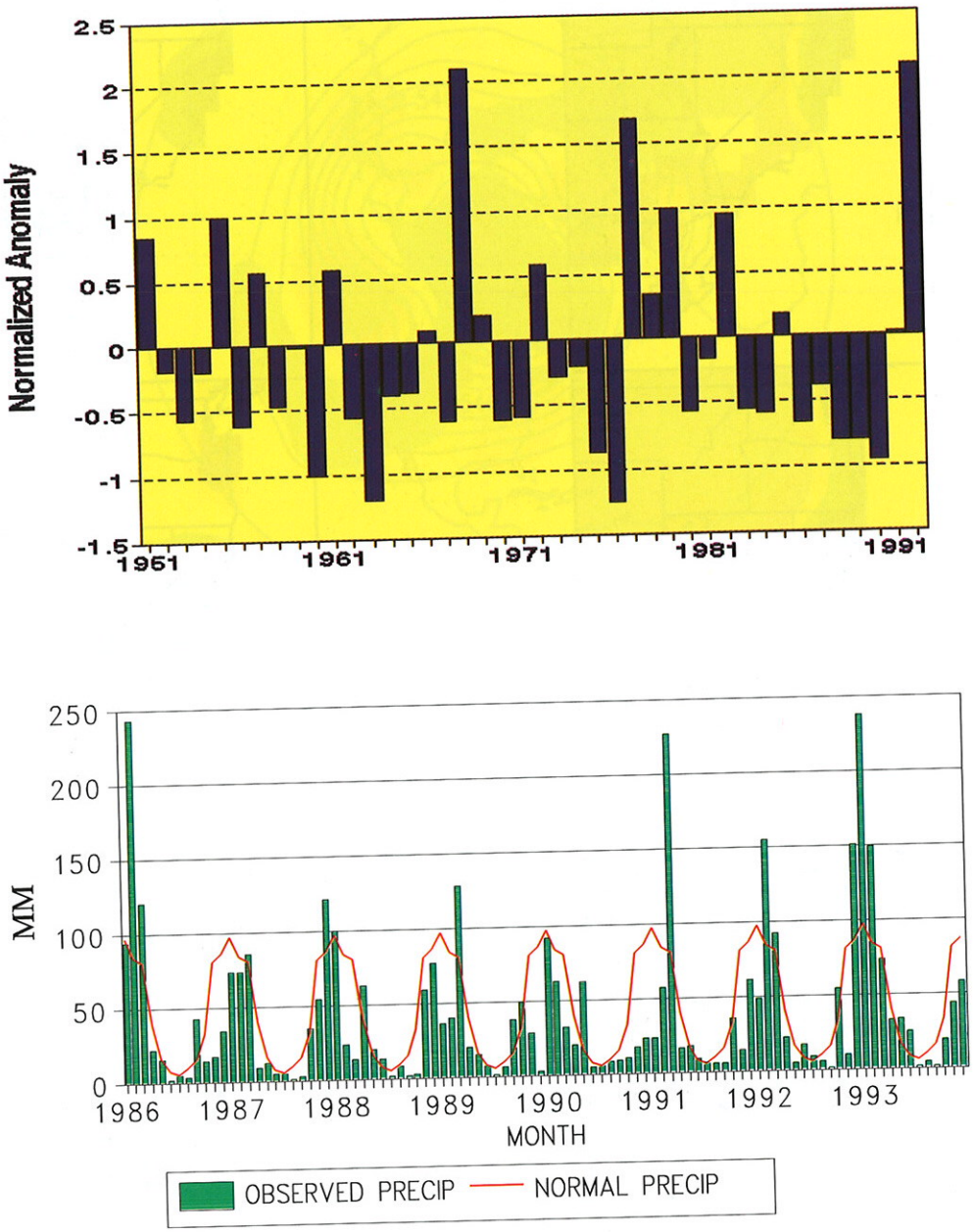

Figure 3.1 Normalized precipitation anomaly for California/Nevada during the December - February period (1951/52-1992/93) (top) and monthly mean precipitation totals (mm) in California (January 1986 - December 1993) (bottom). Solid red curve shows the mean annual cycle (1961-1990) of precipitation. (Source: (top) - CAC, (bottom) - NCDC)

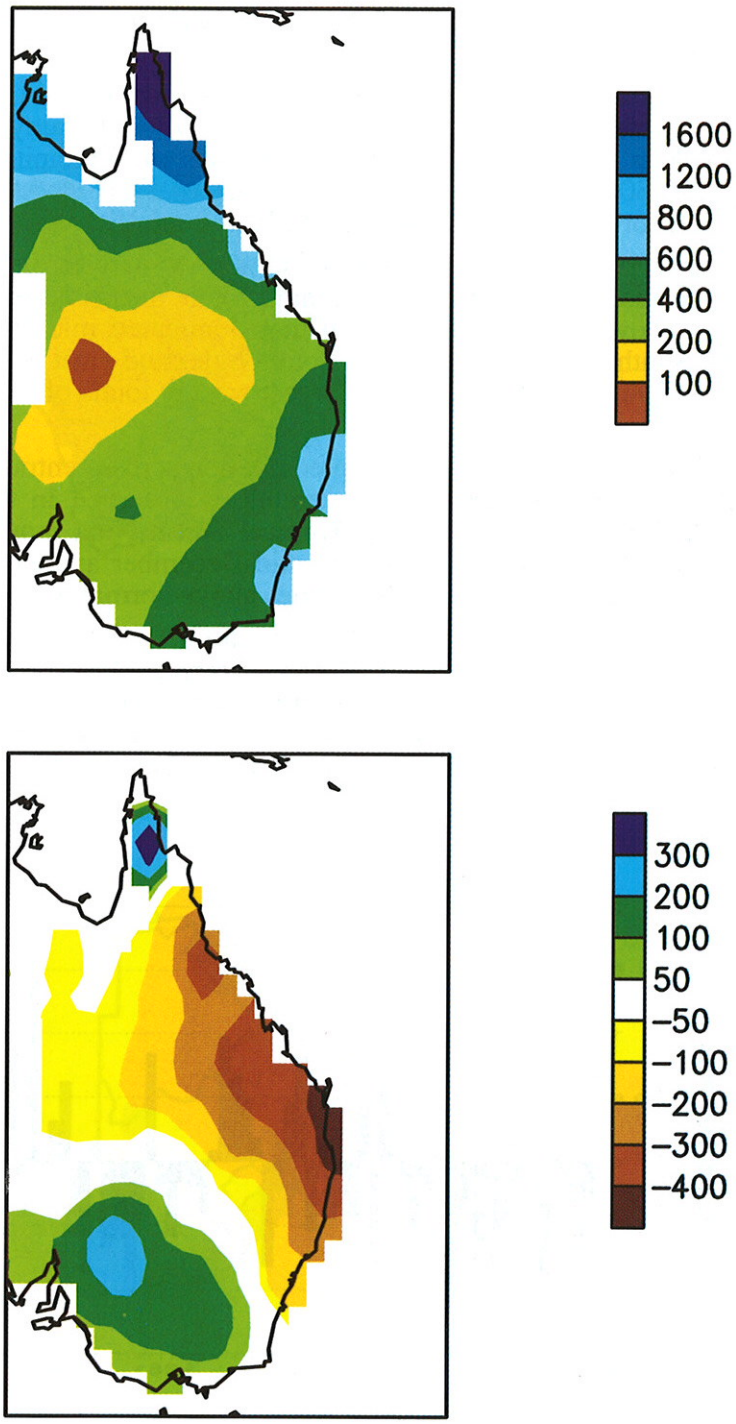

Figure 3.9 Total precipitation (top) and departure from normal (mm) (bottom) for eastern Australia for October 1992 - May 1993. (Source: CAC)

d. The Midwest Floods of June-July 1993

The midwestern United States experienced one of its worst flooding events on record during June-July 1993. The region of extensive flooding encompassed nine states, including eastern North and South Dakota, eastern Nebraska, northwestern Kansas, southern Minnesota, western and southern Wisconsin, and much of Illinois, Iowa, and the northern half of Missouri. In fact, all major river systems in southern Wisconsin, Iowa, Missouri and Illinois experienced either major or record flooding during June and July (**Fig. 3.10**).

The enormity of the flooding on the Mississippi and Missouri Rivers is summarized in **Fig. 3.11**. The Mississippi River at St. Louis, Missouri was above flood stage for a record 80 days, and above record flood stage for 23 consecutive days between 17 July and 8 August (**Fig. 3.11, top**). Similarly, the Mississippi River at Davenport, Iowa was above flood stage for 43 days (**Fig. 3.11, bottom**). Farther south, the Missouri River at Kansas City, Missouri was above flood stage for 30 consecutive days, and above record flood stage for several days at the end of July (**Fig. 3.11, middle**).

Three atmospheric factors are identified as playing a crucial role in the formation, duration and intensity of the Midwest floods. First, selected analyses of the long-term Palmer Drought Severity Index (**Fig. 3.12**) indicate that above-normal soil moisture conditions persisted throughout much of the Midwest and central Plains for nearly nine months preceding the onset of the floods. Above-normal soil moisture conditions began to develop in Iowa, Missouri and the Plains states during August 1992, nearly one year prior to the onset of the floods (**Fig. 3.12a**). By the end of November 1992 (**Fig. 3.12b**), the area with above-normal soil moisture levels had expanded considerably, with much of the Midwest and Plains states reporting extremely moist soil conditions. These conditions were exacerbated during the winter and spring months by a continuation of above-normal precipitation, which produced near-saturated soil conditions throughout the impending flood region by the end of March (**Fig. 3.12c**). Thus, this region was preconditioned for potential major hydrologic problems even well prior to the onset of the floods. Soil moisture levels then quickly became saturated with the onset of the excessive and focused rainfall events during June and July. During August, the heavy rains became more sporadic and less focused than had been observed for the prior two months. Nonetheless, saturated soil conditions continued into the fall season throughout the Midwest and Plains states (**Fig. 3.12d**).

The second major factor crucial to the flood event was the repetition of excessive and focused rainfall events during June and July. These rainfall events tended to be organized into large mesoscale convective complexes, which often developed at night along a quasi-stationary frontal boundary that persisted over the flood region. Much of Iowa, Missouri, Kansas, southern Minnesota and northwestern Illinois received in excess of 400 mm of precipitation during June - August (**Fig. 3.13, top**), while much of central Iowa, northern Missouri and portions of western Illinois received over 600 mm of rainfall.

Overall, the northern and central Plains states, along with much of the Midwest, received more than twice the normal precipitation during the period, with recorded rainfall anomalies of 200 mm and 400 mm, respectively (**Fig. 3.13, bottom**). These inundating rains quickly brought soil moisture levels to maximum capacity throughout the northern Mississippi River Valley by mid-June, resulting in widespread flooding. In contrast, summer rainfall totals of 100-200 mm over the Carolinas and Virginia, and 200-300 mm of precipitation over Georgia and the southeastern coastal United States were much below normal, resulting in moderate drought conditions in these regions for much of the summer (**Fig. 3.12d**).

The third major factor was an anomalous atmospheric circulation extending from the central North Pacific eastward to the western North Atlantic (**Fig. 3.14**). At 500 mb the mean circulation during the period was characterized by negative height anomalies over the central North Pacific, which reflected an amplification of the climatological-mean Pacific trough, and a broad region of weak positive height anomalies over the Gulf of Alaska. Over North America negative height anomalies dominated the western United States and western Canada, while weak positive

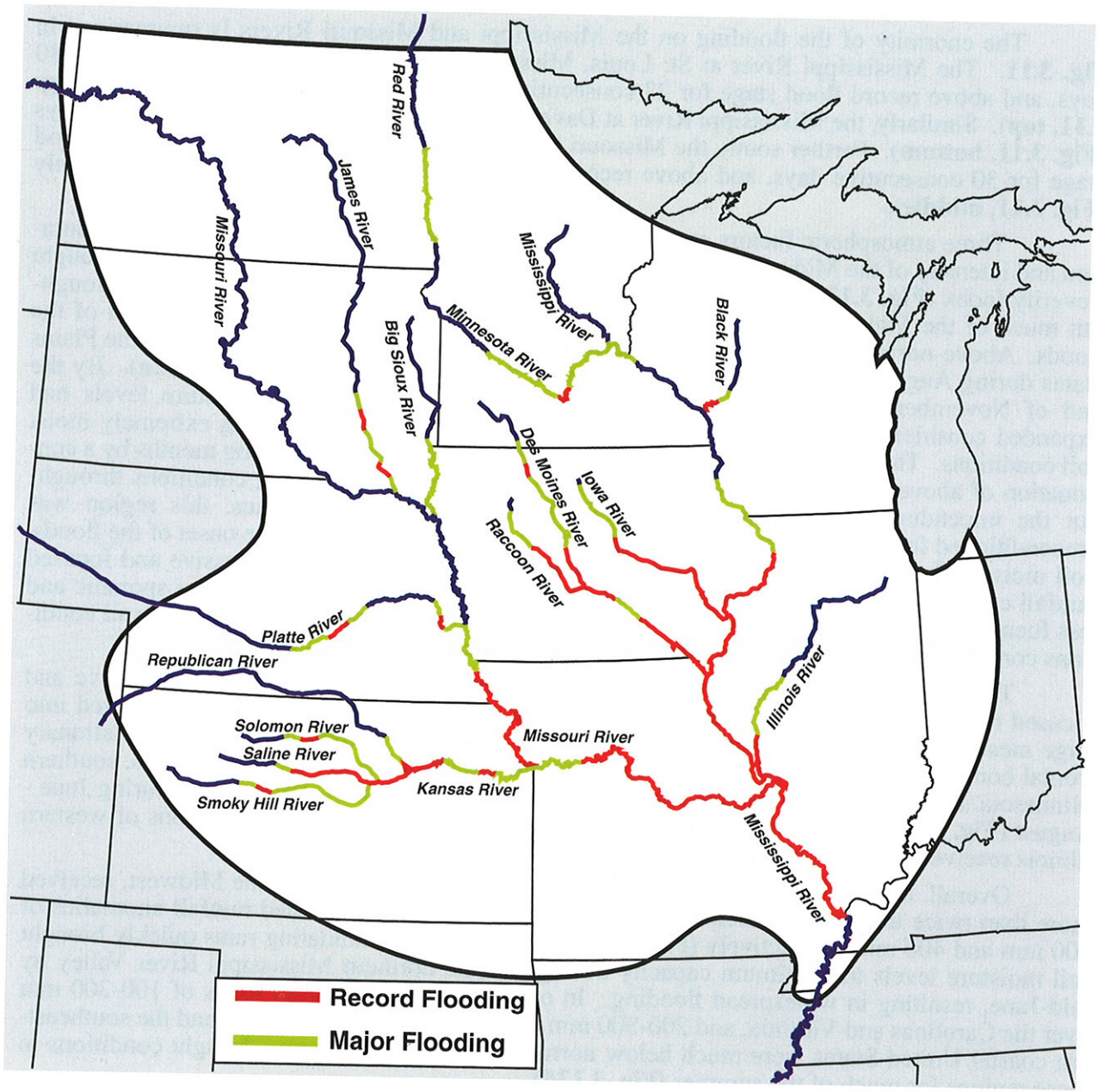

Figure 3.10 Major river systems in the nine-state flood region. Green (red) shading indicates regions of major (record) flooding during the Midwest floods of June-July 1993. (Source: Office of Hydrology)

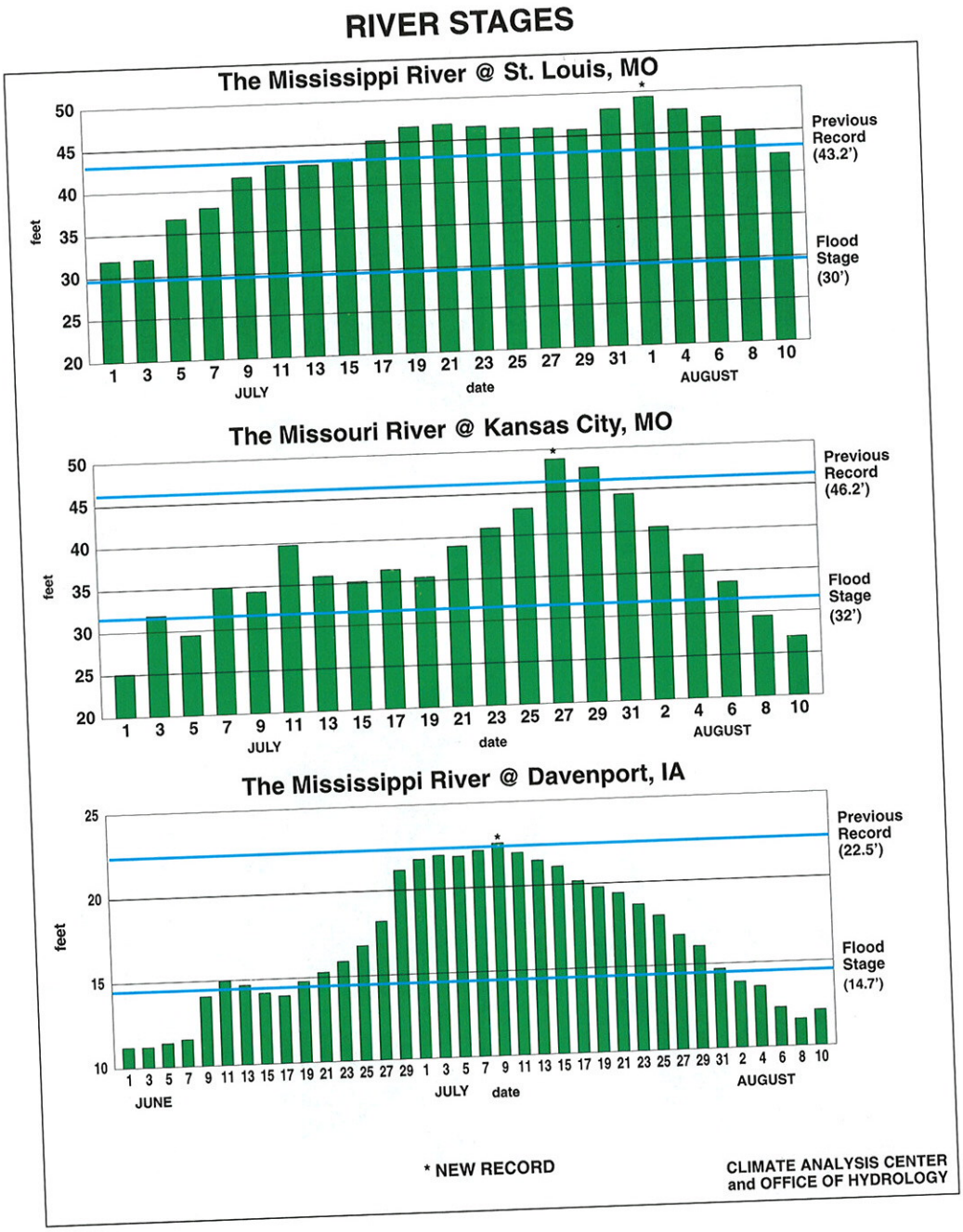

Figure 3.11 Histograms showing river levels for select locations along the Mississippi River (top and bottom) and Missouri River (middle) during the Midwest floods. (Source: CAC and Office of Hydrology)

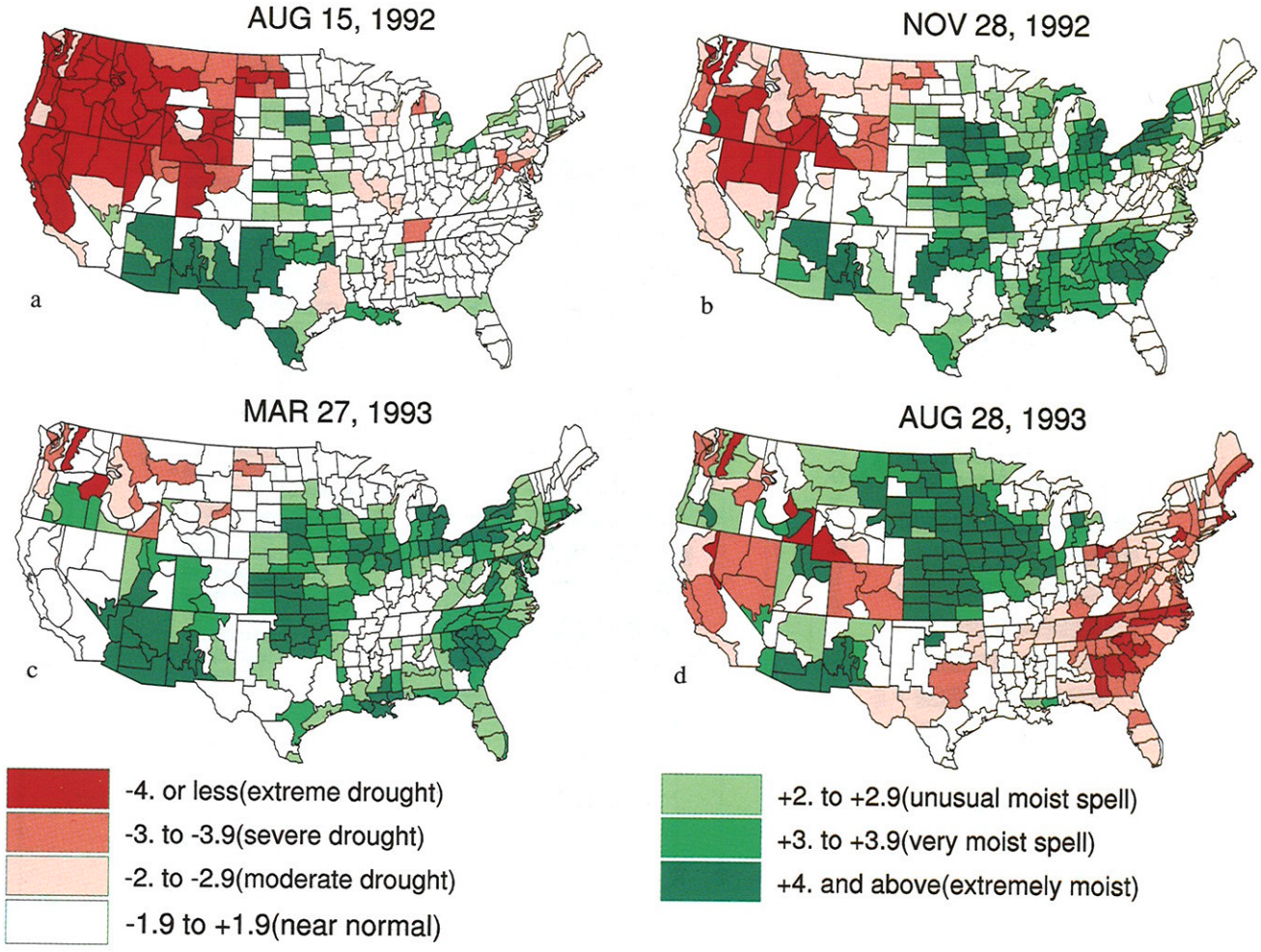

Figure 3.12 Palmer long-term drought severity index for: (a) 15 August. 1992, (b) 28 November, 1992, (c) 27 March 1993, and (d) 28 August 1993. (Source: CAC)

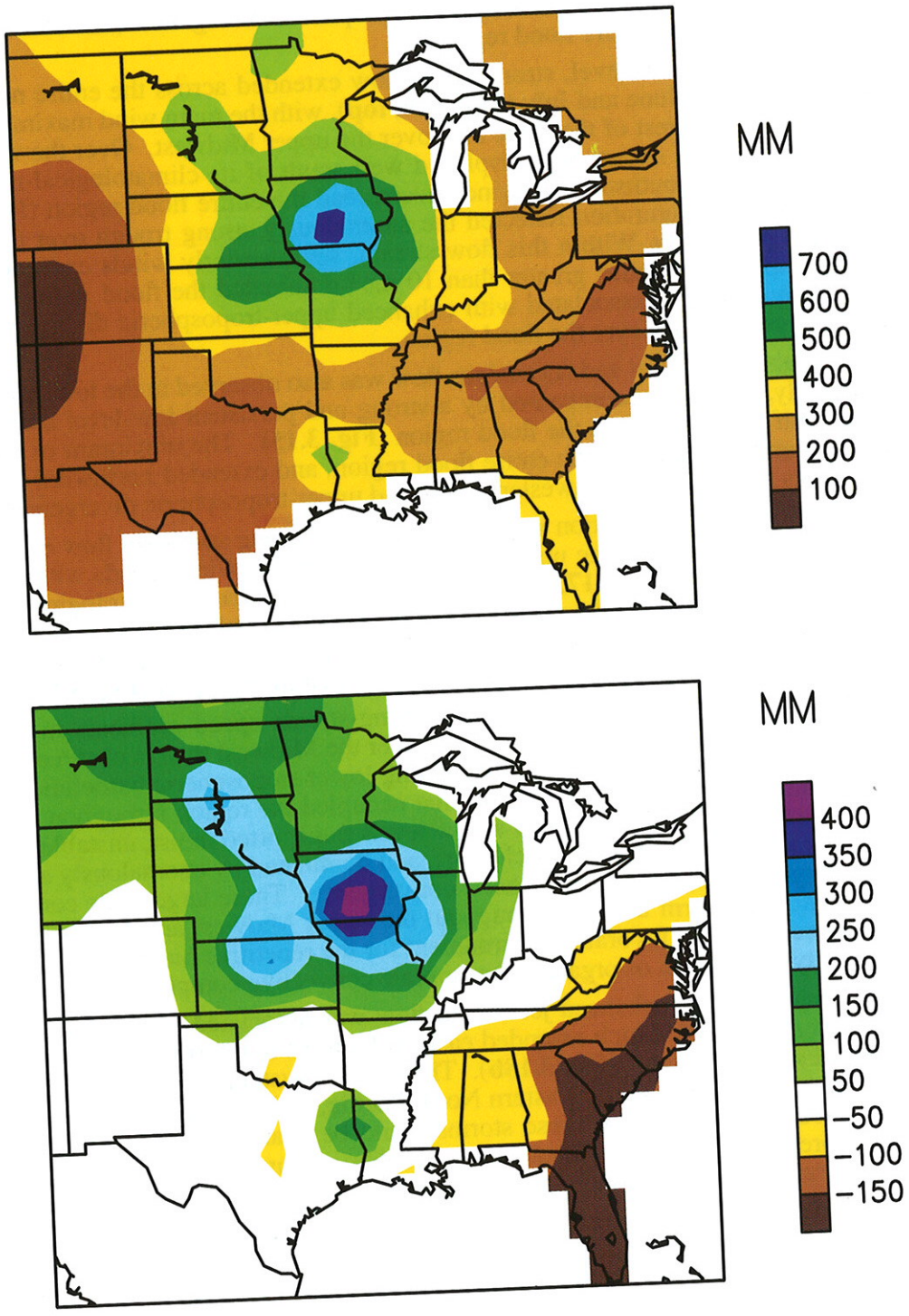

Figure 3.13 Precipitation: total (top) and anomalous (mm) (bottom) during June-August 1993. Anomalies are computed with respect to the 1961-1990 base period. (Source: CAC)

height anomalies covered much of the eastern United States and Canada. This anomaly pattern was associated with a persistent and large amplitude trough in the west and a mean ridge centered over the Great Lakes. These features were accompanied by anomalous southwesterly geostrophic flow, along with broad mid- and upper-tropospheric divergence (not shown) and ascending motion, throughout the entire flood region.

At the jet stream level, strong zonal flow extended across the entire northern half of the United States during June and July (**Fig. 3.16, top**), with the main wind maximum in excess of 30 ms^{-1} centered in the crest of the ridge axis over the upper Midwest. Over the western and central United States, the jet stream was displaced well south of its climatological-mean position, and anomalously strong southwesterly winds overspread the entire flood region (**Fig. 3.16, bottom**). This entire flow configuration reflected the anomalously strong trough over the western United States noted previously. Within this flow stream, southwesterly winds exceeded 25 ms^{-1} everywhere, and speed anomalies greater than 10 ms^{-1} dominated the flood region. This very strong southwesterly flow was associated with enhanced upper-tropospheric divergence and ascending motion centered directly over the flood region.

A highly persistent and anomalous flow was also observed in the lower troposphere during June and July, and was accompanied by a strong and persistent low-level transport of moisture from the Gulf of Mexico into the flood region (**Fig. 3.15**). The maximum of moisture transport during the period overspread the entire flood region, and extended northward beneath the region of anomalous upper-level southwesterly flow and upper-tropospheric divergence.

At 850 mb the circulation was dominated by a strong southerly flow extending northward from the Gulf of Mexico to the upper Midwest (**Fig. 3.17**). Wind speeds within this flow stream ranged from 6-10 ms^{-1} (**Fig. 3.17, top**) and were 1.5-2 times their climatological values (**Fig. 3.17, bottom**), with southerly wind anomalies of 2-4 ms^{-1} observed throughout the central part of the country. This region was also characterized by enhanced lower-tropospheric convergence (not shown), and coincided with the area of maximum moisture transport (**Fig. 3.15**).

Additionally, both cross-stream and along-stream speed gradients in the 850-mb wind field were much larger during June-July 1993 over the Midwest than is observed climatologically. This wind structure reflected anomalously strong lower-tropospheric baroclinicity, and was associated with an enhanced frontal boundary that occupied the region throughout the period. Thus, the anomalously strong southerly flow at low levels transported moist, unstable air northward into a region characterized by strong baroclinicity, and dominated by anomalously strong upper-tropospheric divergence and lower-tropospheric convergence. These large-scale conditions, combined with above-normal storm activity throughout the upper Midwest and Plains states (**Fig. 3.18a**), created an exceptionally favorable environment for the repetitive build-up and release of convective instability in the form of organized mesoscale convective complexes in the flood region.

During June, the enhanced jet stream flow was associated with a particularly anomalous and vigorous storm track which extended eastward almost uninterrupted from the date line to the upper Midwest United States (**Fig. 3.18b**). These storm systems passed through the anomalously deep Pacific trough, traversed the eastern North Pacific, and subsequently moved directly into the central United States. Each of these storms could be characterized qualitatively as having an intensity more typical of "cool season" cyclones than of summertime systems, and each of these systems produced extremely heavy precipitation as they moved into the flood region.

During July, above-normal storm activity continued over the North Pacific and northern Plains states (**Figs. 3.18c**). Interestingly, comparatively few cyclones propagated directly into the flood region from the eastern North Pacific during the month. Instead, cyclones weakened while moving into the mean trough position over the western United States, and then re-amplified in the broad southwesterly flow located downstream of the trough axis, producing a secondary maximum of anomalously strong storm activity over the western portion of the flood region. This anomalous storm track, in combination with the extremely persistent flow configuration described previously, continued to produce intense convective activity over the flood region.

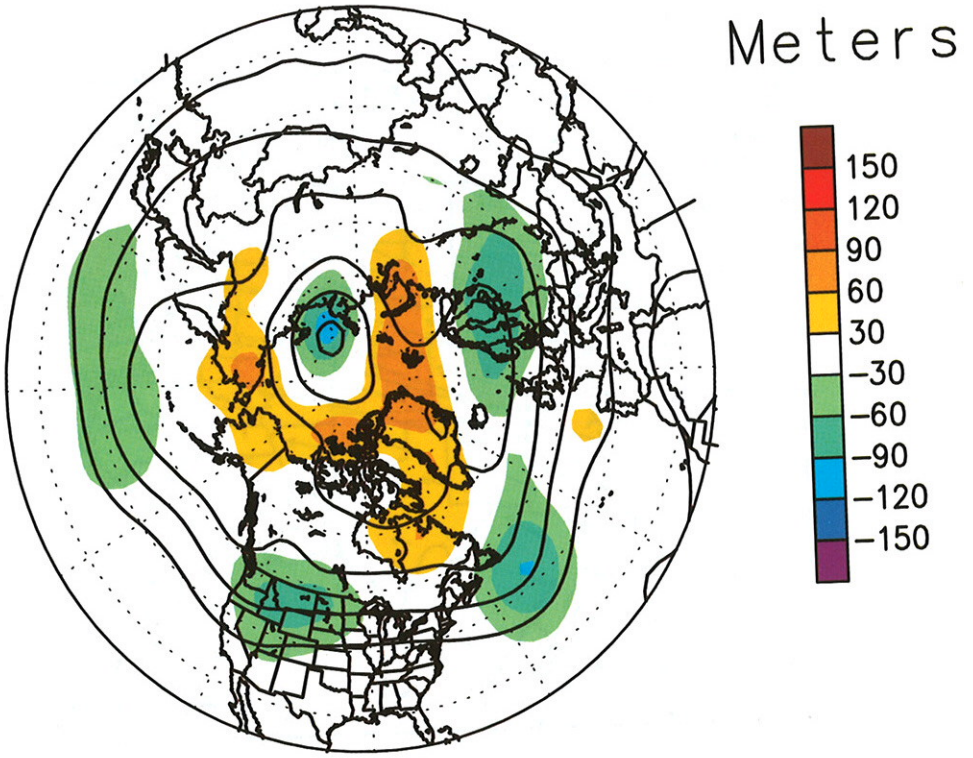

Figure 3.14 Mean 500-mb heights (contours, interval is 120 m) and anomalies (shaded) during June-July 1993. Anomalies are departures from the 1979-1988 base period. (Source: CAC)

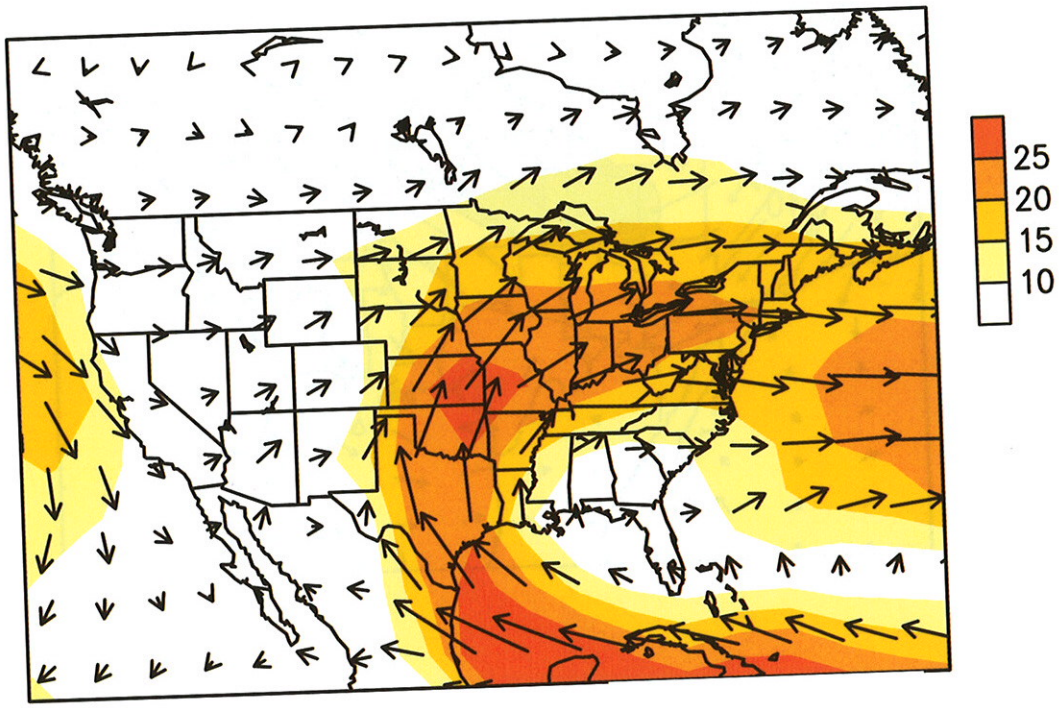

Figure 3.15 Mean vertically-integrated moisture transport (shaded, units are 10^{-3} $kgm^{-3}s^{-1}$) and 850-mb vector wind (ms^{-1}) during June-July 1993. (Source: CAC)

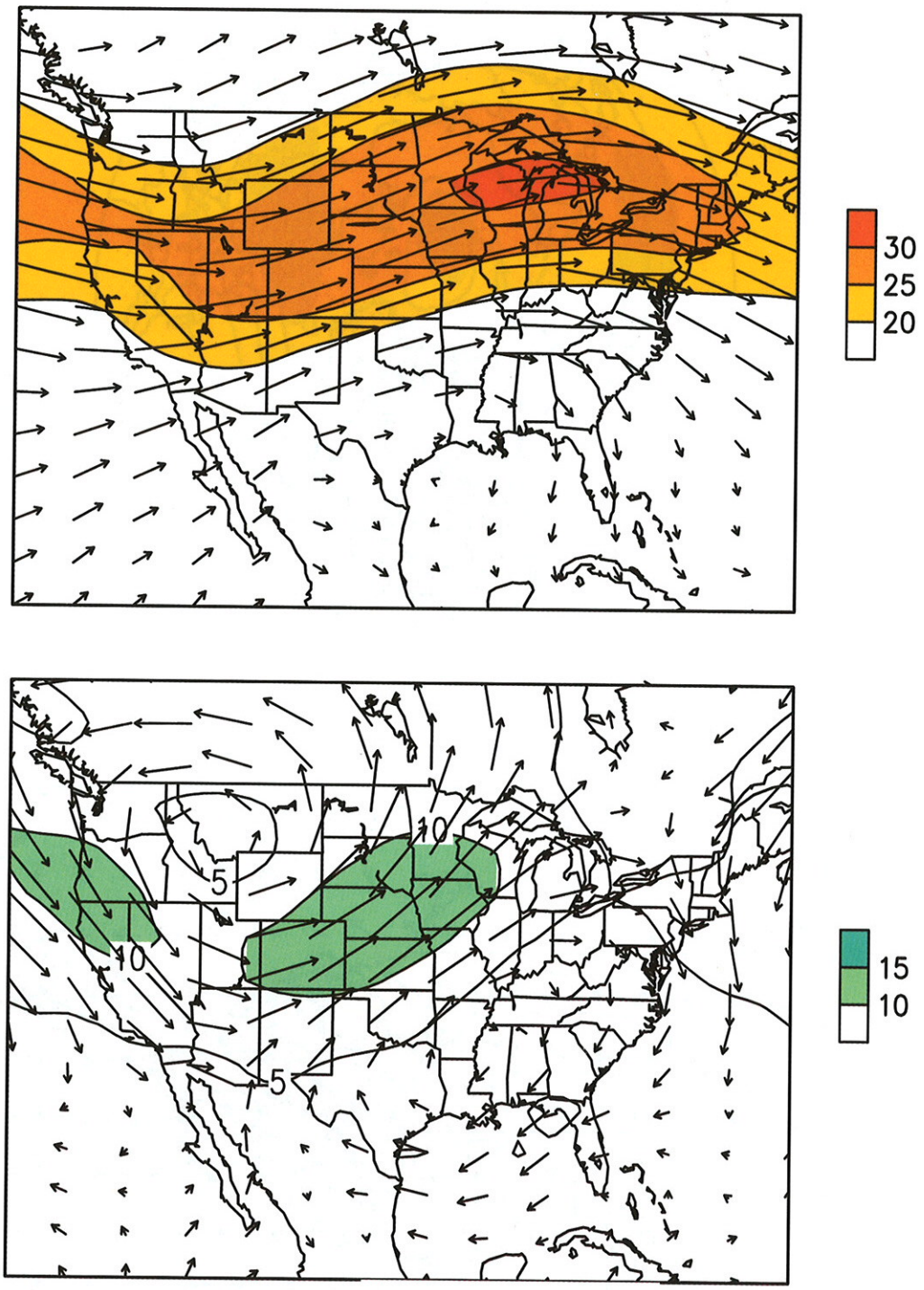

Figure 3.16 Mean (top) and anomalous (bottom) 200-mb vector wind for June-July 1993. Anomalies are departures from the 1979-1988 base period. Contour interval for isotachs is 10 (5) ms^{-1} for the mean (anomalous) wind. (Source: CAC)

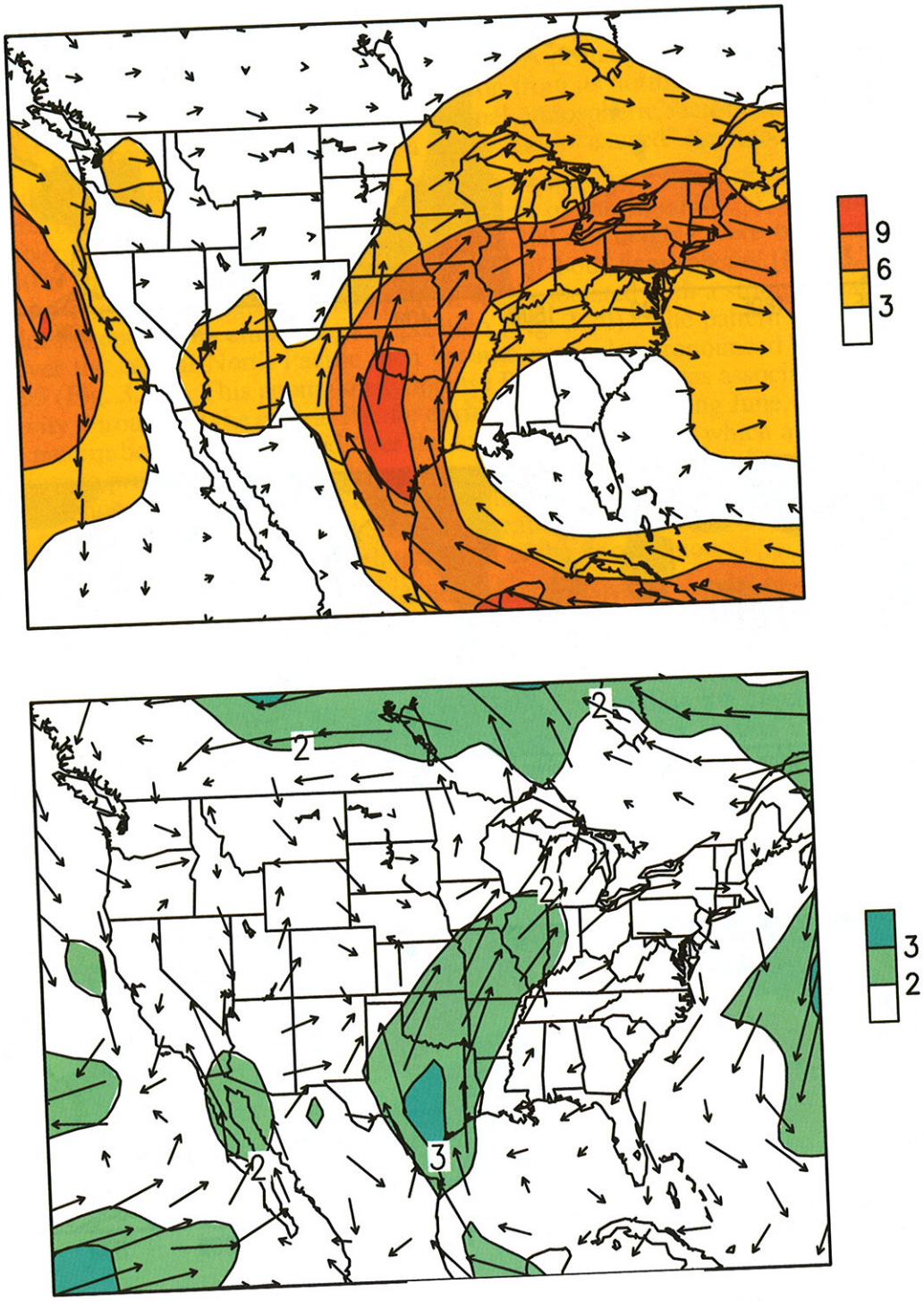

Figure 3.17 Mean (top) and anomalous (bottom) 850-mb vector wind for June-July 1993. Anomalies are departures from the 1979-1988 base period. Contour interval for isotachs is 5 ms^{-1}. (Source: CAC)

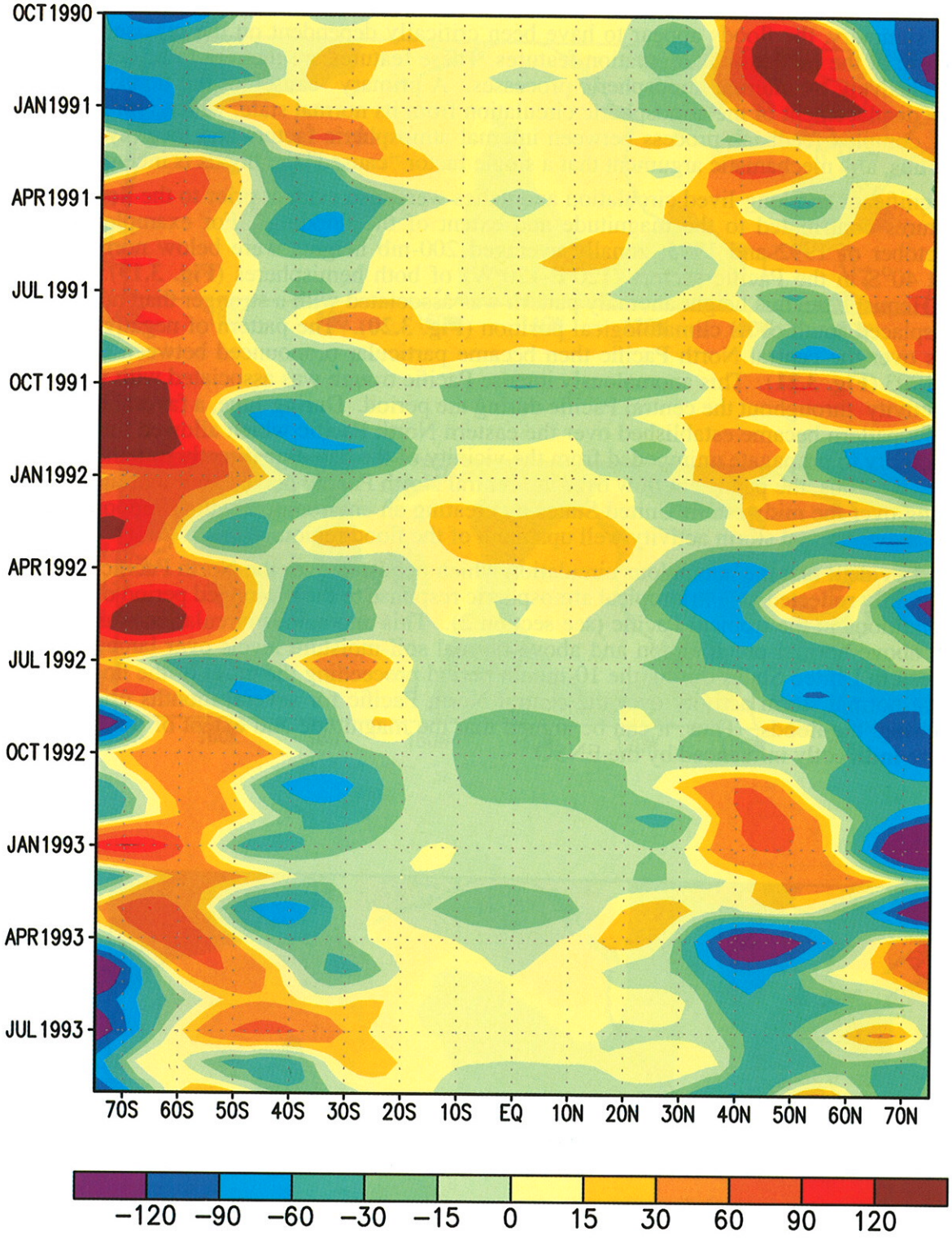

Figure 3.19 Time-latitude section of 200-mb height anomalies (m) averaged over the Pacific sector (120°E-120°W) for October 1990-December 1993. Anomalies are departures from the 1979-1988 base period. (Source: CAC)

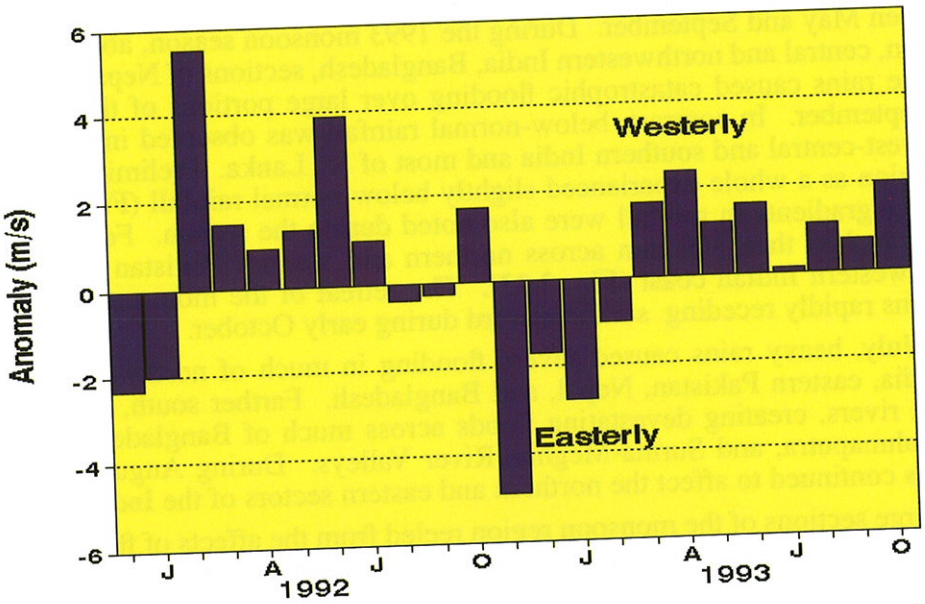

Figure 3.20 Zonally-averaged 200-mb zonal wind anomaly (ms^{-1}) at 30°N from December 1991-October 1993. Anomalies are departures from the 1979-1988 base period. (Source: CAC)

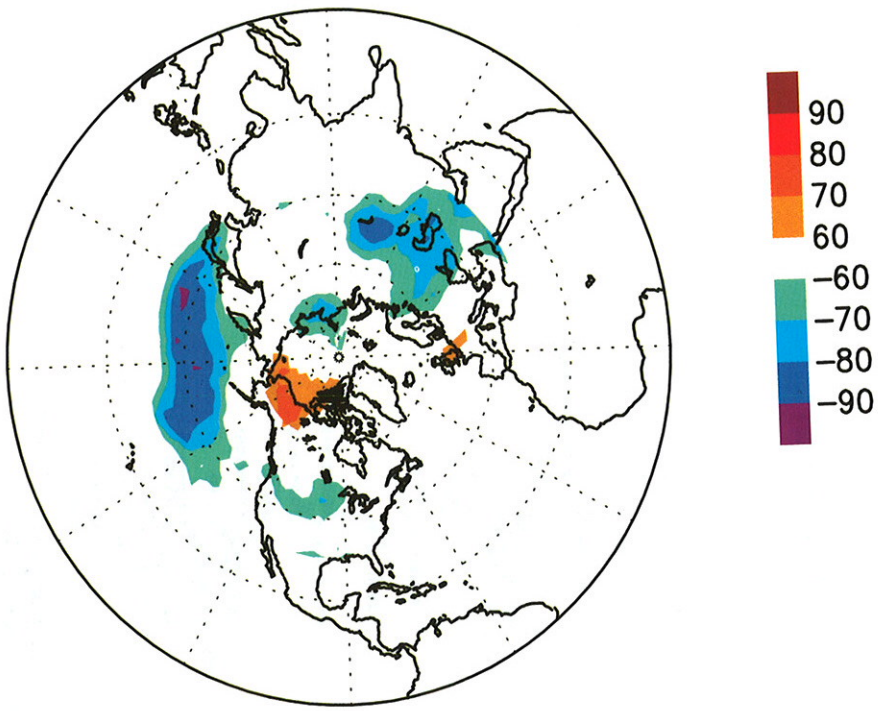

Figure 3.21 Percentage of days in which positive (red shading) and negative (blue shading) low-pass filtered (retaining periods > 30 days) height anomalies at 500 mb were observed between February - July 1993. (Source: CAC)

e. Indian Summer Monsoon

Much of the mean annual precipitation in India typically occurs during the Indian summer monsoon between May and September. During the 1993 monsoon season, above-normal rainfall covered northern, central and northwestern India, Bangladesh, sections of Nepal, and southeastern Pakistan. These rains caused catastrophic flooding over large portions of the monsoon region from July to September. In contrast, below-normal rainfall was observed in northern Pakistan, north-central, west-central and southern India and most of Sri Lanka. Preliminary estimates suggest that the region as a whole experienced slightly below normal rainfall (**Fig. 3.22**), similar to 1992. Very large gradients in rainfall were also noted during the season. For example, rainfall totals ranged from less than 100 mm across northern and western Pakistan to over 3,000 mm along the southwestern Indian coast (**Fig. 3.23**). The retreat of the monsoonal rains was fairly typical, with rains rapidly receding southeastward during early October.

During July, heavy rains caused severe flooding in much of northwestern and extreme northeastern India, eastern Pakistan, Nepal, and Bangladesh. Farther south, heavy rains fell on already-swollen rivers, creating devastating floods across much of Bangladesh, especially near the Ganges, Brahmaputra, and Surma-Meghna River Valleys. During August, scattered flood-related problems continued to affect the northern and eastern sectors of the Indian Subcontinent.

While large sections of the monsoon region reeled from the affects of flooding, acutely dry conditions gripped the western and central sections of the Indian Subcontinent during August. The lack of rainfall adversely affected crops to some extent from west-central India eastward to Bangladesh.

Monsoon rainfall typically starts to decline in September across the northern half of the subcontinent. However, heavy rains persisted in this region during September 1993. Early in the month, heavy rains caused additional flooding in western Nepal and northeastern India. During mid-September, renewed flooding occurred in northern India and southwestern Nepal. As the month ended, heavy rains continued to the south and east of north-central India.

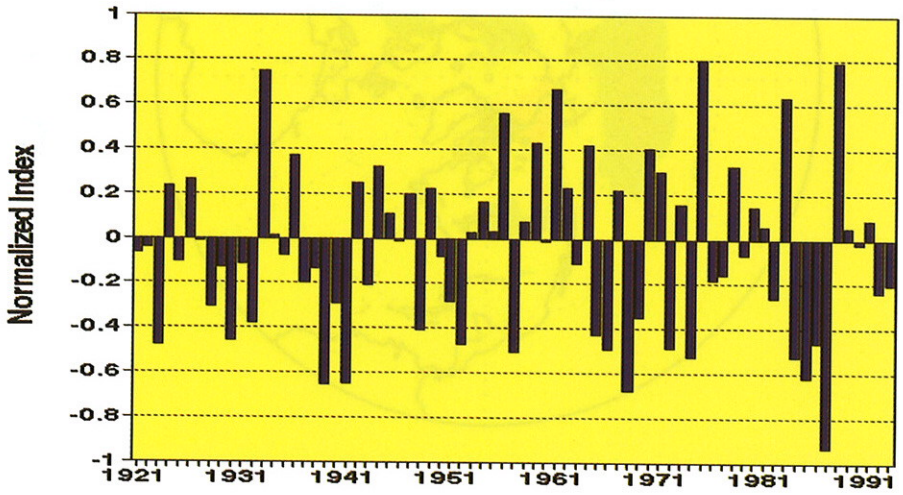

Figure 3.22 Precipitation index (average gamma percentiles of station precipitation within the region) for India (June - September). (Source: CAC)

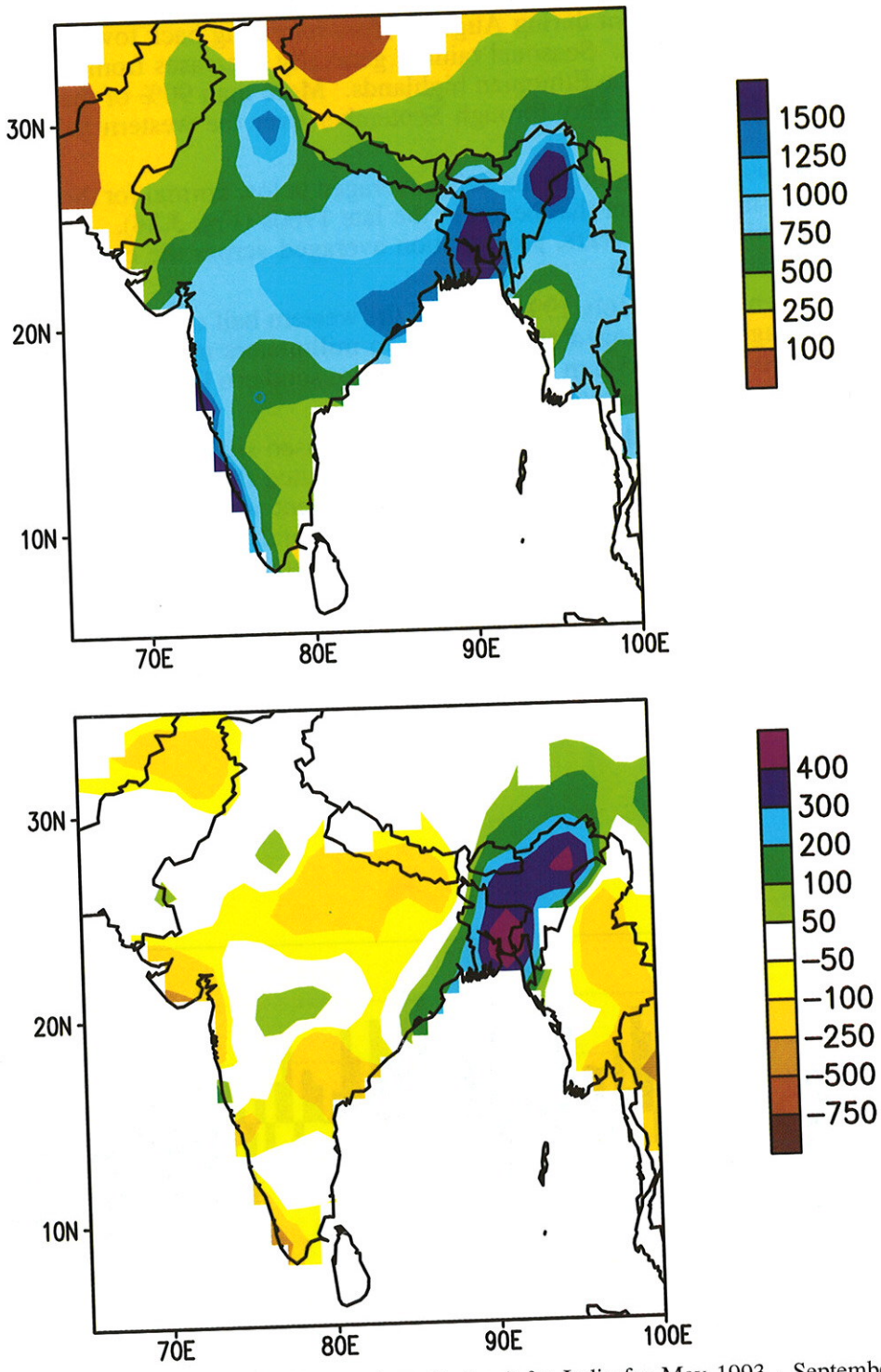

Figure 3.23 Precipitation (mm): total (top) and anomalous (bottom) for India for May 1993 - September 1993. (Source: CAC)

f. Western African Rainy Season

Precipitation patterns tend to be very distinct across the African Sahel. Rains near the equator normally spread northward during the last half of spring and early summer, and reach a maximum northward extent during August before retreating back toward the equator during late summer and early autumn. Seasonal rainfall generally decreases from south to north, except for locally heavy rains over the Ethiopian highlands. More than 90% of the mean annual precipitation typically falls during May through September over the western half of the Sahel north of 12°N.

The 1993 rainy season in the Sahel averaged below normal for the fifth year in a row, continuing a long-term drought that began in the late 1960s (**Fig. 3.24**). Although 1993 was not as dry as the previous three years, precipitation averaged across the entire Sahel was significantly below the 1951-1980 mean.

Between May and July 1993, most of the western half of the Sahel received below-normal rainfall, although totals ranged from under two millimeters in northwestern Senegal and southwestern Mali to 500 - 1165 mm in western Guinea, southern Cote d'Ivoire, central Ghana, northern Togo and parts of Cameroon.

During August and September, rainfall increased significantly across the northern tier of the Sahel, although few locations completely eliminated the moisture deficits that had accumulated through July. The most significant improvement was observed in northern Senegal and southwestern Mauritania, where 135 to 375 mm of rainfall was recorded. In contrast, below-normal precipitation totals persisted over Liberia, central and southern Cote d'Ivoire, eastern Guinea, and western and coastal Ghana.

Abnormally wet conditions were confined to isolated regions in southern Senegal, central Burkina Faso, central Mali, central Niger, and southern Cameroon. These regions received a surplus of between 50 - 200 mm during May-September (**Fig. 3.25**).

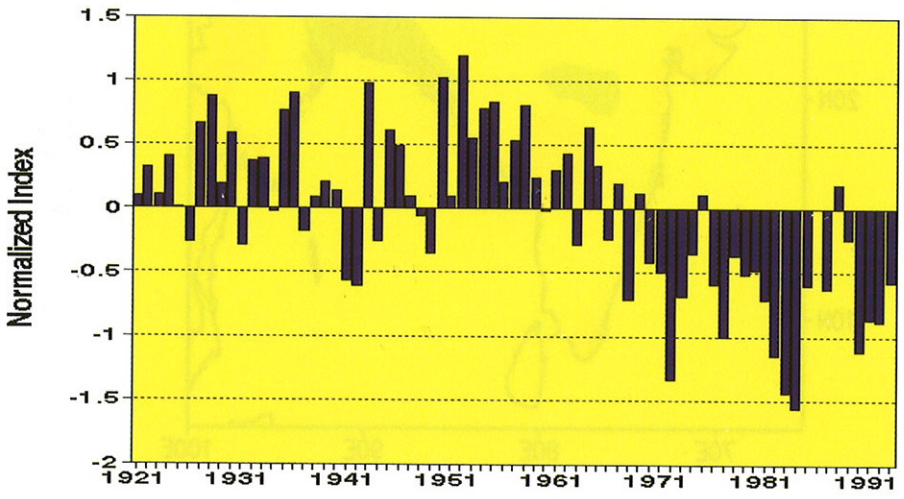

Figure 3.24 Precipitation index (average gamma percentiles of station precipitation within the region) for the western Sahel (June - September). (Source: CAC)

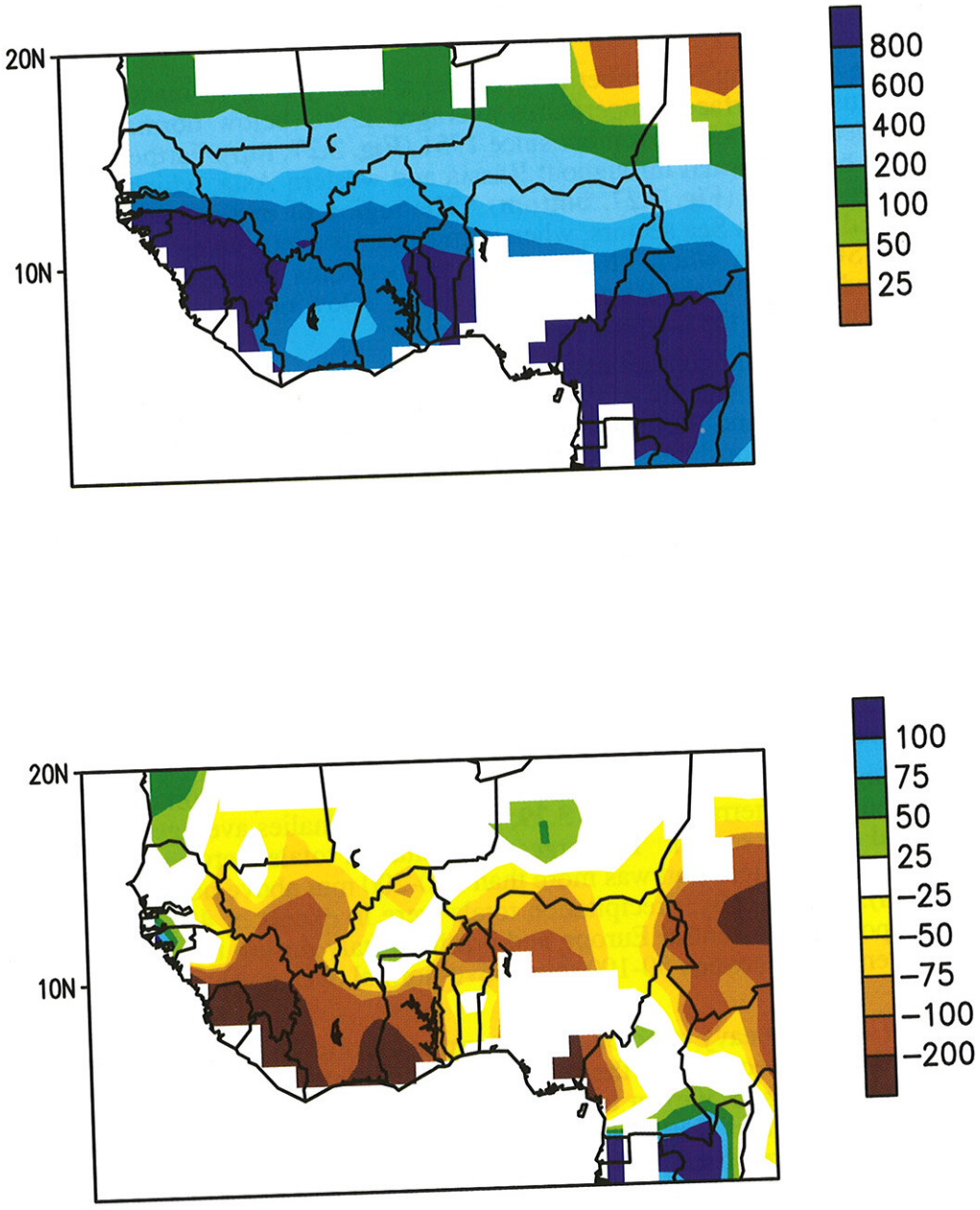

Figure 3.25 Precipitation (mm): total (top) and anomalous (bottom) for the western Sahel for May 1993 - September 1993. (Source: CAC)

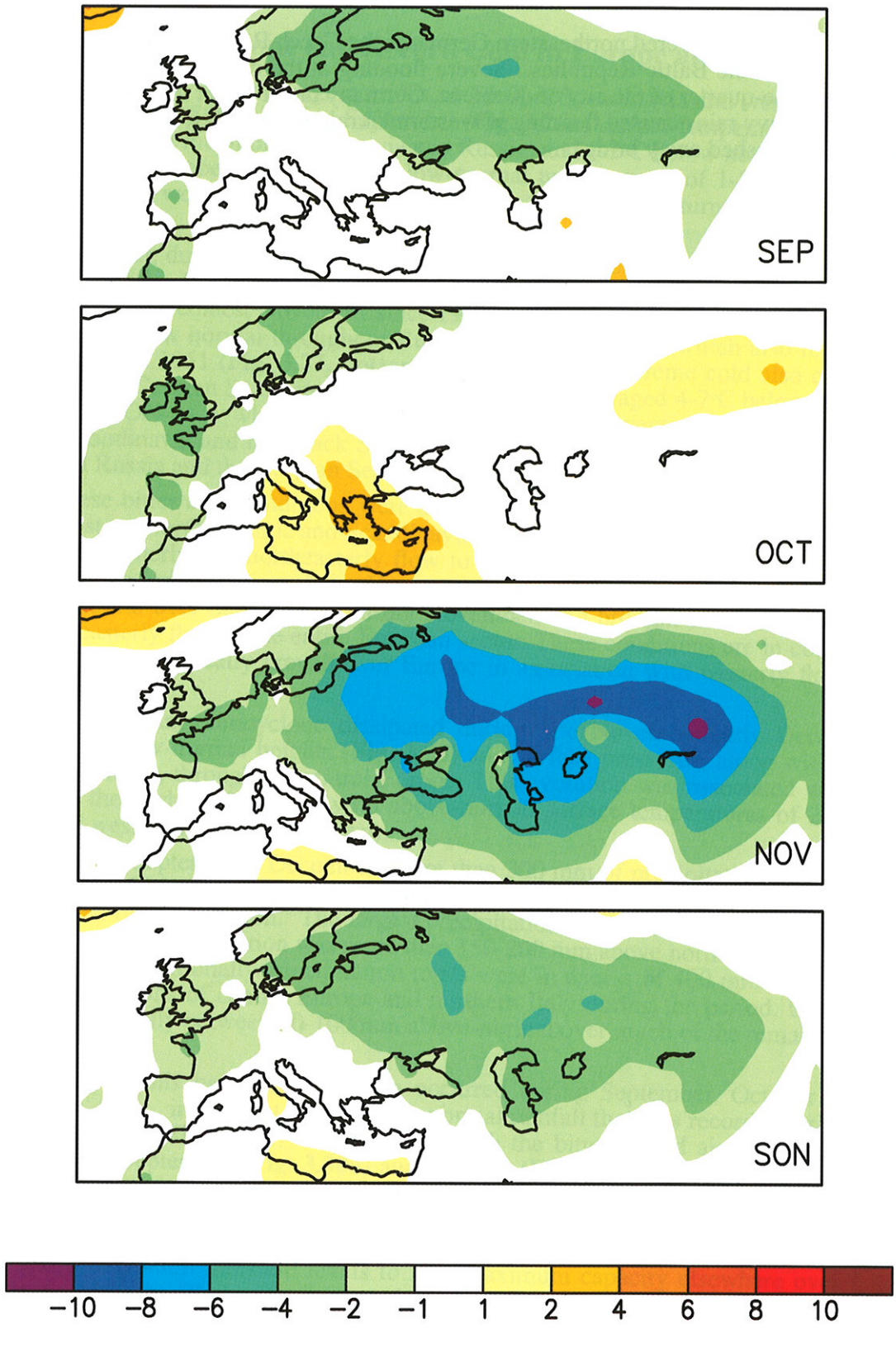

Figure 3.26 Surface temperature anomalies (°C) for: (a) September, (b) October, (c) November, and (d) September-November 1993 for Europe and western Asia. (Source: CAC)

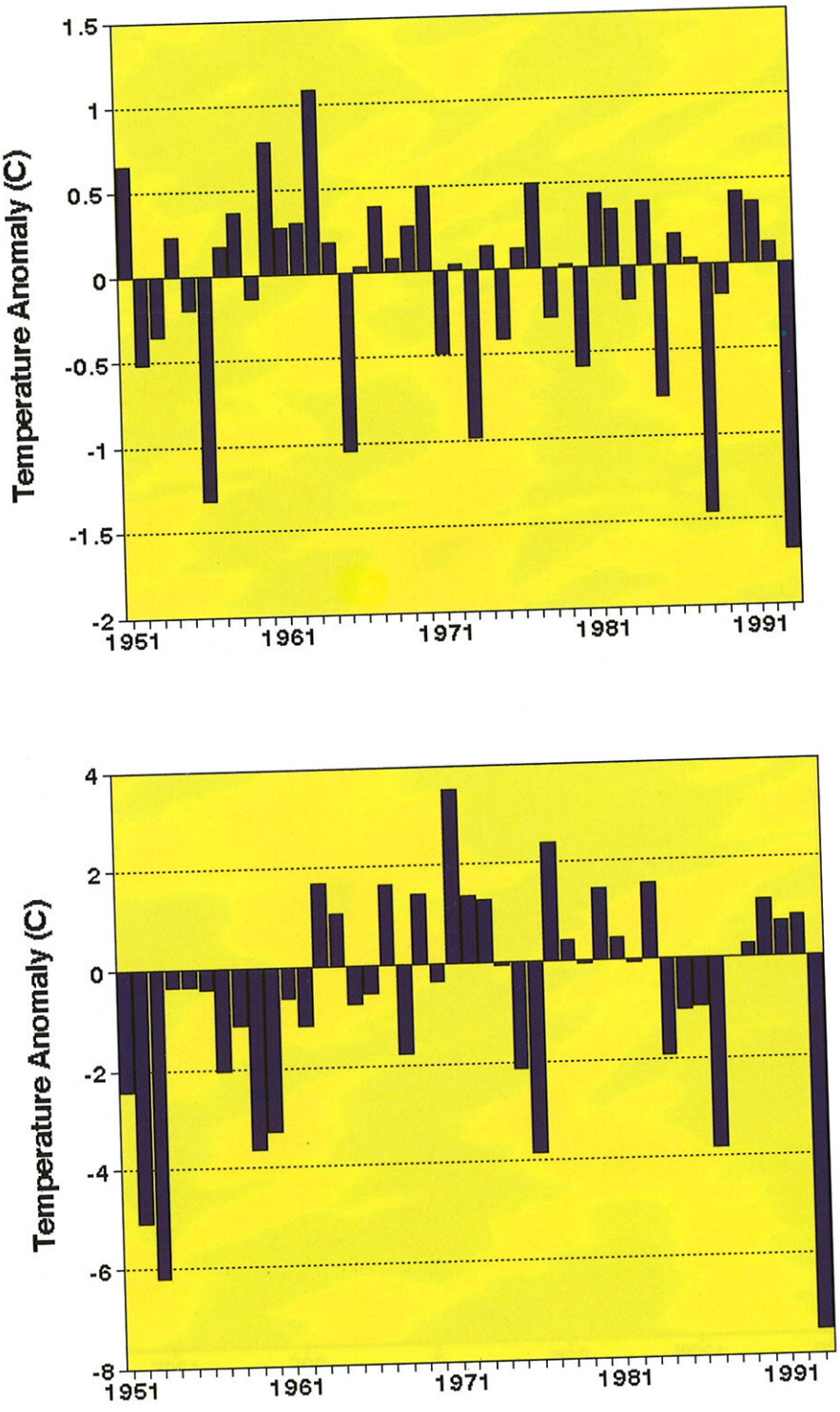

Figure 3.27 Time series of November temperature anomalies (°C) averaged over Europe (top) and western Asia (bottom). (Source: CAC)

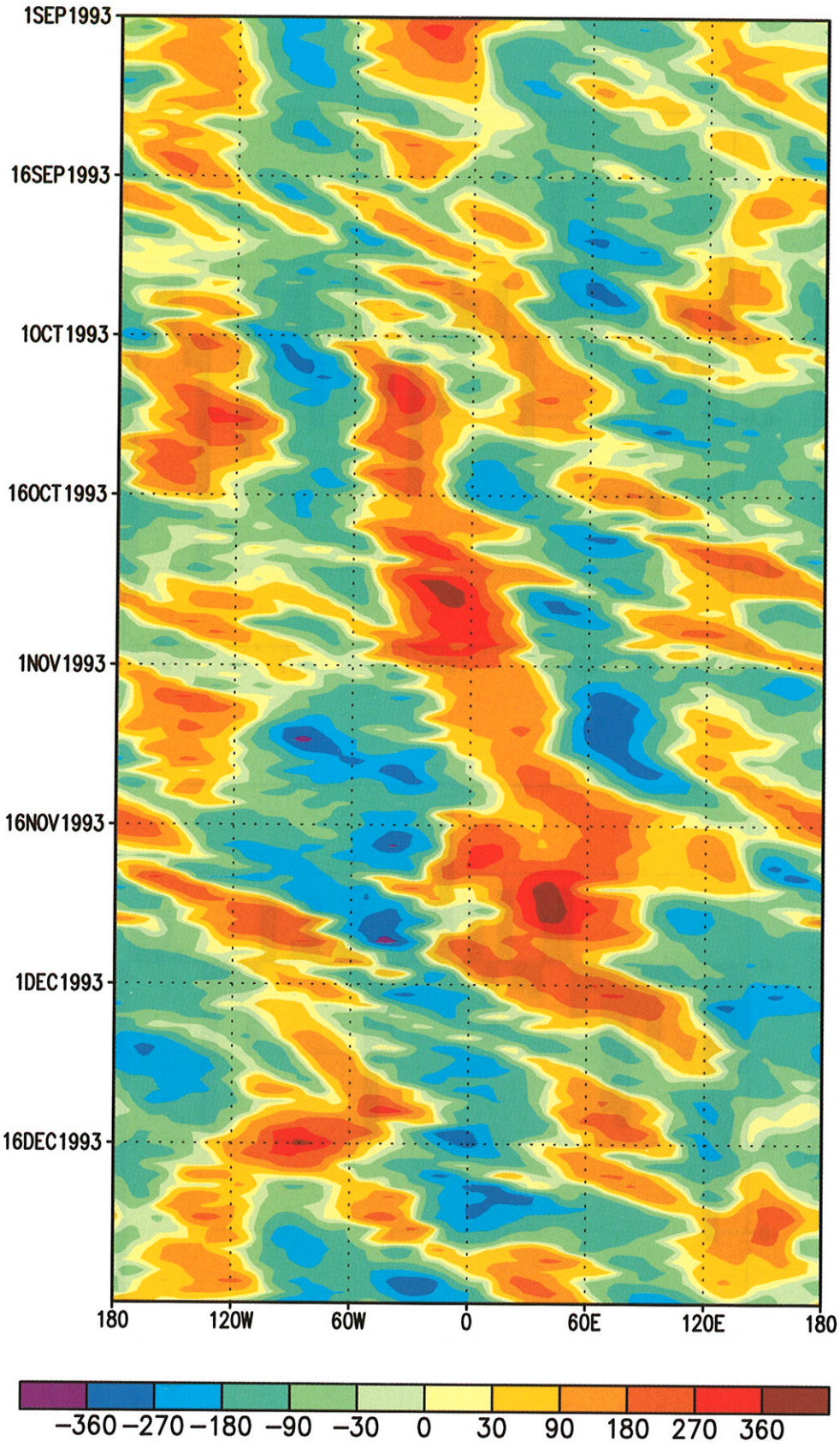

Figure 3.28 Time-longitude section of 500-mb height anomalies (m) during September - December 1993 averaged over the 5° latitude band centered on 60°N. (Source: CAC)

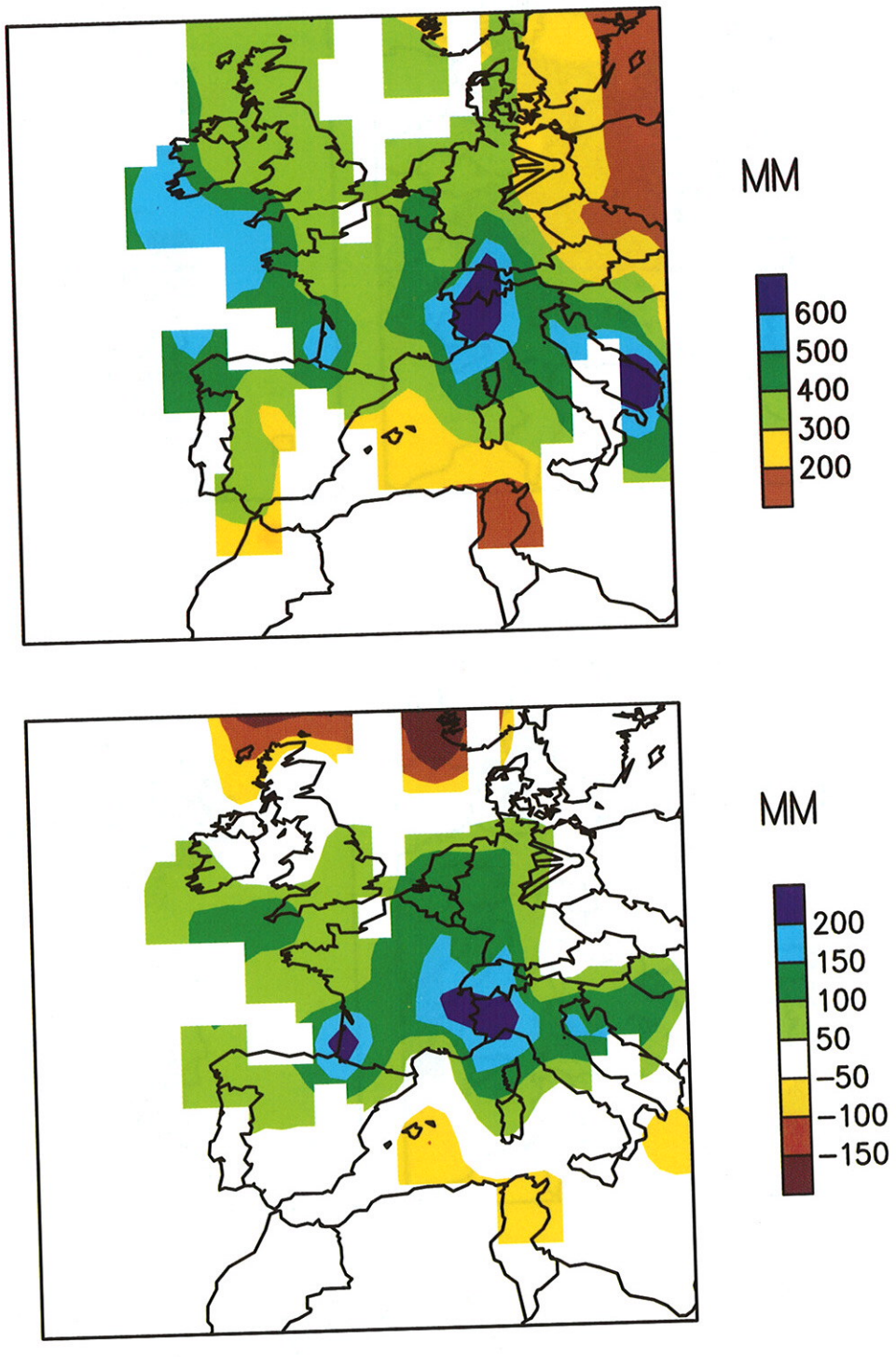

Figure 3.29 Precipitation (mm): total (top) and anomalous (bottom) for September - December 1993. (Source: CAC)

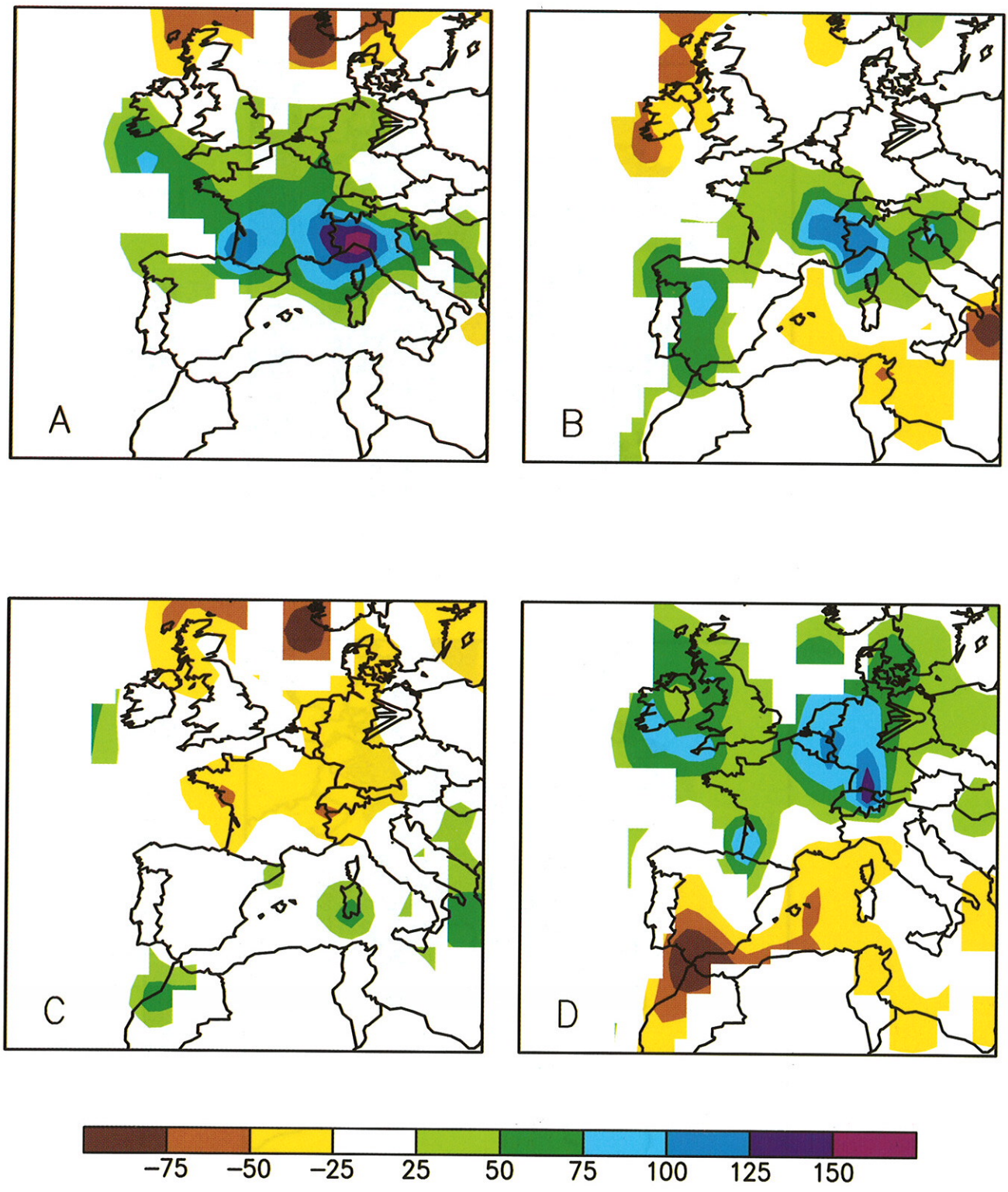

Figure 3.30 Anomalous precipitation (mm) for (a) September, (b) October, (c) November, and (d) December 1993. (Source: CAC)

h. United States Temperature and Precipitation Anomalies and Tornado Activity

The contiguous United States experienced temperatures that were much below the long-term mean (**Fig. 3.31**) during January-December 1993, and the year ranked as the 13th coldest on record (the record for the nationally-averaged temperature begins in 1895). The year also broke a string of three consecutive years with above to much-above average temperatures. It was only the second year of the last eight with temperatures below the long-term mean, and it was the coldest year since 1985. Annual temperatures averaged lower-than-normal for more than 70% of the contiguous United States. In the extreme categories (upper or lower 10th percentile), nearly a fourth of the country averaged much colder than normal while only two percent averaged much warmer than normal.

A tenth or more of the contiguous United States was much colder than normal during eight months in 1993, while only three months had a tenth or more of the country much warmer than normal (**Fig. 3.32**). The coldest months were February, September, and November. The circulation pattern during July was especially strong, with an upper-level trough over the northwest and north central states and a strong upper-level ridge over the southeastern states. This resulted in marked extremes in precipitation and temperature. Approximately a third of the country was much colder than normal and a fourth much warmer than normal, while record flooding occurred in the Midwest (see section 3d for more details).

The first half of 1993 was generally wet, with ten percent or more of the nation experiencing unusually wet conditions during five of the six months (**Fig. 3.33**). The unusually strong circulation pattern during July resulted in large parts of the nation (nearly a third each) experiencing either very wet or very dry conditions. Subsequent months were characterized more by dry conditions than by anomalous wetness.

According to preliminary data from the National Weather Service National Severe Storms Forecast Center, there were 1194 tornadoes across the United States during 1993 (**Fig. 3.34**). This total is second only to the 1297 tornadoes observed in 1992. The annual average for the 1953-92 period is 781. It should be noted that the preliminary tornado count is generally higher than the final count and that the tornado observations have generally improved with time.

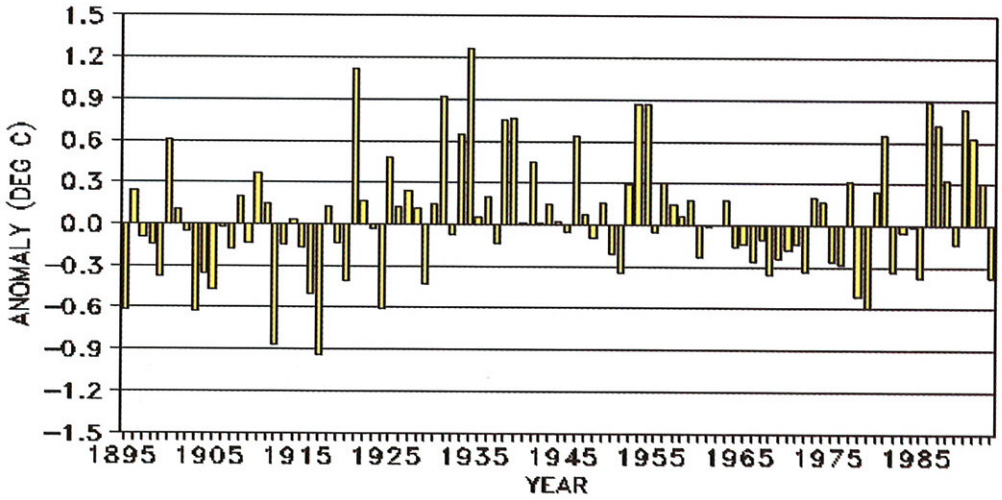

Figure 3.31 Annual surface temperature anomalies (°C) for the contiguous United States. Anomalies are computed from the 1961-1990 base period. (Source: NCDC)

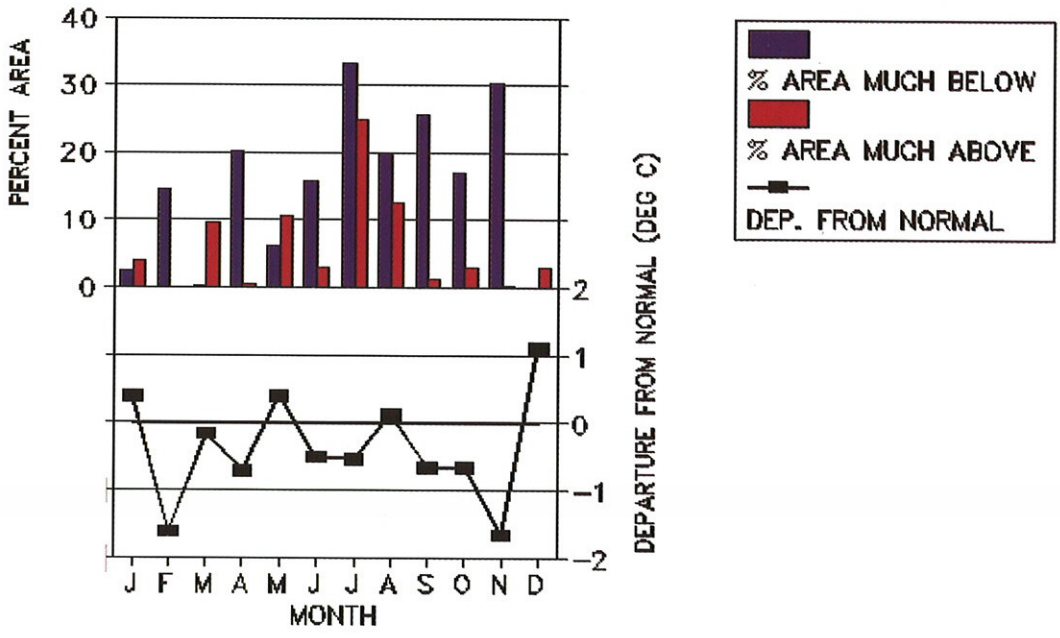

Figure 3.32 Percent area of the contiguous United States experiencing monthly mean temperatures in the upper and lower tenth percentile (top) and the monthly temperature departures from the 1961-1990 base period averaged across the contiguous U. S. (bottom). (Source: NCDC)

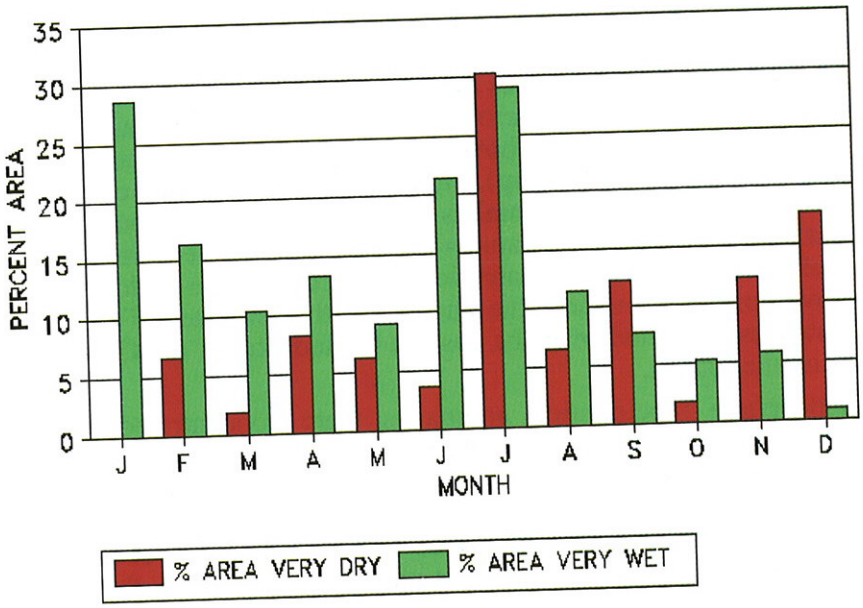

Figure 3.33 Percent area of the contiguous United States experiencing monthly mean precipitation totals in the upper and lower tenth percentile. Precipitation amounts in the upper tenth percentile are categorized as very wet and amounts in the lowest tenth percentile are categorized as very dry. (Source: NCDC)

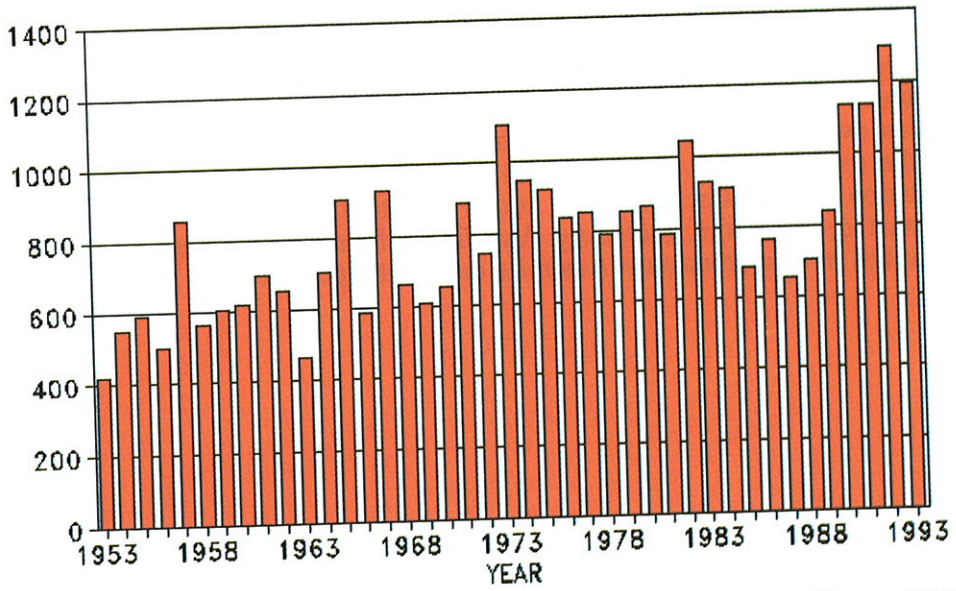

Figure 3.34 Annual number of observed tornadoes in the United States (1953-1993). (Source: NCDC)

4. SEASONAL SUMMARIES

a. December 1992-February 1993

In the Northern Hemisphere, above-normal surface temperatures covered Scandinavia, northern Europe, the former Soviet Union and much of central Asia during December 1992-February 1993 (DJF) (**Fig. 4.1, top**). Temperatures averaged 2-3°C above-normal over this region as a whole, and more than 4-5°C above-normal across the high latitudes of Eurasia. These anomalous temperatures tended to be associated with above-normal 500-mb heights and abnormally strong southwesterly geostrophic flow (**Fig. 4.2, top**), along with reduced snow cover and snow depth (not shown). Large surface temperature anomalies were also observed throughout North America during the season. At high latitudes, temperatures averaged 1°C above-normal over north-central Canada, and 3-5°C below-normal over the Labrador Sea sector. In the middle latitudes, temperatures were 2-4°C above-normal throughout the Pacific Northwest states. Farther south and east, above-normal temperatures prevailed over the eastern United States, the Gulf Coast States, and much of Mexico during the season.

Northern Hemisphere precipitation anomalies were concentrated primarily over the United States, Canada, southern Europe, and China (**Fig. 4.1, bottom**). Over North America, below-normal precipitation covered much of central Canada from coast to coast. Farther south, well-above-normal precipitation dominated the southwestern United States throughout the season, in association with a persistent large-amplitude trough centered over the region (**Fig. 4.2, top**). This feature was accompanied by significant winter storm activity throughout the region, and with a stronger-than-normal subtropical jet stream which extended northeastward from Hawaii to the southwestern United States. In California, this above-normal precipitation, along with a significantly above-normal snowpack at higher elevations, alleviated long-term drought conditions that had plagued the state since 1986 (see section 3a). Above-normal rainfall also covered the central United States during the season. This region had received excess precipitation since mid-summer 1992, and the continuation of these conditions during DJF helped to bring soil-moisture levels increasingly close to saturation in the region. These soil conditions eventually contributed to the overall magnitude of the Midwest floods of June-July 1993 (see section 3d).

In the Southern Hemisphere, summer surface temperature anomalies were relatively small (**Fig. 4.1, top**). Precipitation anomalies generally reflected the persistent ENSO episode, except for wetter-than-normal conditions in northern and southern Australia. At high latitudes, the Southern Hemisphere circulation was dominated by an anomalous zonal wave-one pattern, with positive anomalies over the south-central South Pacific and Antarctic Peninsula, and negative anomalies over the remainder of Antarctica and the southern Indian Ocean. In the middle latitudes, the circulation was characterized by broad negative anomalies over the central South Pacific and Indian Ocean sectors, including Australia. This latter feature was associated with above-normal rainfall over southeastern Australia during the period.

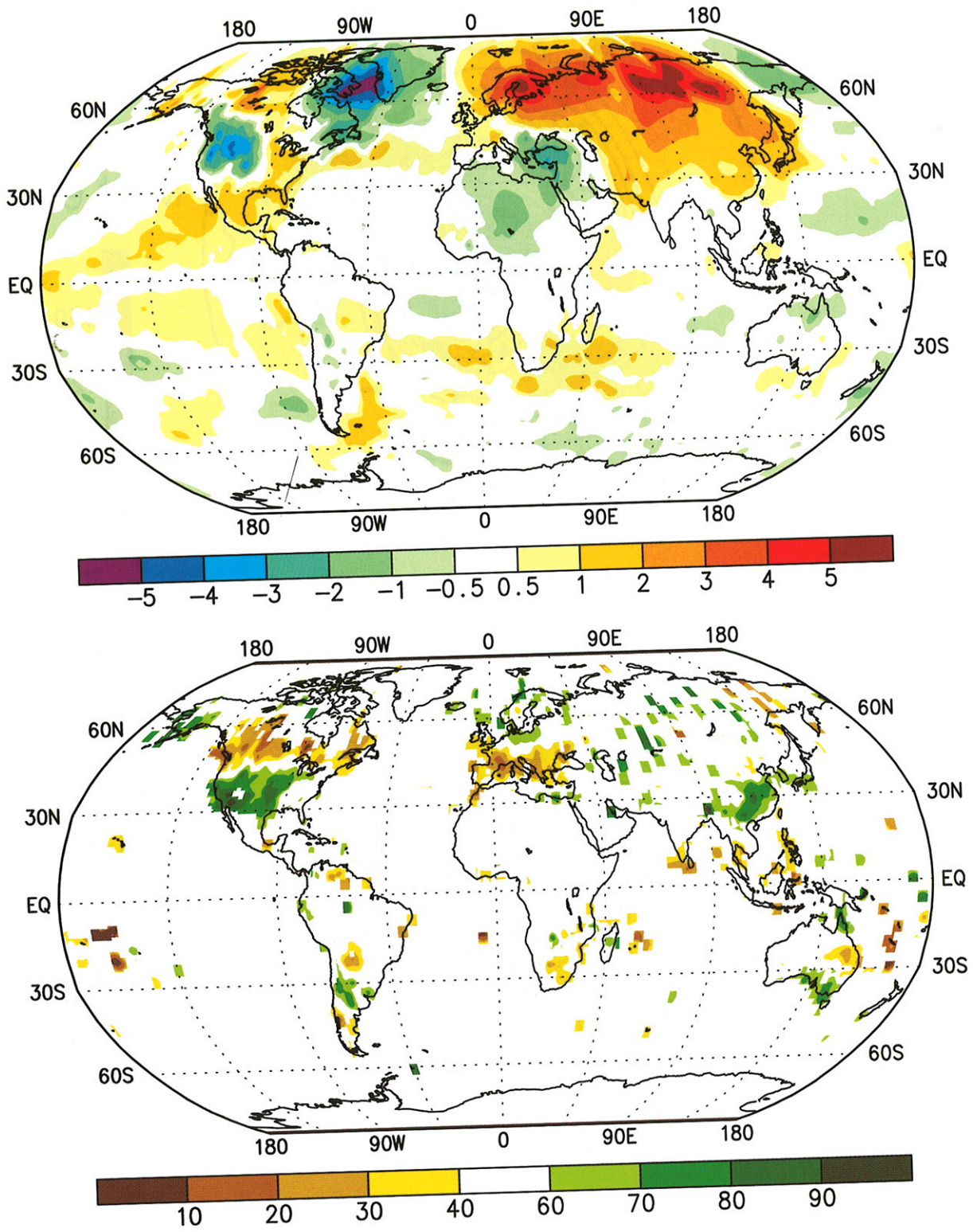

Figure 4.1 Surface temperature anomalies (°C) (top) and precipitation percentiles based on a gamma distribution fit to the 1961-1990 base period (bottom) for December 1992 - February 1993. Temperature anomalies are based on station data over land (1961-1990 base period) and sea surface temperature data (SST) over water (COADS/ ICE climatology). Analysis omitted in data-sparse regions. (Source: CAC)

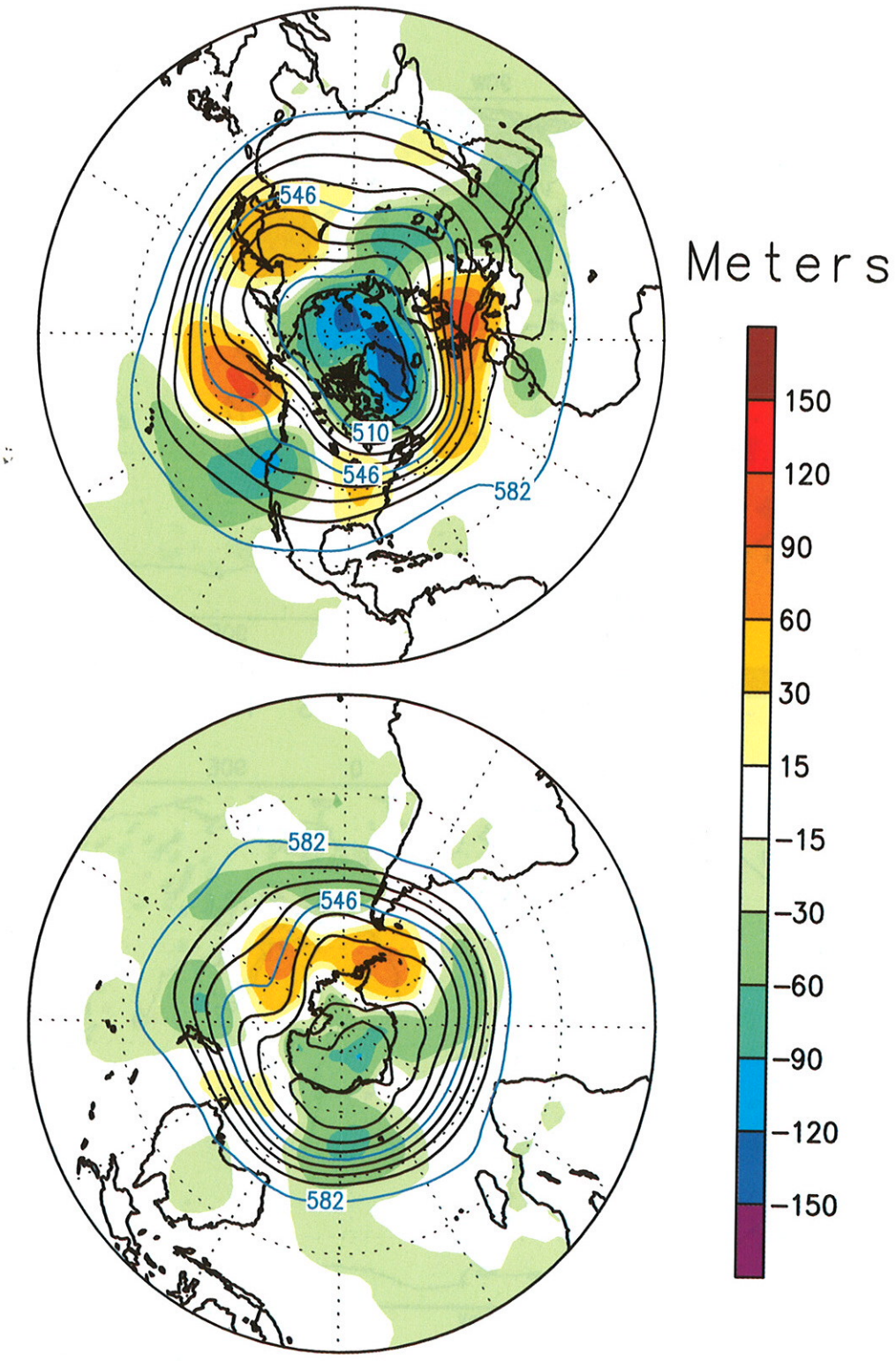

Figure 4.2. Northern Hemisphere (top) and Southern Hemisphere (bottom) 500-mb geopotential height (contours, interval is 9 dm) and anomalies (shading, in m) for December 1992 - February 1993. Anomalies are departures from the 1979-1988 base period. (Source: CAC)

b. March-May 1993

The western half of North America experienced above-normal temperatures (**Fig. 4.3, top**) during March through May (MAM) in association with a stronger than normal 500-mb ridge over the region (**Fig. 4.4, top**). These conditions were opposite to those which prevailed during DJF. In addition during MAM, the ridge over the western United States and Canada was undercut by stronger-than-normal westerlies throughout the Pacific Northwest, which brought enhanced precipitation to the region (**Fig. 4.3, bottom**). Over the eastern United States, below-normal temperatures and 500-mb heights prevailed during the season. This was also a reversal of the conditions that were observed during DJF. Elsewhere, above-normal rainfall continued over the central United States during MAM. This region had received above-normal rainfall since July 1992, and soil-moisture levels were near peak capacity prior to MAM. The above-normal rainfall during MAM further exacerbated these conditions, and created the potential for severe hydrologic problems throughout the Midwest.

Over large portions of Europe and the Middle East, the temperature and rainfall anomaly patterns during March-May persisted from the winter season. For example, above-normal surface temperatures continued over Europe and Scandinavia, while below-normal rainfall totals persisted throughout central Europe. Farther east, below-normal temperatures continued from the winter season over the eastern Mediterranean Sea, Turkey and the Black Sea sector.

The 500-mb circulation during the season (**Fig. 4.4, top**) was dominated by significantly below-normal heights throughout the middle latitudes of the North Pacific, reflecting an anomalously intense trough over the region. This feature is consistent with the presence of mature ENSO conditions in the tropical Pacific during the period. Negative height anomalies also dominated the Mediterranean Sea and Middle East during the season, in association with below-normal temperatures and rainfall throughout the region.

In the Southern Hemisphere, above-normal surface temperatures and below-normal rainfall dominated the subtropics near 28°S. These conditions were particularly prevalent over southern Africa, where anomalously warm and dry conditions persisted from DJF. Warmer and drier-than-normal conditions were also prominent over Australia, where above-normal temperatures dominated the entire continent and below-normal rainfall persisted from DJF in the east. Farther south, above-normal rainfall continued from DJF over large portions of central Argentina. Elsewhere, above-normal surface temperatures and above-normal SST's continued from DJF over the western South Atlantic just east of central Argentina, and over the region to the south of Africa.

The Southern Hemisphere circulation (**Fig. 4.4, bottom**) was dominated by below-normal 500-mb heights over Antarctica during the season, reflecting an enhanced circumpolar vortex over the region. This feature was flanked by positive height anomalies in the high latitudes of the southern extratropics. Farther north, negative height anomalies prevailed during the season over the central South Pacific. This feature is similar to that noted in the extratropical North Pacific, and may be linked to the redevelopment of mature ENSO conditions in the tropical Pacific.

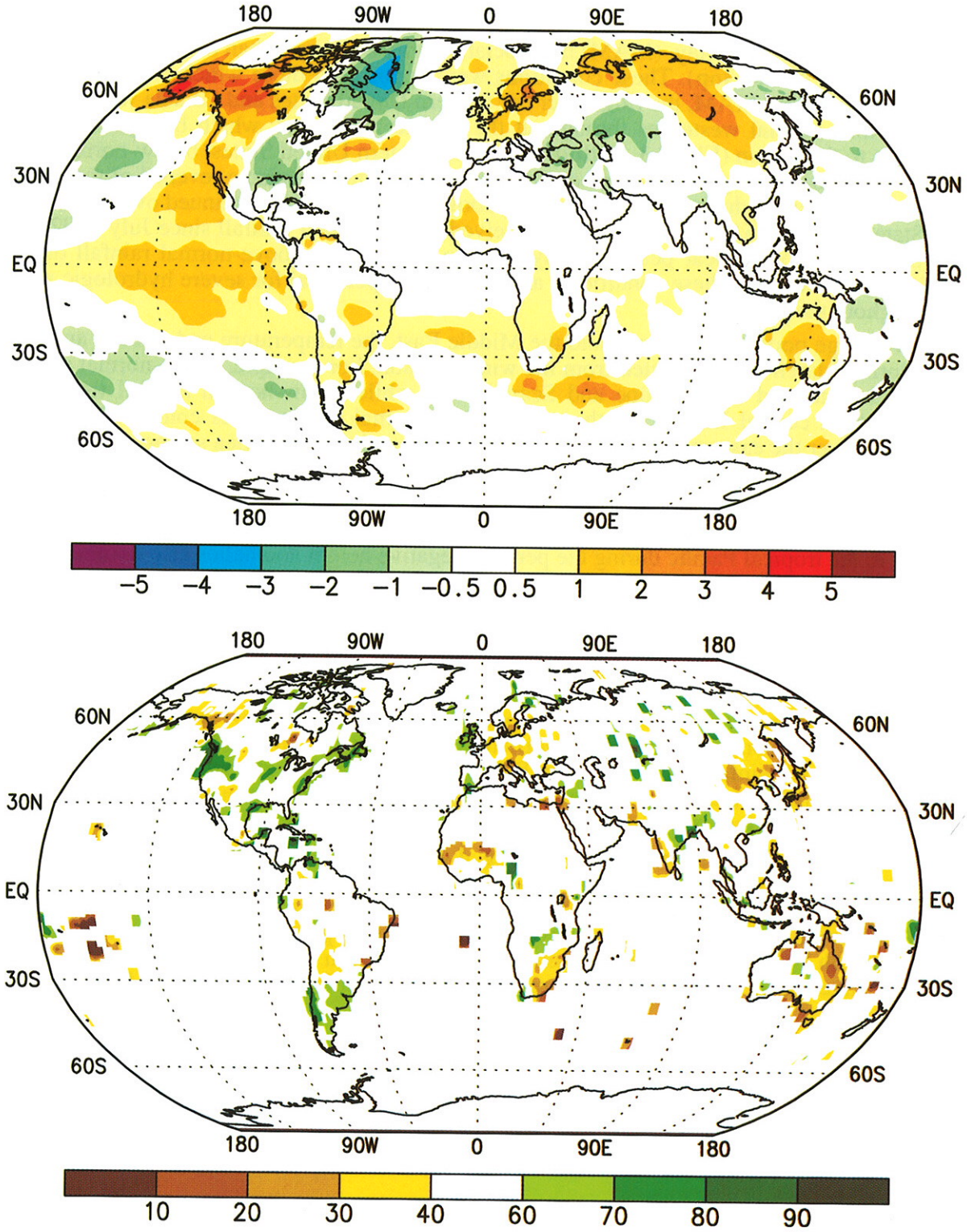

Figure 4.3 Surface temperature anomalies (°C) (top) and precipitation percentiles based on a gamma distribution fit to the 1961-1990 base period (bottom) for March - May 1993. Temperature anomalies are based on station data over land (1961-1990 base period) and sea surface temperature data (SST) over water (COADS/ICE climatology). Analysis omitted in data-sparse regions. (Source: CAC)

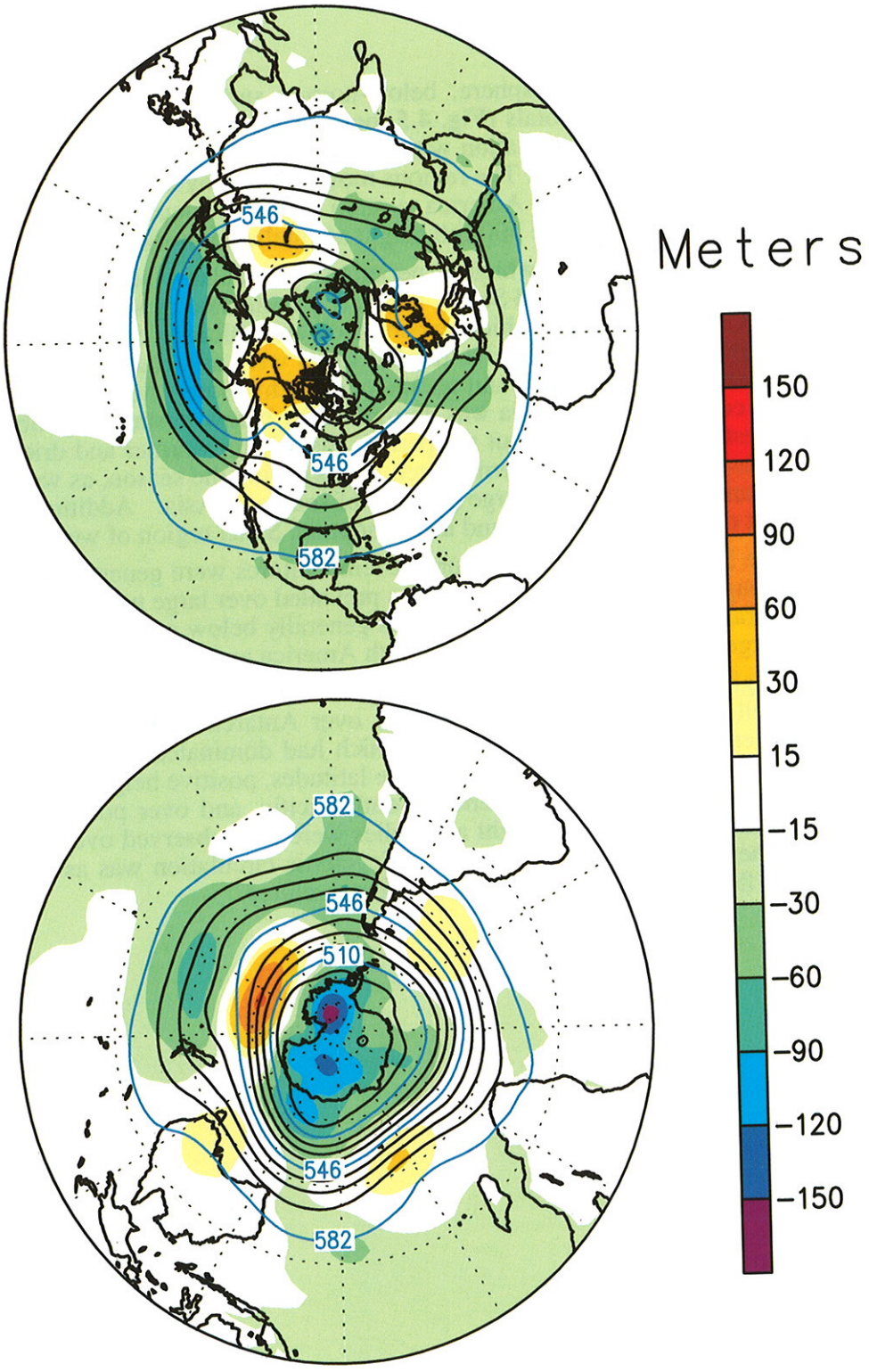

Figure 4.4 Northern Hemisphere (top) and Southern Hemisphere (bottom) 500-mb geopotential height (contours, interval is 9 dm) and anomalies (shading, in m) for March - May 1993. Anomalies are departures from the 1979-1988 base period. (Source: CAC)

c. June-August 1993

In the Northern Hemisphere, below-normal surface temperatures (**Fig. 4.5, top**) and above-normal precipitation totals (**Fig. 4.5, bottom**) dominated the middle latitudes during June through August (JJA), in association with generally below-normal height anomalies throughout the extratropics (**Fig. 4.6, top**). The regions most affected by colder and wetter than normal conditions included western North America, eastern China and Japan, and north-central Europe and western Russia, where negative 500-mb height anomalies prevailed throughout the season.

Two specific regions which experienced particularly severe conditions during June-August were the Midwest United States, which was inundated by severe and widespread flooding, and eastern China and Japan, which experienced anomalously cold and wet conditions. In the Midwest United States, the excessive rainfall totals were associated with below-normal 500-mb heights and extremely persistent and anomalous southwesterly flow throughout the region (**Fig. 4.6, top**). In contrast, eastern Asia was dominated by below-normal 500-mb heights and anomalous northwesterly flow throughout the period. Elsewhere, warmer and drier than normal conditions were observed over the eastern United States during the season, as well as in the vicinity of the Mediterranean Sea and over large portions of southeast Asia. Additionally, monsoon rainfall was deficient over southern India, and throughout the Sahel region of western Africa.

In the Southern Hemisphere, surface temperatures were generally near normal during the season, although above-normal temperatures prevailed over large portions of southern Africa and eastern Australia. Precipitation over land was generally below normal during the season, particularly over large portions of south-central South America and over northeastern Peru.

At high latitudes, the Southern Hemisphere circulation during JJA continued to be dominated by well-below-normal 500-mb heights over Antarctica (**Fig. 4.6, bottom**). This feature reflected an enhanced circumpolar vortex which had dominated the region for six consecutive months by the end of the season. In the middle latitudes, positive height anomalies continued over southeastern Australia across the central South Pacific, and over portions of the southwestern South Atlantic. Weak positive height anomalies were also observed over southern South Africa. In each of these regions, the anomalous anticyclonic circulation was associated with enhanced equatorward flow and above-normal surface temperatures.

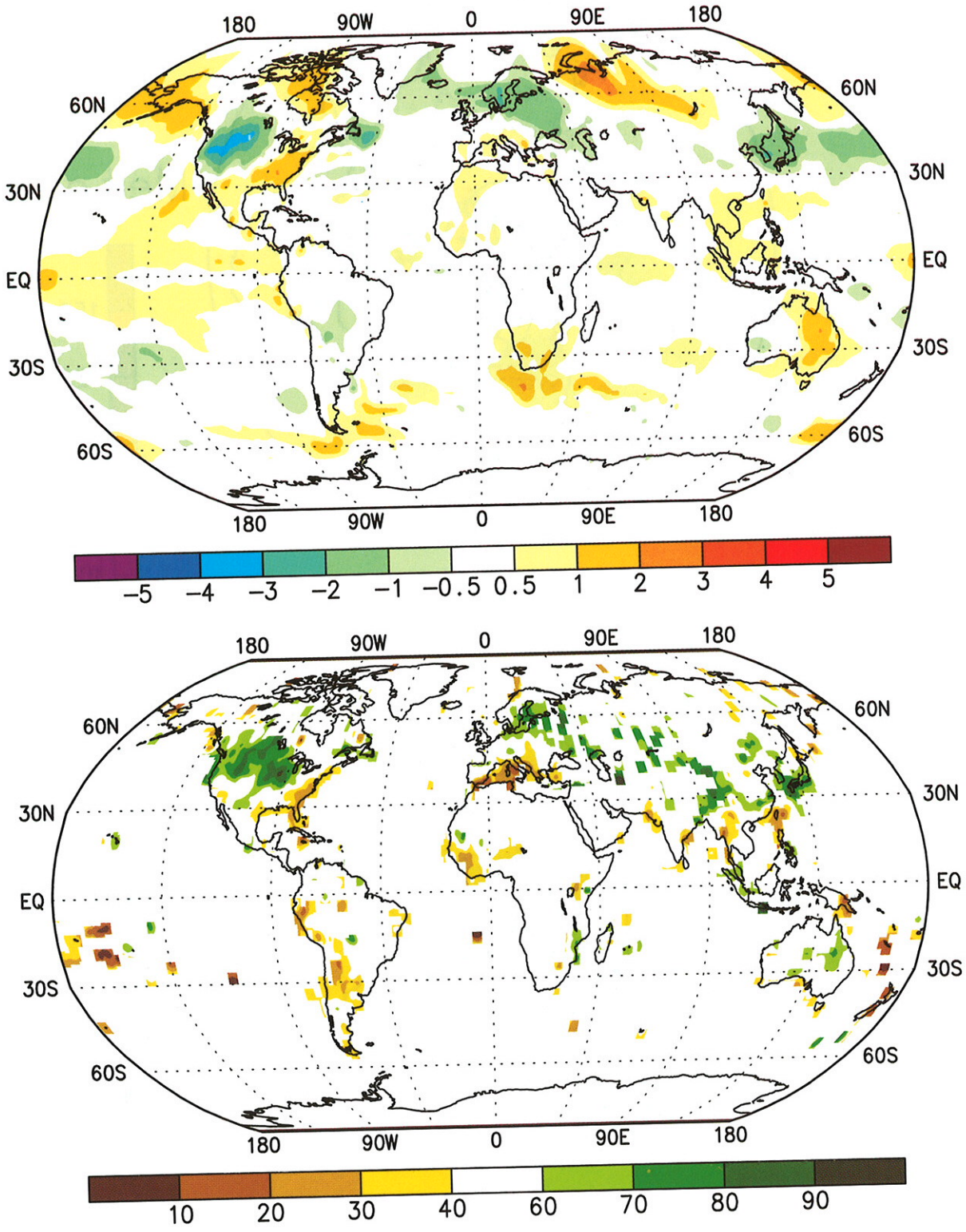

Figure 4.5 Surface temperature anomalies (°C) (top) and precipitation percentiles based on a gamma distribution fit to the 1961-1990 base period (bottom) for June - August 1993. Temperature anomalies are based on station data over land (1961-1990 base period) and sea surface temperature data (SST) over water (COADS/ICE climatology). Analysis omitted in data-sparse regions. (Source: CAC)

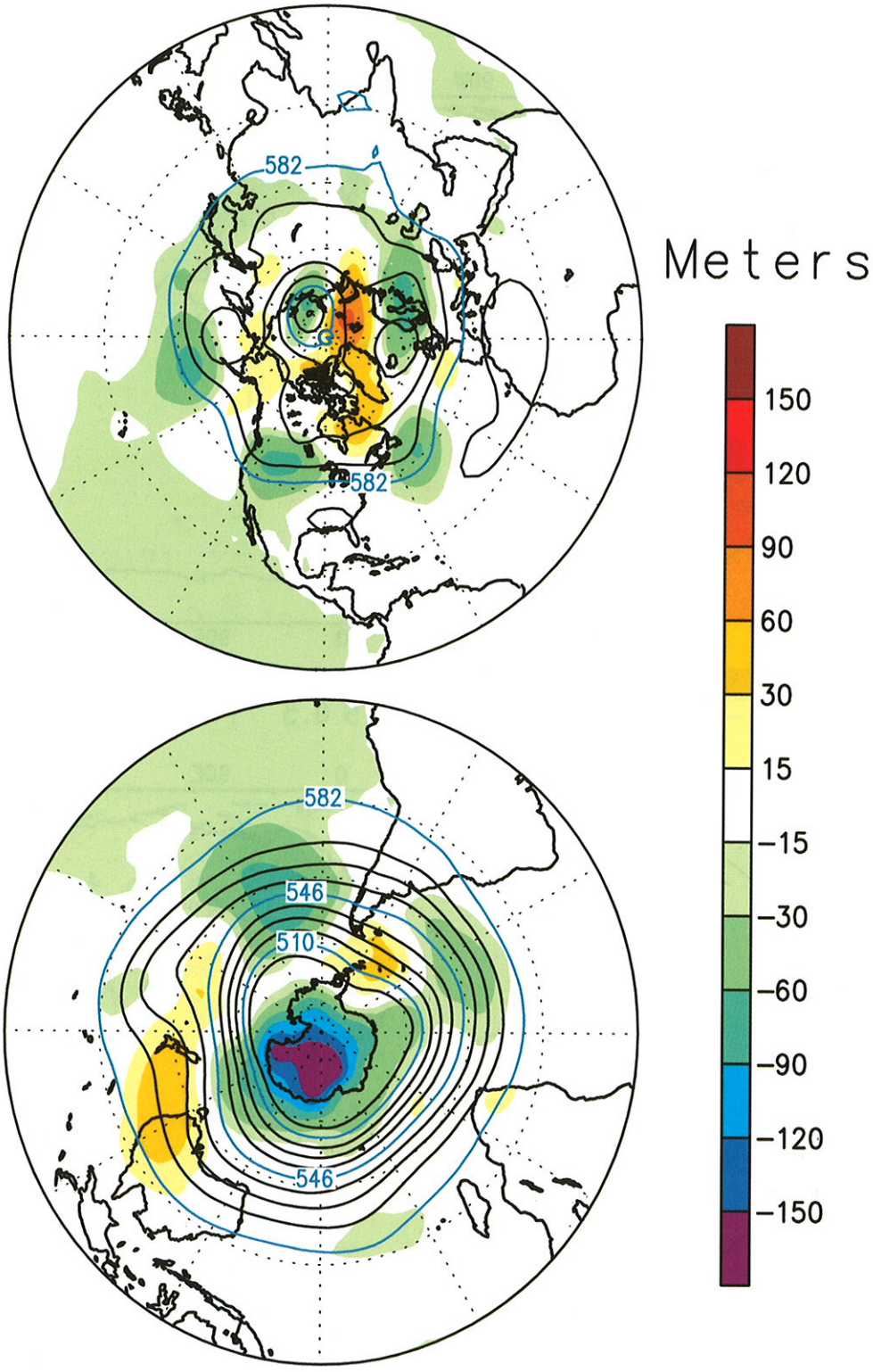

Figure 4.6 Northern Hemisphere (top) and Southern Hemisphere (bottom) 500-mb geopotential height (contours, interval is 9 dm) and anomalies (shading, in m) for June - August 1993. Anomalies are departures from the 1979-1988 base period. (Source: CAC)

d. September-November 1993

Over North America, above-normal temperatures covered Alaska and western Canada during September-November (SON), while below-normal temperatures dominated the central United States and central Canada (Fig. 4.7, top). These anomalies were associated with above-normal 500-mb heights and anomalous southerly flow over the Gulf of Alaska, and with below-normal 500-mb heights and anomalous northwesterly flow over central Canada and the Great Lakes (Fig. 4.8, top). This anomalous circulation was accompanied by above-normal precipitation over southern Alaska and over the central and eastern United States, and by below-normal precipitation over the northwestern United States and southwestern Canada (Fig. 4.7, bottom). In the Midwest, the continuation of above-normal precipitation for the sixth consecutive season beginning mid-summer 1992, kept soil-moisture levels near maximum capacity.

Record cold gripped large portions of Europe, Scandinavia and western Asia during SON (**Fig. 4.7, top**) (see section 3g). Temperatures averaged 1-2°C below normal over Europe, Scandinavia and the Black Sea during the season, and 3-4°C below normal over large portions of western and central Russia and the Caspian Sea sector. These anomalies were particularly pronounced during November, with Europe, Russia and central Asia all reporting their coldest November since at least 1951 (**Fig. 3.28**). These record cold conditions were associated with a major blocking anticyclone centered over the eastern North Atlantic and Scandinavia throughout SON (**Fig. 4.8, top**). This feature brought anomalous northerly and northeasterly flow to the region, along with a marked decrease in the strength of westerly, onshore flow. These conditions are in contrast to the mild conditions that typically prevail over Europe in association with westerly flow off the North Atlantic.

Additionally, above-normal rainfall covered large portions of central Europe and northern Italy (**Fig. 4.7, bottom**), in association with a stronger than normal trough at 500-mb. Well above-normal precipitation then continued during December over much of the region, resulting in a swath of locally heavy flooding extended from western Europe eastward to Israel (see section 3g).

In the Southern Hemisphere, temperatures were near normal during SON over much of South America and Australia (**Fig. 4.7, top**). In Africa, above-normal temperatures were confined to the eastern Sahel region and to southwestern Africa. Excessive precipitation characterized large portions of the Southern Hemisphere in a belt near 30°S (**Fig. 4.7, bottom**), with above-normal precipitation reported over Northern Argentina and Uruguay, over most of south Africa, and over eastern Australia. These regions were associated with positive 500-mb height anomalies (**Fig. 4.8, bottom**) and with anomalous poleward geostrophic flow in the middle and upper troposphere. At higher latitudes, negative height anomalies and an enhanced circumpolar vortex continued to dominate the circulation over Antarctica. During October, this enhanced circumpolar vortex was associated with record low ozone values and with an area of significant ozone depletion encompassing an area as large as the Antarctic subcontinent (see section 1c).

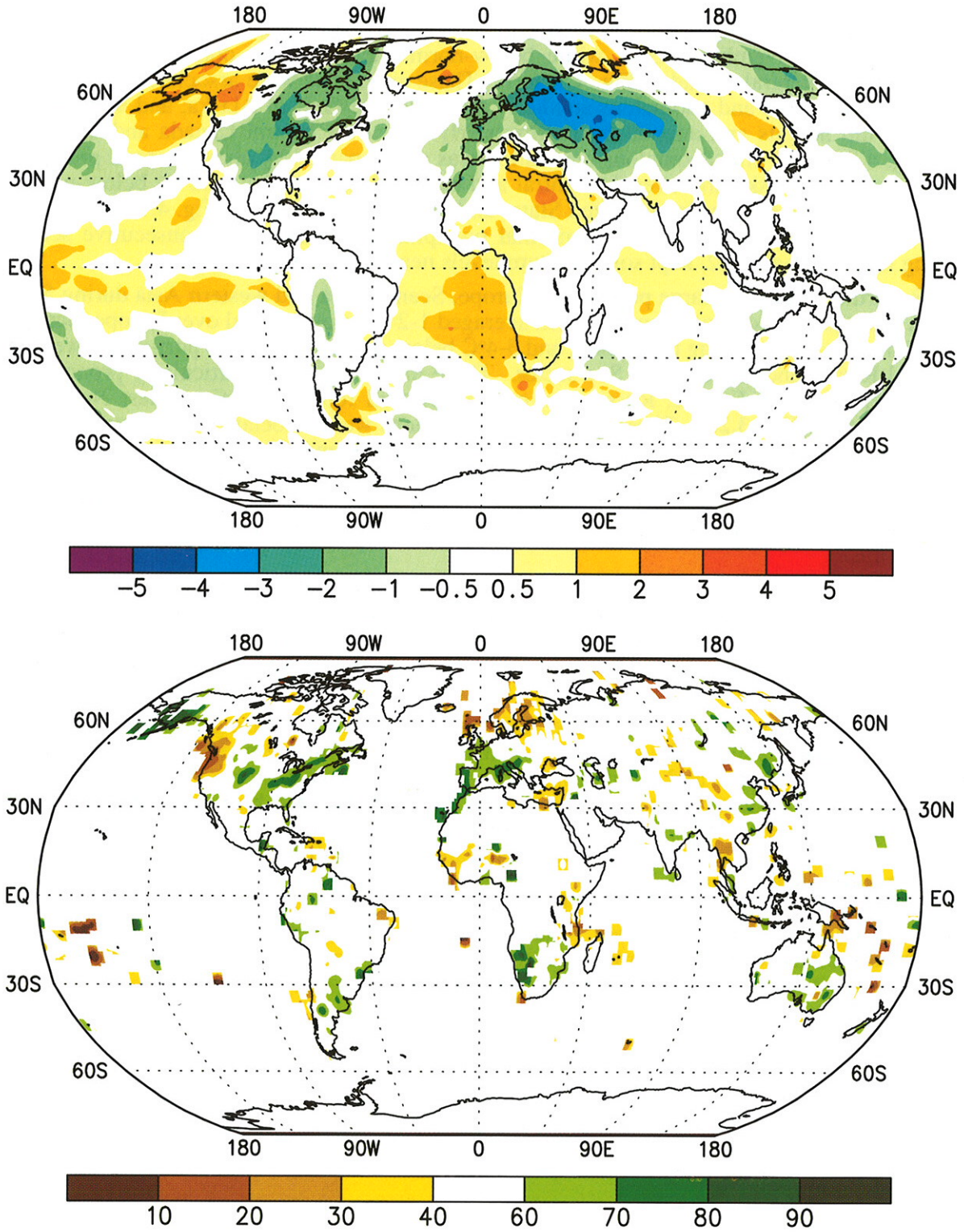

Figure 4.7 Surface temperature anomalies (°C) (top) and precipitation percentiles based on a gamma distribution fit to the 1961-1990 base period (bottom) for September - November 1993. Temperature anomalies are based on station data over land (1961-1990 base period) and sea surface temperature data (SST) over water (COADS/ ICE climatology). Analysis omitted in data-sparse regions. (Source: CAC)

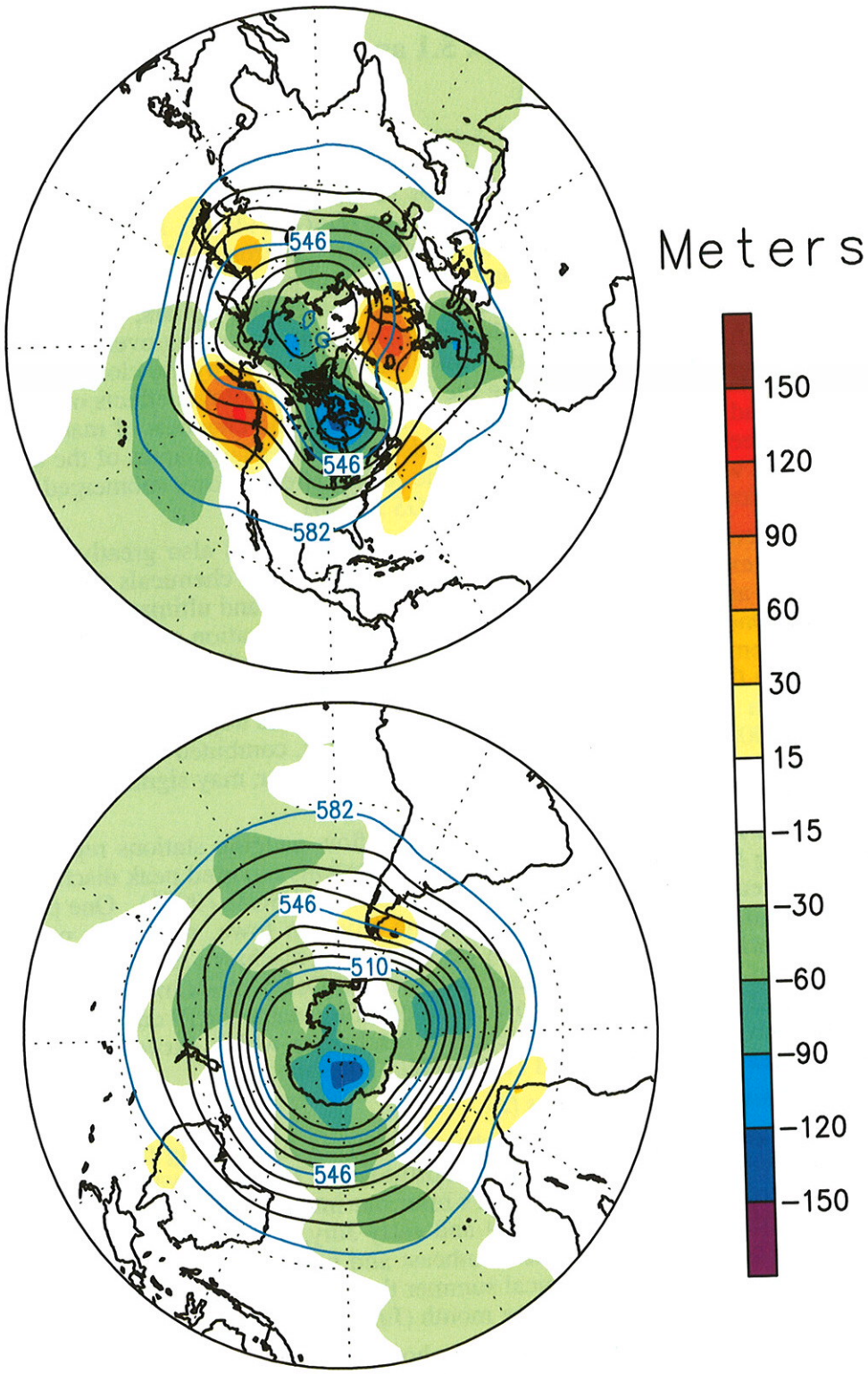

Figure 4.8 Northern Hemisphere (top) and Southern Hemisphere (bottom) 500-mb geopotential height (contours, interval is 9 dm) and anomalies (shading, in m) for September - November 1993. Anomalies are departures from the 1979-1988 base period. (Source: CAC)

5. CLIMATE IMPACTS (Figs. 5.1 and 5.2)

Central United States (1)

The midwestern United States experienced one of its worst flooding events on record during June-July 1993 (see section 3d). According to the United States Geological Survey (USGS), the damages from the floods in terms of property damage, disrupted business, and personal trauma was unmatched in United States history (*USGS 1993a*). More than 12 million acres were inundated by the floods, according to the International Erosion Control Association (*IECA 1993*), 26 people were killed and more than thirty thousand people were forced to evacuate their homes. Property damage alone was expected to exceed 10 billion dollars, and many major roads were either closed or submerged during the floods, severely disrupting overland transportation and the distribution of goods. Transportation was further disrupted by the closing of the Mississippi and Missouri Rivers to navigation during the event. The hydrologic effects of the floods were severe and widespread. Numerous levees failed, the banks and channels of many rivers were severely eroded, and deep layers of sediment were deposited over large areas of the adjacent flood plains. This situation was exacerbated because the record stream flows submerged many areas that had not been previously affected by floods (*USGS 1993b*).

The normal transport of agricultural chemicals was also greatly affected by the floods. For example, extraordinarily large amounts of agricultural chemicals were flushed into the Mississippi River and many of its tributaries (*USGS 1993c*), and ultimately transported into the Gulf of Mexico. One particular item of interest is the concentration and transport of atrazine through the river systems, a widely used but potentially toxic fertilizer. The total load of atrazine discharged to the Gulf of Mexico between April and August (539,000 kg) was 80% larger than the same period in 1991 and 225% larger than in 1992. This huge discharge of atrazine, along with nitrates (827,000 tons) and other fertilizer compounds, combined with an abnormally large transport of freshwater into the Gulf of Mexico in mid-summer, may significantly affect the ecosystem along the Louisiana coast (*USGS 1993c*).

In the nine-state flood area, 41 stream-flow-gauging stations reported record peak discharges during June and July. Additionally, 45 stations reported peak discharges with recurrence intervals of greater than 100 years during this period (*USGS, 1993b*). One particular river which experienced major flooding was the Raccoon River in Iowa, where the peak discharge at Van Meter was nearly twice as large as any previous peak discharge recorded at that site in almost 80 years of record. Flooding of the Raccoon River at Des Moines inundated the city's water treatment plant, and forced the city to go without drinking water for 19 days. Elsewhere, the Missouri River at Boonville, Missouri also reported discharges which exceeded previous historic flood peak discharges in 1951, 1903 and 1844 (*USGS 1993b*).

Southeastern United States (2)

Moisture shortages were first observed during April along the South Atlantic Coast. In May and June, subnormal rains fell from northeastern Texas eastward to the Atlantic Coast, with the exception of Tropical Storm Arlene's brief but intense rains in mid-June. Scattered showers brought limited relief during late June and early July, but an intense heat wave aggravated the unusually dry conditions across the Southeast and mid-Atlantic during mid-July. Although the heat wave was short-lived, the typical summer thunderstorms did not ensue as Dallas-Fort Worth, TX endured the first precipitation-free month (July) in 90 years.

Temperatures averaged up to 3°C above normal across the southeastern quarter of the country through June and July, with Augusta, GA reaching at least 35°C on 47 of the 61 days during the period. Dry weather persisted well into August, and the dryness spread southward into northeastern Mexico during the last half of the month. Hurricane Emily brushed the Outer Banks of North Carolina as September approached, dropping over 175 mm of rain on Cape Hatteras, but recurved northeastward and denied relief to the rest of the area.

Precipitation increased in September, but scattered areas with continuing moisture shortages were observed well into October before abundant rains and early-season snows provided relief from the long-term dryness. According to the U. S. Department of Agriculture, the combined effects of the floods and drought generated corn and soybean yield drops of 33% and 17%, respectively, from the previous year's favorable output.

Eastern United States (3)

In mid-March, the "Storm of the Century" brought significant snows as far south as southern Alabama and northern Florida while 30 to 120 cm of snow buried the northeastern quarter of the country from Tennessee and North Carolina northeastward across the eastern Ohio Valley, northern mid-Atlantic, and New England. To the south of the wintry conditions, a line of severe thunderstorms generated a storm surge of 3-4 meters along the Gulf Coast of Florida, with wind gusts exceeding 160 kph, and a deadly tornado outbreak. The storm claimed more than 240 lives, caused an estimated one billion dollars in damage, and may have generated several billion dollars in snow removal expenses. In addition, central pressures dropped to an estimated 960 mb in central Delaware, and several new low-pressure records were broken along the storm's path up the Atlantic Coast, some of which dated back to Hurricane Hazel (October 1954).

Western United States (4)

The long-term drought in the Far West was broken when excess winter (1992-93) precipitation, exceeding 600% of normal in parts of Arizona and southern California, significantly increased the region's snowpack and raised river and reservoir levels. One feature of the 1992-93 wet season was the relative "coldness" of the storms that affected the region, allowing a greater than normal proportion of each storm's precipitation to fall as snow, especially in the higher elevations of California and Oregon. Deep mountain snowpack is critical, since spring and summer snowmelt provides much of the region's usable water. Reservoir storage in California reached the highest level since 1987, and precipitation in water-critical areas, total water-year runoff, and snow water content were at or above the levels measured during the "flood" season of 1985-1986. Unfortunately, drought relief in California, Nevada, and Arizona was accompanied by flash floods and mudslides, particularly in January. Serious flooding in Arizona and southern California claimed several lives and caused considerable property and crop damage as Arizona's Gila River swelled to over 50 times its normal flow at the head of the Safford Valley.

Southern California (5)

During late October and early November, the pressure gradient between high pressure centered over Utah and a low in northwestern Mexico provided strong Santa Ana (easterly) winds across southern California. These gusty winds, blowing off the Southwestern deserts, created very low relative humidities and high temperatures, generating an extremely hazardous fire situation. In addition, last winter's (1992-93) ample precipitation had resulted in the abundant growth of grasses, which combined with dead brush and timber from the previous long-term drought (1986-1992) to provide ample fuel for the rapid spread of fires. Whipped by the strong Santa Ana winds, dozens of wildfires charred over 800 km^2 of land, destroyed more than 1,000 homes, claimed 4 lives, injured hundreds, displaced thousands of people, and caused an estimated one billion dollars in damage.

Europe (6)

Much above normal rainfall during August and parts of September and October (see **10**) left much of the region's soils saturated (see section 3g). In early December, strong storms pounded Europe with 145 kph wind gusts and torrential rains, generating the worst flooding in 60 years across parts of France, Belgium, the Netherlands, Luxemburg, and Germany. The floods claimed several lives, forced thousands of individuals to flee their homes and caused more than $580 million (U. S.) in damage in Germany alone, according to press reports. Severe flooding at the confluence of the Mosel and Rhine Rivers left one-quarter of Koblenz under water. Between 130 to 275 mm of precipitation drenched the already-saturated region in December.

Japan and Southeastern Asia (7)

Very heavy rain saturated much of the region during May and June, with considerable flooding reported in southern China and Taiwan. Shortly thereafter, abundant rains fell on much of Japan from mid-June through mid-August. Over 2,000 mm inundated parts of Kyushu during the period as tropical cyclones affected the islands, generating localized flooding and taking several lives. Farther south, a steady progression of tropical cyclones brought strong winds and torrential rains to the Philippines, Vietnam, and southeastern China beginning in late July. The Philippines were affected by 32 tropical systems during 1993 (the most on record for a single year), with as much as nine times the normal precipitation deluging parts of southern Luzon during the last 45 days of the year. Strong winds and flooding with the tropical systems reportedly took hundreds of lives across the Philippines and Vietnam through the last three months of 1993. Across Japan, relatively dry weather prevailed during most of October and November, but heavy precipitation resumed in early December. As December ended, surplus precipitation continued to fall on southern Japan.

Europe and Northwestern Africa (8)

Little or no precipitation fell on southwestern Europe and northwestern Africa during early January. This dryness spread eastward and northward as the month progressed. The prolonged dry spell reportedly affected the winter wheat crop of Morocco and forced restrictions on irrigation and reductions in hydroelectric output. Except for some brief rains in early March, the abnormally dry weather persisted until widespread rains dampened much of Europe in mid-April. The relief, however, was short-lived, with abnormally warm and dry conditions slowly redeveloping through May and covering most of southern Europe through the summer. Readings soared to 39°C in Athens, Greece as stagnant air created a severe pollution episode in June, and highs exceeded 40°C in parts of Italy, Greece, and Bulgaria in late August. Cooler air eventually overspread the Continent in early September, providing relief from the late-summer heat wave, and by the middle of the month, powerful storms ended the dry spell across most of the region. In parts of southeastern Europe the prolonged dryness observed through much of 1993 continued a trend of consistently below-normal precipitation since late 1991. During December 1991 through mid-November 1993, less than half of the normal precipitation fell on southeastern Bulgaria and many of the Greek islands. These prolonged drought conditions had forced Greece to enact numerous water conservation measures, but a wet and stormy November helped the parched region.

Southeastern Europe, Southwestern Asia, and Northeastern Africa (9)

Heavy snow reportedly paralyzed portions of Turkey and widespread flooding affected Baghdad, Iraq during January 1993. In addition, repeated blasts of cold air plunged through the region, dropping lows to -7°C in northern Saudi Arabia, -27°C in northeastern Turkey, and -40°C in the higher elevations of west-central Iran. Some parts of the Iranian desert reportedly observed snow for the first time in fifteen years. Typically dry and mild conditions returned in early February, but by mid-month, very cold air penetrated as far south as southern Egypt and central Saudi Arabia while abnormally wet weather covered much of the Middle East. Cold and wet conditions persisted across most of the region through March, and by late in the month, exceptionally chilly air swept as far south as central Sahelian Africa, with lows dropping below 10°C and weekly departures reaching -11°C at isolated locations of northwestern Africa. From early March through late April, 25 to 125 mm of precipitation fell from southern Syria southward and eastward across eastern Jordan, most of Saudi Arabia, and western Iran. These totals were more than twice the normal across much of Saudi Arabia, and over 12 times the normal in central and northwestern parts of the country.

Southern and Southeastern Europe (10)

Powerful storms during the middle of September abruptly ended the dry spell across much of southern Europe, but much of the eastern Mediterranean remained dry until mid-November. Flash flooding at the end of September claimed over a dozen lives, blocked several major roads and railways, and caused hundreds of millions of dollars (U. S.) in damages across southern and eastern France, Switzerland, and northern Italy. Locarno, a Swiss lakeside resort, was flooded as Lake Maggiore rose to within a few centimeters of its record level reached in 1907. The heavy rains, however, replenished drought-depleted reservoirs in southern France and central Spain. Farther east, unusually warm and dry weather covered Greece, Turkey, and the Middle East until mid-November when torrential rains brought the dry spell to an abrupt end and caused flooding that forced evacuations across Greece. Abundant precipitation continued until mid-December. At the end of the year, localized flooding claimed two lives, closed highways, and disrupted electrical power in southern Israel, with Elat receiving 43 mm (80% of its normal annual rainfall) during 20-23 December.

Southern and East-Central Africa (11)

Above-normal convective activity brought torrential downpours to Zimbabwe, northern Mozambique, most of Malawi, Tanzania, and Kenya during the first few months of the year, continuing to alleviate drought conditions which affected the area in 1991 and much of 1992, but also caused localized flooding. More than twice the normal rainfall was measured across western South Africa, eastern Zimbabwe, northern Namibia, and parts of Kenya in February and again in April. In sharp contrast, less than half of normal rainfall was measured across northern South Africa and southern Mozambique during January and early February. During March, below normal rains were observed from central Mozambique and central Zimbabwe southeastward to northern South Africa and southern Namibia. Although pockets of unfavorable dry conditions were observed, the 1992-93 wet season reportedly allowed southern Africa to largely recover from the previous season's drought.

Southern and Southeastern Africa (12)

Early wet-season rains fell on large sections of southern Africa, with some areas receiving five times the normal amount during late September and early October. By the end of October, drier weather returned to the region; however, heavy rains were again reported in early December which persisted through the end of the year. Much of South Africa and parts of Zimbabwe, Botswana, and southern Mozambique received over 125% of normal rain from late September through the end of the year, with some areas reporting up to two and a half times normal.

Indian Subcontinent and Sri Lanka (13)

The 1993 monsoon was very intense over much of northwestern and extreme eastern India, eastern Pakistan, Nepal, and Bangladesh, with weekly totals of up to 990 mm generating severe flooding that isolated the northeastern section of India from the remainder of the country (see section 3e). Heavy runoff, added to already-swollen rivers, also caused devastating floods across much of Bangladesh. The most severe flooding, however, swept through the Katmandu Valley of Nepal, creating that country's worst natural disaster (in terms of property loss) on record. By early August, at least 4200 lives had been lost across northern and eastern sections of the subcontinent as the flooding finally eased. The monsoon continued its annual retreat in late August, but heavy rains again soaked parts of Nepal and northern India at the beginning of September. Brief but torrential downpours inundated southern India in mid-October and again in mid-November, and a tropical cyclone lashed Sri Lanka and southern India in early December, accompanied by additional unseasonably heavy rains. From mid-October through early December, 500 to 935 mm of rain fell on parts of southern India and Sri Lanka, compared to normals of 250 to 650 mm.

Taiwan and Lower Ryukyu Islands (14)

Unusually dry conditions prevailed on Taiwan and the lower Ryukyu Islands from early July through the end of the year. Most typhoons missed the islands in 1993 as they recurved northeastward towards Japan or drifted further south across the Philippines and South China Sea. Scattered showers brought limited relief to northern Taiwan in early October, but the dry weather returned and persisted through the end of December. During the second half of the year, most of the island received less than half of normal rainfall. This was reportedly Taiwan's worst drought in four decades, causing water rationing in the north and reducing rice production.

Southern and Eastern Australia (15)

Abundant rains fell on eastern Australia in late September and continued through early November, with only brief respites during early and late October. Rainfall totals from early October to mid-December were between two and five times the normal amount in parts of South Australia, New South Wales, and Victoria (see section 3c).

Australia, Indonesia, and the Philippines (16)

The year began with heavy rains in southeastern Australia, but the wet spell ended by February (see section 3c). Farther north, torrential rains in late January and early February caused flooding in northern Australia and parts of Indonesia, but eliminated short-term moisture deficits in the southern Philippines. By the middle of the month, the heavy rains spread into northeastern Australia while additional flooding affected western Java. In sharp contrast, the southern half of Queensland received little or no rain, and this dryness spread northward across the province during late February and most of March. Dry weather continued across most of northeastern and eastern Australia through April, but short-term moisture deficits declined as the typically dry time of year approached. During the first four months of 1993, only 30% to 70% of normal rains fell on the Cape York Peninsula while 10% to 50% of normal was measured across the remainder of central and northern Queensland.

Central South America (17)

During most of the year, many areas experienced either short-term wet or dry spells. The first two weeks of January featured more than twice-normal rainfall in Uruguay, Paraguay, and adjacent parts of Brazil and Argentina, but dry weather prevailed during late January and early February. Heavy rains returned to Uruguay in mid-February. A short respite was experienced from late February through March, but widespread heavy rains of 50 to 250 mm again fell during most of April. Meanwhile, abnormally dry weather affected parts of Paraguay, southern Bolivia, and northern Argentina in March, and a heat wave aggravated the dry conditions in Argentina. Moisture deficits spread northward into Brazil during most of April and early May, eventually encompassing a large area from drought-stricken northeastern Brazil southwestward through northern and western Argentina. Meanwhile, torrential rains deluged south-central Chile, Uruguay, northeastern Argentina, and southeastern Paraguay during the first half of May as up to 400 mm fell within three weeks. In the middle of the month, scattered showers brought some relief to the dry areas, and by June, conditions had returned to near normal, except for persistent rainfall deficits in parts of Paraguay and north-central Argentina. Several weeks of light rain allowed precipitation shortages to develop across northeastern Argentina during July and August, spreading across southeastern Brazil and western Uruguay by the end of August. Widespread dryness continued to plague the region until late September showers provided limited relief. However, July - September totals of only 25% to 60% of normal were common across Uruguay and adjacent Argentina. In October, heavy rains began across Uruguay by mid-month, eventually generating significant short-term moisture surpluses by mid-December throughout east-central South America.

Caribbean, Central America, and Mexico (18)

In late June and early July, the first named Atlantic tropical storm of the season, Arlene, brought heavy rains (over 300 mm at some places) to the south-central United States and northern Mexico. Meanwhile, Pacific Tropical Storm Beatrix and Hurricane Calvin battered central and western Mexico, aggravating five weeks of excessively wet weather. Some locations received 500 to 1380 mm of rain during June and early July. Calvin reportedly caused considerable crop damage, flooded roads, dropped 100 to 300 mm of rain, and knocked out utilities along the western Mexican coastline. Farther south, Tropical Storm Bret brought heavy rains and strong winds to northern South America and southern Central America during early August. Although the wind and rainfall were rather modest for a tropical system, thousands were left homeless as mudslides destroyed many of the mountainside dwellings of Caracas, Venezuela. Farther north, rains from Bret forced rivers out of their banks in southern Nicaragua and northern Costa Rica. Four weeks later, torrential rains from Tropical Storm Gert drenched Honduras and Nicaragua in mid-September, claiming dozens of lives and leaving thousands of individuals homeless. Gert then intensified into a hurricane over the Gulf of Campeche and slammed into east-central Mexico. The states of Veracruz, Tamaulipas, San Luis Potosi, and Hidalgo were most affected as excessive rains generated severe flooding.

Fiji Islands (19)

According to the National Disaster Management Council of Fiji, Cyclone Kina was the worst storm to strike the South Pacific nation in 57 years, causing considerable damage. Daily rainfall totals approached 200 mm at some locations.

Europe and Western Asia (20)

Unusually low temperatures, averaging as much as 5°C below normal, spread across Scandinavia during the last week of June, but the cool air quickly moved out. In September, temperatures fell below freezing in parts of Sweden, Finland, and northwestern Russia as an early-autumn cold wave covered most of northern Europe (see section 3g). Cold air continued to cover the region through September and most of October, with weekly departures reaching -7°C at a few locations. More chilly weather overspread the continent during late October and early November as early-season snows dusted both Paris and London in mid-month, with the latter location reporting its first November snowfall since 1969. By the end of the month, weekly departures reached -11°C in eastern Europe and plummeted to -17°C in parts of Russia. During December, lows plunged to -50°C and weekly departures reached -14°C in southwestern Asia as the cold air shifted southeastward.

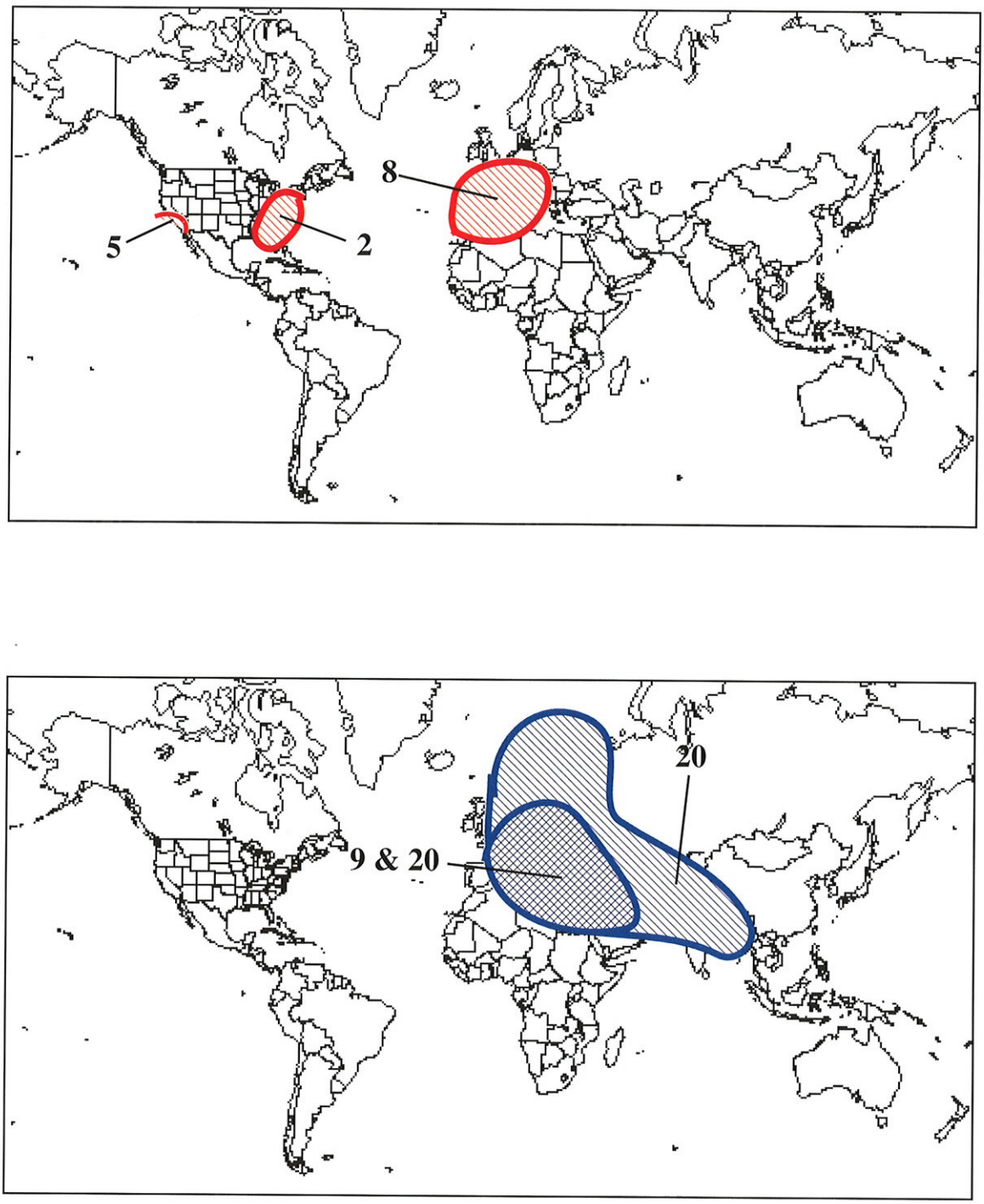

Figure 5.1 Significant above-normal temperature anomalies (top) and below-normal temperature anomalies (bottom) during 1993. The numbers are keyed to the descriptive paragraphs. (Source: CAC)

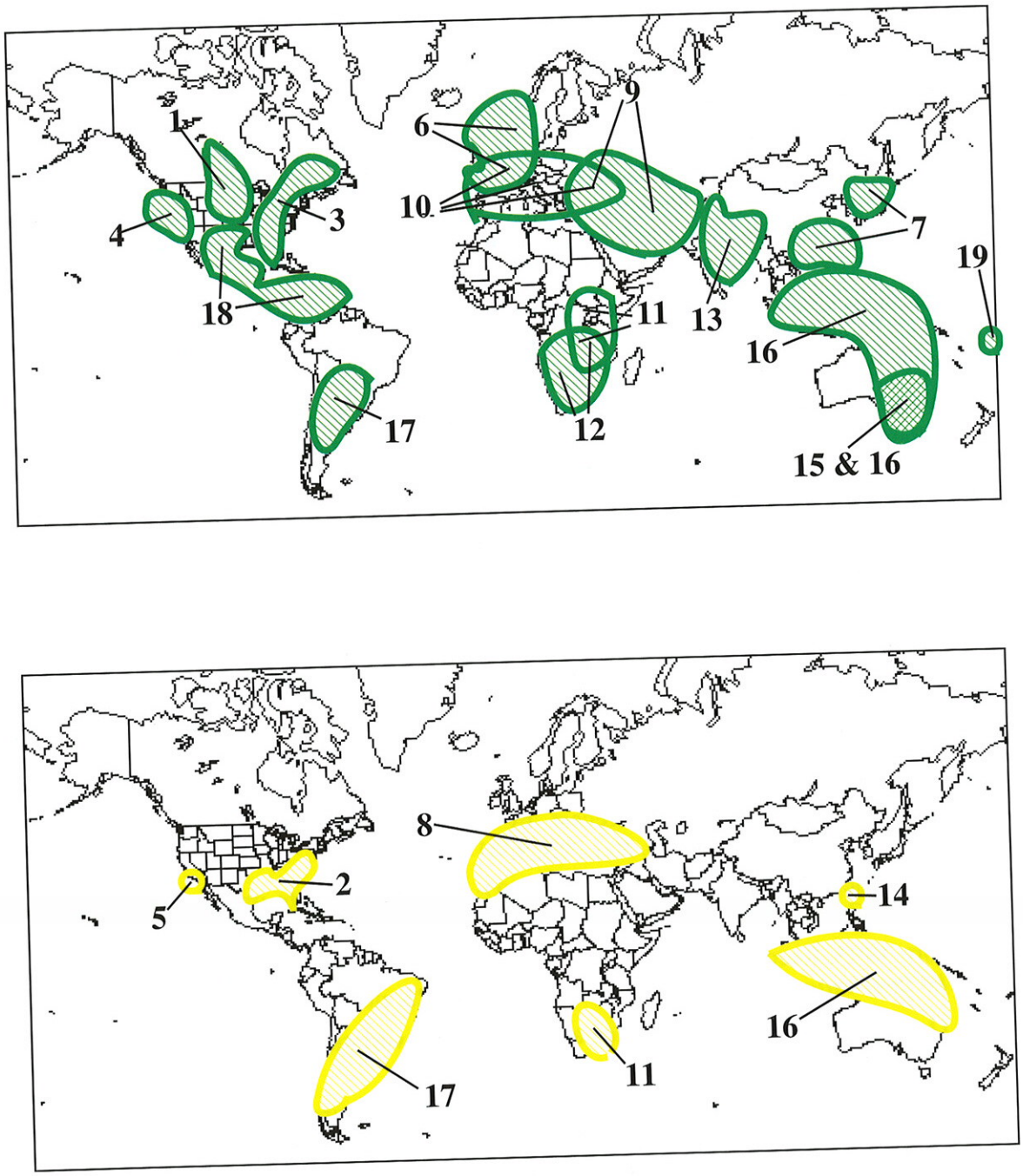

Figure 5.2 Significant above-normal precipitation anomalies (top) and below-normal precipitation anomalies (bottom) during 1993. The numbers are keyed to the descriptive paragraphs. (Source: CAC)

REFERENCES

Arkin, P. A., and B. N. Meisner, 1987: The relationship between large-scale convective rainfall and cold cloud cover over the western hemisphere during 1982-1984. *Mon. Wea. Rev.*, **115**, 51-74.

Arkin, P. A., and P. P. Xie, 1994: The Global Precipitation Climatology Project: First Algorithm Intercomparison Project. *Bull. Amer. Met. Soc.*, (in press).

Bottomley, M., C. K. Folland, J. Hsiung, R. E. Newell and D. E. Parker, 1990: Global Ocean Surface Temperature Atlas (GOSTA). Joint Meteorological Office/Massachusetts Institute of Technology Project. Project supported by US Dept of Energy, US National Science Foundation and US Office of Naval Research. Publication funded by UK Depts. of Energy and Environment. 20 + iv pp and 313 plates, HMSO, London.

Climate Analysis Center, 1991: Climate assessment: A decadal review 1981-1990. M. S. Halpert and C. F. Ropelewski editors. Dept. of Commerce, NOAA/NWS/NMC, Climate Analysis Center [U. S. Printing Office: 1991 - 281-557/40426], 109 pp.

Dlugokencky, E. J., K. A. Masarie, P. M. Lang, P. P. Tans, L. P. Steele and E. G. Nisbet, 1994: A dramatic decrease in the growth rate of atmospheric methane in the Northern Hemisphere during 1992. *Geophys. Res. Let.*, **21**, 45-48.

Ellis, H. T., and R. F. Pueschel, 1971: Solar radiation: Absence of air pollution trends at Mauna Loa. *Science*, **172**, 845-846.

Folland, C. K., T. R. Karl, N. Nicholls, B. S. Nyenzi, D. E. Parker and K. Ya. Vinnikov, 1992: Observed climate variability and change. Section C of *Climate Change 1992 - The Supplementary Report to the IPCC Scientific Assessment*, (Eds., J. T. Houghton, B. A. Callander and S. K. Varney). WMO/UNEP, IPCC, Cambridge University Press, 135-170.

Folland, C. K., and D. E. Parker, 1994: Correction of instrumental biases in historical sea surface temperature data. Submitted to *Quarterly Journal Royal Meteorological Society.*

Hansen, J., J. Fung, A. Lacis, D. Rind, S. Lebedeff, R. Ruedy, G. Russell and P. Stone, 1988: Global climate changes as forecast by Goddard Institute for Space Studies three-dimensional model. *J. Geoph. Res.*, **93**, 9341-9364.

Hansen, J., A. Lacis, R. Ruedy and M. Sato, 1992: Potential climate impact of Mount Pinatubo eruption. *Geoph. Res. Lett.*, **19**, 215-218.

IECA Report, 1993: Record flooding tests the effectiveness of erosion control practices. *Bulletin of the International Erosion Control Association*, **25**, no. 2, 28 pp.

Jones, P. D., 1988: Hemispheric surface air temperature variations: recent trends and an update to 1987. *J. Climate*, **1**, 654-660.

Keeling, C. D., R. B. Bacastow, and T. P. Whorf, 1982: Measurements of the concentration of carbon dioxide at Mauna Loa Observatory, Hawaii. *Carbon Dioxide Review: 1982*. W. C. Clark, Editor. Oxford University Press, New York, 377-385.

Leetmaa, A., and M. Ji, 1989: Operational hindcasting of the tropical Pacific. *Dyn. Atmos. and Oceans*, **13**, 465-490.

Matveev, L. T., 1986: Global field of cloudiness. *Hydrometeoizdat*, Leningrad, 179 pp (in Russian).

Mokhov, I., and M. E. Schlesinger, 1993: Analysis of global cloudiness: 1. Comparison of Meteor, Nimbus-7, and ISCCP satellite data. *J. Geophys. Rev.*, **98**, 12849-868.

Reynolds, R. W., 1988: A real-time global sea surface temperature analysis. *J. Climate*, **1**, 75-86.

Ropelewski, C. F., and M. S. Halpert, 1987: Global and regional scale patterns associated with the El Niño/Southern Oscillation. *Mon. Wea. Rev.*, **115**, 1606-1626.

Rossow, W. B., A. W. Walker and L. C. Garder, 1993: Comparisons of ISCCP and other cloud amounts. *J. of Climate*, **6**, 2394-2418.

Spencer, R. W., J. R. Christy and N. C. Grody, 1990: Global atmospheric temperature monitoring with satellite microwave measurements: Method and results 1979-84. *J. Climate*, **3**, 1111-1128.

Steele, L. P., E. J. Dlugokencky, P. M. Lang, P. P. Tans, R. C. Martin and K. A. Masarie, 1992: Slowing down the global accumulation of atmospheric methane during the 1980's. *Nature*, **358**, 313-316.

Thorning, K. W., P. P. Tans and W. D. Komhyr, 1989: Atmospheric carbon dioxide at Mauna Loa Observatory 2. Analysis of the NOAA/GMCC data, 1974-1985. *J. Geophys. Res.*, **94**, 8549-8565.

USGS, 1993a: Precipitation in the upper Mississippi River basin, July through August 1993. United States Geological Survey, Circular 1120-B, 13 pp.

USGS, 1993b: Flood discharges in the upper Mississippi River basin, July through August 1993. United States Geological Survey, Circular 1120-A, 14 pp.

USGS, 1993c: Occurrence and transport of agricultural chemicals in the Mississippi River basin, July through August 1993. United States Geological Survey, Circular 1120-C, 22 pp.